FH Vorarlberg
University of Applied Sciences

Computational Intelligence Methods for Solving Partial Differential Equations

an experimental study on performance and accuracy

Master Thesis

Submitted in Fulfillment of the Degree

Master of Science in Engineering, MSc

Vorarlberg University of Applied Sciences

Master's in Mechatronics

Support Vorarlberg University of Applied Sciences

Dr.-Ing. Finck Steffen

Handed in by

Schwartze Nicolai, BSc

51835415

Dornbirn, 31.08.2020

Abstract

Computational Intelligence Method for Solving Partial Differential Equations

This master thesis investigates a Computational Intelligence-based method for solving PDEs. The proposed strategy formulates the residual of a PDE as a fitness function. The solution is approximated by a finite sum of Gauss kernels. An appropriate optimisation technique, in this case JADE, is deployed that searches for the best fitting parameters for these kernels. This field is fairly young, a comprehensive literature research reveals several past papers that investigate similar techniques.

To evaluate the performance of the solver, a comprehensive testbed is defined. It consists of 11 different Poisson equations. The solving time, the memory consumption and the approximation quality are compared to the state of the art open-source Finite Element solver NGSolve.

The first experiment tests a serial JADE. The results are not as good as comparable work in the literature. Further, a strange behaviour is observed, where the fitness and the quality do not match.

The second experiment implements a parallel JADE, which allows to make use of parallel hardware. This significantly speeds up the solving time.

The third experiment implements a parallel JADE with adaptive kernels. It starts with one kernel and introduce more kernels along the solving process. A significant improvement is observed on one PDE, that is purposely built to be solvable. On all other testbed PDEs the quality-difference is not conclusive.

The last experiment investigates the discrepancy between the fitness and the quality. Therefore, a new kernel is defined. This kernel inherits all features of the Gauss kernel and extends it with a sine function. As a result, the observed inconsistency between fitness and quality is mitigated.

The thesis closes with a proposal for further investigations. The concepts here should be reconsidered by using better performing optimisation algorithms from the literature, like CMA-ES. Beyond that, an adaptive scheme for the collocation points could be tested. Finally, the fitness function should be further examined.

Kurzreferat

Computational Intelligence Methoden zum Lösen partieller Differentialgleichungen

Diese Masterarbeit untersucht eine Computational Intelligence Methode zum Lösen von PDEs. Diese Strategie formuliert das Residuum der PDE als Fitnessfunktion. Die Lösung wird durch eine endliche Summe von Gauß-Kernel approximiert. Ein geeigneter Optimierungsalgorithmus, in diesem Fall JADE, sucht die passenden Parameter für diese Kernel. Dieses Forschungsfeld ist relativ neu, eine umfassende Literaturrecherche zeigt mehrere Paper, die ähnliche Algorithmen behandeln.

Um die Performance des Solvers zu bewerten, wird ein Testbed definiert. Es besteht aus 11 verschiedenen Poisson-Gleichungen. Die Lösungszeit, der Speicherbedarf und die Approximationsqualität werden mit dem open-source Finite Elemente Solver NGSolve verglichen.

Das erste Experiment testet eine serielle JADE. Die Ergebnisse sind nicht so gut wie vergleichbare Arbeiten in der Literatur. Weiterhin wird ein Verhalten beobachtet, bei dem Fitness und Qualität nicht übereinstimmen.

Das zweite Experiment implementiert eine parallele JADE. Somit kann parallele Hardware genutzt werden. Dadurch wird die Lösungsdauer erheblich verkürzt.

Das dritte Experiment implementiert eine parallele JADE mit adaptiven Kernels. Der Solver beginnt mit einem Kernel und führt weitere Kernels während des Lösungsprozesses ein. Eine signifikante Verbesserung wird bei einer PDE beobachtet, die speziell dafür ausgelegt wurde. Bei allen anderen Testbed-PDEs ist der Qualitätsunterschied nicht aufschlussreich.

Das letzte Experiment untersucht die Diskrepanz zwischen Fitness und Qualität. Dazu wird ein neuer Kernel definiert. Dieser Kernel hat alle Eigenschaften des Gauß-Kernels. Zusätzlich wird er mit einer Sinusfunktion erweitert. Dadurch werden die beobachteten Unterschiede zwischen Fitness und Qualität verringert.

In weiterführenden Arbeiten sollten die hier eingeführten Konzepte mit anderen Optimierungsalgorithmen, wie zum Beispiel einer CMA-ES, überprüft werden. Darüber hinaus könnte ein adaptiver Prozess für die Collocation Punkte getestet werden. Schließlich sollte die Fitnessfunktion weiter untersucht werden.

Contents

List of Figures **VII**

List of Tables **X**

List of Algorithms **XI**

1 Introduction **1**

2 State of the Art **2**
2.1 Finite Element Method 2
2.2 Computational Intelligence Methods 4
2.3 Differential Evolution 10

3 Problem Definition **12**
3.1 Theoretical Foundation 12
3.2 Fitness Function 13
3.3 Candidate Representation 14
3.3.1 Gauss Kernel 15
3.3.2 Gauss Sine Kernel 16

4 Experimental Design **19**
4.1 Testbed 19
4.2 Software Architecture 22
4.3 Performance Metric 23
4.3.1 Solving Time 24
4.3.2 Memory Usage 24
4.3.3 Quality Measurement 25
4.4 Baseline: NGSolve 26
4.4.1 Setup 27
4.4.2 Result 27
4.5 Default CI Parameter 30
4.6 Hardware Infrastructure 33

5 Experiment 0: Serial Memetic JADE **34**
5.1 Hypotheses . . . 34
5.2 Experiment Setup . . . 35
5.3 Results . . . 35
5.4 Discussion . . . 38
5.4.1 Comparison to Literature . . . 38
5.4.2 Solving Time/Memory Usage . . . 38
5.4.3 PDE 0A . . . 39
5.4.4 PDE 5 . . . 40

6 Experiment 1: Parallel Population JADE **43**
6.1 Hypotheses . . . 43
6.2 Experiment Setup . . . 44
6.3 Results . . . 44
6.4 Discussion . . . 46
6.4.1 Memory Usage . . . 46
6.4.2 Solving Time . . . 47
6.4.3 PDE 4 . . . 48

7 Experiment 2: Adaptive Number of Kernels **50**
7.1 Hypotheses . . . 50
7.2 Experiment Setup . . . 52
7.3 Results . . . 53
7.4 Discussion . . . 55
7.4.1 Solving Time . . . 55
7.4.2 Memory Usage . . . 56
7.4.3 PDE 0A . . . 56
7.4.4 Significantly Worse Quality . . . 57
7.4.5 PDE 5 . . . 60
7.4.6 PDE 6 . . . 61

8 Experiment 3: Gauss-Sinus Kernel **64**
8.1 Hypotheses . . . 64
8.2 Experiment Setup . . . 64
8.3 Results . . . 65
8.4 Discussion . . . 67
8.4.1 Solving Time . . . 67
8.4.2 Memory Usage . . . 67
8.4.3 PDE 0A and PDE 6 . . . 67
8.4.4 PDE 0B . . . 68
8.4.5 PDE 5 . . . 68

9 Limitations **71**
9.1 Testbed 71
9.2 Fulfilment of Boundary Condition 71
9.3 Computational Effort 72

10 Theoretical Notes **74**
10.1 Universial Approximation Theorem 74
10.2 Multimodality and Symmetry 76

11 Conclusion **78**

12 Further Work **80**

Acronyms **81**

Bibliography **83**

Appendices **89**

A Differential Evolution Pseudocodes **90**
A.1 JADE Pseudocode 91
A.2 SHADE Pseudocode 92
A.3 L-SHADE Pseudocode 93

B Testbed **94**

C Software Architecture **106**

D Post-Processing Module Description **108**

E Solve Method **111**

F pJADE **112**

G paJADE **114**

H Adaptive Kernel Scheme **116**

I PDE 2 3 4 and 7 Kernel Adaption **118**

List of Figures

3.1 3D plot of a single Gauss kernel with the parameters $\omega = 1$, $\gamma = 1$, $c_0 = 0$ and $c_1 = 0$ 15
3.2 3D plot of a single Gauss Sine kernel with the parameters $\omega = 1$, $\gamma = 1$, $c_0 = 0$, $c_1 = 0$, $f = 1$, $\varphi = 0$ 17

4.1 This reduced Unified Modeling Language (UML) class diagram gives an overview of the testbed design and its interfaces and classes. . . 23
4.2 Aliasing Error: sharp inaccuracies in between collocation points . . 26
4.3 Boxplot: time (in seconds) needed to solve the testbed Partial Differential Equation (PDE) (without PDE3) 28
4.4 Boxplot: memory (in Mbyte) needed to solve the testbed PDE (without PDE3) 29
4.5 PDE 3 performance metrics at different Degree of Freedom (DOF) budgets. 30
4.6 Comparison of time and memory effort on PDE 3 at $5 \cdot 10^4$ DOF. . 30
4.7 Weighting factor φ and ξ on every collocation point 32
4.8 Collocation points used in the testbed. For the PDEs 0A and 0B with the larger domain, the lower limits x_0L and x_1L are replaced with -2 and the upper limits x_0U and x_1U are replaced with 2. The points are still equally spaced. 33

5.1 Relative solving time results of memetic JADE after 10^4 Number of Function Evaluation (#FE). 37
5.2 Relative memory usage results of memetic JADE after 10^4 #FE. . 37
5.3 Comparison of two typical PDE 0A solutions. 40
5.4 Comparison of best solution after 10^4 and 10^6 #FE. 40
5.5 Histograms of the fitness and the L2 norm reached with 10^4 #FE and 10^6 #FE on PDE 5. 41
5.6 Fitness value and L2 Norm of one individual at every generation on PDE 5. 42

6.1 Relative solving time results of parallel memetic JADE after 10^4 #FE. 45
6.2 Relative memory usage results of parallel memetic JADE after 10^4 #FE. 45
6.3 Mean speed-up of parallel JADE with 95% confidence interval. . . 47
6.4 Comparison of the absolute error of the worst solution on PDE 4 by a parallel and a serial memetic JADE at 10^6 #FE 48
6.5 Histogram of the L2 norm data obtained by the serial and the parallel JADE on PDE 4 from table 6.1. 49
6.6 Boxplot of the L2 norm data from table 6.1 on PDE 4. 49

7.1 Flowchart of the adaptive kernel scheme. 51
7.2 Relative solving time results of parallel memetic JADE with adaptive kernels after 10^4 #FE. 53
7.3 Relative memory usage results of parallel memetic JADE with adaptive kernels after 10^4 #FE. 54
7.4 Number of kernels of the proposed solution by the paJADE per PDE at 10^6 #FE 55
7.5 3D plot and comparison of unnecessary 6^{th} kernels on PDE 0A. . . 57
7.6 Semi-logarithmic plot of the correlation between the L2 norm and the number of kernels. The results are taken at 10^6 #FE on the PDEs 2, 3, 4 and 7. The corresponding R^2 values of the linear regression are denoted. 57
7.7 Comparison of $minError$ against the number of kernels and the achieved solution quality. 58
7.8 Semi-logarithmic plot of the correlation between the L2 norm and the number of kernels. The results are produced with a $minError = 10^-1$ after 10^6 #FE. 59
7.9 Boxplot of solution quality on PDE 5 with a budget of 10^6 #FE. Comparison of distribution with and without outliers. 60
7.10 3D plot of the outlier solution produced by the adaptive kernel scheme on PDE 5 after 10^6 #FE. 61
7.11 Comparison of the L2 norm reached by the paJADE and a non-adaptive pJADE on PDE 6 after 10^6 #FE. 62
7.12 These wrong solutions are generated with paJADE after 10^6 #FE and represent local optima where JADE gets stuck. 62
7.13 Kernel bar plot of the false solution, represented in figure 7.12a . . 63
7.14 Kernel bar plot of the false solution, represented in figure 7.12b . . 63

8.1 Relative solving time results of parallel memetic JADE with Gauss Sine Kernel (GSK) after 10^4 #FE. 65
8.2 Relative memory usage results of parallel memetic JADE with GSK after 10^4 #FE. 66
8.3 Comparisons of best solution absolute error by memetic parallel JADE using Gauss Kernel (GaK) and GSK after 10^6 #FE. 68
8.4 Comparison of the best and the worst result generated by memetic pJADE with GSK after 10^6 #FE. 69
8.5 Histograms of GSK and GaK L2 norm and fitness value on PDE 5 after 10^6 #FE. 69
8.6 Fitness value and L2 Norm of an exemplary individual at every generation on PDE 5 using a GSK. 70

9.1 Empirical Runtime Distribution of all algorithms on the 11 testbed PDEs at target values $5 \cdot 10^{-2}$, $1 \cdot 10^{-2}$, $5 \cdot 10^{-3}$ and $1 \cdot 10^{-3}$. . . . 73

10.1 Distribution of exemplary optima on the fitness function in 3D space. 77

B.1 PDE 0A Gauss Kernel solution plot 95
B.2 PDE 0B Gauss Sine Kernel solution plot 96
B.3 PDE 1 Polynomial 2D solution plot 97
B.4 PDE 2 Chaquet PDE 1 solution plot 98
B.5 PDE 3 Chaquet PDE 3 solution plot 99
B.6 PDE 4 Sine Bump 2D solution plot 100
B.7 PDE 5 Arctan Circular Wave Front solution plot 101
B.8 PDE 6 Peak 2D solution plot 102
B.9 PDE 7 Boundary Line Singularity solution plot 103
B.10 PDE 8 Interior Point Singularity solution plot 104
B.11 PDE 9 Arctan Wave Front Homogeneous Boundary Conditions 2D solution plot 105

C.1 This UML class diagram describes the software architecture defined to prepare, run and evaluate the experiments. 107

D.1 Example distributions for different results of the statsWilcoxon method. 110

I.1 Kernel Bars Plot on the worst result of PDE2 in experiment 2. . . 118
I.2 Kernel Bars Plot on the best result of PDE2 in experiment 2. . . . 118
I.3 Kernel Bars Plot on the worst result of PDE3 in experiment 2. . . 118
I.4 Kernel Bars Plot on the best result of PDE3 in experiment 2. . . . 119
I.5 Kernel Bars Plot on the worst result of PDE4 in experiment 2. . . 119
I.6 Kernel Bars Plot on the best result of PDE4 in experiment 2. . . . 119
I.7 Kernel Bars Plot on the worst result of PDE7 in experiment 2. . . 119
I.8 Kernel Bars Plot on the best result of PDE7 in experiment 2. . . . 119

List of Tables

2.1 Literature research on the general topic of stochastic solver and their application. The papers are sorted by date of release. 9

4.1 These are the results obtained by the Finite Element Method (FEM) solver in terms of distance to the analytical solution. The solver achieves the smallest deviation in PDE 3. 28
4.2 These predefined parameters are used for the following numerical experiments. 31
4.3 Comparison of the machines used for the experiments. 33

5.1 This table compares the results obtained with the serial memetic JADE to the numerical results obtained by similar work in literature. The same metric must be used, thus the RMSE as defined in equation (4.1) is calculated. 35
5.2 L2 norm reached with serial JADE at 10^4 #FE and 10^6 #FE . . . 36

6.1 This table compares the results obtained by the parallel and the serial JADE. All results are obtained at 10^6 #FE. The serial data is the same as already presented in table 5.2. 46

7.1 Comparison of the achieved L2 norm by the pJADE and the paJADE at 10^6 #FE. The pJADE data is directly taken from table 6.1. . . 54
7.2 Statistical comparison of the achieved L2 norm by paJADE with $minError = 0$ and $minError = 10^{-1}$ after 10^6 #FE. The data with $minError = 0$ is directly taken from table 7.1. 59

8.1 Statistical comparison of the the parallel JADE using the GaK and the GSK. 66

List of Algorithms

5.1 Pseudocode of memetic JADE 34

6.1 Pseudocode of memetic parallel JADE 44

A.1 JADE Pseudocode 91
A.2 SHADE Pseudocode 92
A.3 L-SHADE Pseudocode 93

E.1 Solve Method Pseudocode 111

F.1 Pseudocode of pJADE 113

G.1 Pseudocode of paJADE 115

H.1 Pseudocode of memetic parallel JADE with adaptive kernels 117

1 Introduction

Differential equations are a very powerful mathematical tool to describe the universe. From fluid dynamic and heat flow in mechanical engineering or electrodynamics and circuit-design in electrical engineering to the fluctuation of stock market prices and even the movement of astronomical objects - most dynamic processes can be modelled by them. But only a tiny fraction of them are currently analytically solvable. The rise of the computer paved the way for approximating the solution of a differential equation numerically. There are plenty of different solver methods ranging from simple single step solvers like the Forward-Euler (FE) method over more complex multistep solvers like the Adams–Bashforth (AB) method to whole Finite Element Method (FEM) solver packages. Most of these solvers are specialised for one kind of differential equation, leveraging some special properties of the problem to be most efficient in time and error. But there are very few generalised methods that can solve many different types of equations. This lack of a universal solver is the main motivation of the present master thesis.

There is already a small, yet steadily growing research community interested in tying together the concepts of computational intelligence and numerical solver for differential equations. In chapter 2.2 a brief overview of related work done within the last 20 years is given. The main idea of all listed papers is to reformulate the original problem into an optimisation problem, which in turn is then solved using an evolutionary algorithm. The main focus of this thesis lies on two-dimensional Partial Differential Equations (PDE). The results are then compared to the analytical solution as well as a state of the art FEM solver.

This master thesis tries to answer the following questions: Is it possible to improve the results obtained in other research papers by using a modern variant of the Differential Evolution (DE) optimisation algorithm? How well does this method stack up against classical FEM packages for solving PDEs considering time and memory usage as well as numerical error? Is there a meaningful way to reduce the time consumption by making use of a parallel computation architecture?

2 State of the Art

This chapter provides an overview of the current state of the art in solving PDE. Included are the widely used FEM as well as heuristic optimisation methods. Further, an introduction to the DE framework is given, which provides the basis for the algorithms described in this thesis.

2.1 Finite Element Method

Currently, the Finite Element Method is the go-to approach to solve partial differential equations. The domain Ω on which the PDE is posed, is discretised into multiple smaller elements - as the name suggests. Thus, FEM counts to the category of meshed methods. The underlying solution function $u(\mathbf{x})$ to the PDE is then approximated by so called "basis-functions" $\Phi(\mathbf{x})$ limited to these finite elements. This thesis uses the open-source Netgen/NGSolve FEM package (Schöberl, Lackner, and Hochsteger 2020).

The general steps taken to solve a PDE with an FEM solver are:

1. Step: Strong Form
   This is the standard formulation of the linear PDE. $\mathbf{L}$ and $\mathbf{B}$ are linear differential operators that include the derivatives.

$$\begin{aligned} \mathbf{x} &\in \mathbb{R}^2 \\ u(\mathbf{x}), f(\mathbf{x}), g(\mathbf{x}) &: \Omega \to \mathbb{R} \\ \mathbf{L}u(\mathbf{x}) &= f(\mathbf{x}) \text{ on } \Omega \\ \mathbf{B}u(\mathbf{x}) &= g(\mathbf{x}) \text{ on } \partial\Omega \end{aligned} \tag{2.1}$$

   Further, only Dirichlet boundary conditions are considered, thus the boundary operator is always the identity matrix $\mathbf{B} = \mathbb{I}$. Therefore, the linear operator on the boundary $\mathbf{B}$ can be disregarded, resulting in

$$u(\mathbf{x})|_{\partial\Omega} = g(\mathbf{x}). \tag{2.2}$$

2. Step: Weak Form
   The next step is to reformulate the strong form into a usable weak form. This is equivalent to the strong form but written in an integral notation. In this

equation, the A, b and c correspond to the constant factors of the derivatives in strong form. For the sake of completeness, this is kept abstract. In the PDEs considered in this work, $A = \mathbb{I}$ and $b = \mathbf{0}$, $c = 0$. Currently, the so-called test-function $v(\mathbf{x})$ is an arbitrary function, but it has to be 0 on the boundary $v(\mathbf{x})|_\Omega = 0$. The choice of the test-function correspond to different FEM types (Shen, Tang, and Wang 2011, p. 6f).

$$\underbrace{\int_\Omega -(\nabla^T A \nabla)u(\mathbf{x})v(\mathbf{x})dV - \int_\Omega b^T \nabla u(\mathbf{x})v(\mathbf{x})dV + \int_\Omega cu(\mathbf{x})v(\mathbf{x})dV}_{a(u,v)} = \underbrace{\int_\Omega f(\mathbf{x})v(\mathbf{x})dV}_{F(v)} \tag{2.3}$$

3. Step: Discretisation of Ω
   Create a mesh of finite elements that span the whole domain. Usually these are triangles. Thus, this step is sometimes called "triangulation".

4. Step: Basis functions
   Choose a basis function $\Phi(\mathbf{x})$ that can be used to approximate the solution $u(\mathbf{x}) \approx u_h(\mathbf{x}) = \sum_{i=1}^{N} u_i \Phi_i(\mathbf{x})$. A common choice are Lagrange or Chebyshev polynomials. In the Galerkin type FEM, the test-function $v(\mathbf{x})$ is the same as the trail-function, thus $v(\mathbf{x}) = \sum_{j=1}^{N} v_j \Phi_j(\mathbf{x})$. The choice of the basis function $\Phi(\mathbf{x})$ largely influences the computational effort. $\Phi(\mathbf{x})$ should have a small support, to produce a thinly populated matrix A in the linear system of equations (2.5) below.

5. Step: Solution
   In the weak form, as seen in equation (2.3), $a(u, v)$ is a continuous bilinear form and $F(v)$ is a continuous linear functional. Substituting u and v with their corresponding approximation from step 4 results in

$$\sum_{j=1}^{N} v_j \sum_{i=1}^{N} u_i a(\Phi_i, \Phi_j) = \sum_{j=1}^{N} v_j F(\Phi_j). \tag{2.4}$$

   Dividing by the v_j values on both sides results in a linear system of equations, where the constant factors u_i need to be determined.

$$\underbrace{\sum_{i=1}^{N} u_i a(\Phi_i, \Phi_j)}_{\mathbf{Au}} = \underbrace{F(\Phi_j)}_{\mathbf{b}} \text{ for } j = 1, ...N \tag{2.5}$$

Modern solvers include more complex and advanced techniques to further improve the solution error and the computation time. Some of the most important concepts

that are also available in NGSolve are listed here.

- Static Condensation:
  Depending on the number of discrete elements, the $\mathbf{A}$ matrix can be very large. Inverting large matrices is very time consuming. Static condensation, also called Guyan reduction (Guyan 1965), reduces this dimensionality by exploiting the structure of $\mathbf{A}$.
- Preconditioner:
  Instead of solving the $\mathbf{A}^{-1}$ exactly, this can also be approximated by a matrix that is similar to $\mathbf{A}^{-1}$. The actual inverse can be iteratively approximated. NGSolve implements multiple different preconditioners and it even allows to create your own method.
- Adaptive Mesh Refinement:
  The accuracy of a FEM-approximated solution mainly depends on the density of the mesh. Typically, finer meshes tend to produce more accurate solutions, but the computation time is longer. This trade-off can be overcome by a self-adaptive mesh. NGSolve implements that in an adaptive loop that executes:
  - Solve PDE (with coarse mesh)
  - Estimate Error (for every element)
  - Mark Elements (that have the greatest error)
  - Refine Elements (that were previously marked)
  - Repeat until degrees of freedom exceed a specified N

2.2 Computational Intelligence Methods

The research community interested in computational intelligence solvers for differential equations has been steadily growing over the past 20 years. This chapter summarises the most important works done in the general field of development and application of such statistical numerical solvers. The following table 2.1 gives a brief overview of these papers and sorts them historically.

In general, all of these papers from the table use the Weighted Residual Method (WRM), or some variant of that concept, to transform their differential equation into an optimisation problem. This serves as the fitness function and is necessary to evaluate a possible candidate solution and perform the evolutionary selection. The fitness function is the function to be optimised. It is also called objective function and these terms are used interchangeably in this thesis. In short, the residual R is defined through the differential equation itself and can be calculated by $R(u(\mathbf{x})) = \mathbf{L}u(\mathbf{x}) - f(\mathbf{x})$. The residual can be thought of as a functional that

substitutes $u(\mathbf{x})$ with an approximate solution $u_{apx}(\mathbf{x})$ and returns a numerical score. The WRM method is further described in chapter 3.1.

Howard and Roberts 2001 is one of the first advances in this field. They approximate a subset of the convection-diffusion equations with Genetic Programming (GP) (Koza 1992). Their main idea is to use a polynomial of variable length as the candidate solution that is forced to satisfy the boundary condition. Their fitness value, as seen in equation (2.6), is calculated by squaring the residual R and integrating it over the domain. Since the polynomials are known, and the problems are restricted to a specific differential equation, the integral can be evaluated analytically.

$$F(u_{apx}(\mathbf{x})) = -\int_{\Omega} R(u_{apx}(\mathbf{x}))^2 dx \tag{2.6}$$

Kirstukas, Bryden, and Ashlock 2005 proposes a three-step procedure. The first step is time consuming and employs GP techniques to find basis functions that span the solution space. The second step is faster and uses a Gram–Schmidt algorithm to compute the basis function multipliers to develop a complete solution for a given set of boundary conditions. Using linear solver methods, a set of coefficients is found that produces a single function that both satisfies the differential equation and the boundary or initial conditions at distinct points over the domain. These points are further called collocation points.

Tsoulos and Lagaris 2006 use Grammatical Evolution (GE) (Ryan, Collins, and Neill 1998) to find solutions to various differential equations. In contrary to GP, GE uses vectors instead of trees to represent the candidate string. The solution is evaluated as an analytical string, constructed of the functions sin, cos, exp and log, as well as all digits and all four basic arithmetic operations. Because the GE step could result in virtually any function, the fitness integral from equation (2.6) can not be calculated analytically. Thus, the integral is approximated by evaluating the residual at collocation points within the domain. This is seen in equation (2.7). The algorithm was tested on multiple problems of Ordinary Differential Equation (ODE), system of ODEs and PDE. Only the results for ODEs were promising.

$$F(u_{apx}(\mathbf{x})) = \sum_{i=1}^{n_C} ||R(u_{apx}(\mathbf{x}_i))||^2 \tag{2.7}$$

Mastorakis 2006 couples a Genetic Algorithm (GA) (Holland 1962) with a Downhill-Simplex (DS) method (Nelder and Mead 1965) for the local solution refinement. The candidates are represented as polynomials of the order 5 where the coefficients are optimised. The boundary condition is directly incorporated into the candidate, thus simplifying the objective function to equation (2.7). The focus here is on unstable ODEs that can not be solved with finite difference methods.

Sobester, Nair, and Keane 2008 tried a radical different approach to incorporate the boundary condition into the solution. They found that using GP for the inner domain is only effective if the algorithm does not have to consider the boundary. They split the solution $u_{apx}(\mathbf{x})$ into two parts where $u_{GP}(\mathbf{x})$ represents the solution for the inner domain and $u_{RBF}(\mathbf{x})$ ensures the boundary condition

$$u(\mathbf{x})_{apx} = u_{GP}(\mathbf{x}) + u(\mathbf{x})_{RBF}. \tag{2.8}$$

At first, the GP step produced a trial solution according to the objective function (2.7). After the GP procedure, a linear combination of radial basis functions $u(\mathbf{x})_{RBF} = \sum_{j=1}^{n_B} \alpha_j \Phi(||\mathbf{x} - \mathbf{x}_j||)$ is specifically tailored to $u_{GP}(\mathbf{x})$ that ensures the boundary condition at all $\mathbf{x}_j$ points on $\partial\Omega$. Finding the parameters α_j can be formulated as a least squares problem.

Howard, Brezulianu, and Kolibal 2011 use a GP scheme to find the solution to a specific set of simplified convection-diffusion equations. They represent a candidate as discrete function value points over the domain. The function between these points is interpolated. The fitness function is similar to equation (2.7) with the exception that the n_C points are not predetermined. These points are sampled randomly in the domain, thus allowing the algorithm to approximate the solution aside from fixed base points.

Chaquet and Carmona 2012 use a simple self-adaptive Evolution Strategy (ES) (as developed by Schwefel 1977 and Rechenberg 1978) to evolve the coefficients of a partial Fourier series. The fitness function is expressed in equation (2.14). This is similar to the fitness function 2.7, but it extends the definition of the boundary to also include Neumann conditions by introducing the linear differential operator $\mathbf{B}$. The limit n_C denotes the number of inner collocation points $\mathbf{x}_i$ within the domain Ω, whereas n_B is the number of discrete points $\mathbf{x}_j$ on the boundary $\partial\Omega$. Further, a penalty factor ϕ shifts the focus of the fitness to the boundary. Additionally, this objective function can also represent systems of differential equations, where the number of equations is denoted by m. To reduce the search dimension (represented by the number of harmonics), they developed a scheme that only optimises one harmonic at a time and freezes the other coefficients. This scheme is based on the often observed principle that lower frequencies are more important in reconstructing a signal than higher ones. Albeit this concept might not be valid for all possible functions, it worked on all differential equations of their testbed.

$$F(u_{apx}(\mathbf{x})) = \frac{\sum_{i=1}^{n_C} ||\mathbf{L}u_{apx}(\mathbf{x}_i) - f(\mathbf{x}_i)||^2 + \phi \sum_{j=1}^{n_B} ||\mathbf{B}u_{apx}(\mathbf{x}_j) - g(\mathbf{x}_j)||^2}{m(n_C + n_B)} \tag{2.9}$$

Babaei 2013 takes a similar approach. They approximate a solution using a partial Fourier series. The optimal parameters for the candidates are found using a Particle Swarm Optimisation (PSO) algorithm (Kennedy and Eberhart 1995). The fitness

function consists of two parts, one for the inner area (equation (2.10)) and one for the boundary (equation (2.11)). These are added together resulting in equation (2.12).

The weighted residual integral WRF is exactly the formulation of the WRM from chapter 3.1. W is an arbitrary weighting function. The absolute values of W and R ensure that only positive values count towards the fitness. Instead of using a sum over collocation points, the integral is evaluated using a numerical integration scheme.

$$WRF(u_{apx}(\mathbf{x})) = \int_{\Omega} |W(\mathbf{x})||R(u_{apx}(\mathbf{x}))|dx \tag{2.10}$$

The boundary condition is incorporated by summing up its normed violations at distinct points $\mathbf{x}_i$. K_j are penality multipliers that shift the focus to different points of the boundary. The concept of this penalty function originates from Rajeev and Krishnamoorthy 1992.

$$PFV(u_{apx}(\mathbf{x})) = WRF(u_{apx}(\mathbf{x})) \cdot \sum_{j=1}^{n_B} K_j \left(\frac{u_{apx}(\mathbf{x}_i)}{g(\mathbf{x}_i)} - 1 \right) \tag{2.11}$$

$$F(u_{apx}(\mathbf{x})) = WRF(u_{apx}(\mathbf{x})) + PFV(u_{apx}(\mathbf{x})) \tag{2.12}$$

Panagant and Bureerat 2014 use polynomials as a candidate representation. They do not specify the order or the type of the polynomial. They test five different simple versions of the optimisation algorithm DE (Storn and Price 1997). Further, they introduce a so called DE-New that increases the population size after every generation. Their proposition is that greater population sizes are better at finding good solutions.

Sadollah et al. 2017 compares three different optimisation algorithms to approximate differential equations: PSO, Harmony Search (HS) (Geem, Kim, and Loganathan 2001) and Water Cycle Algorithm (WCA) (Eskandar et al. 2012). They use the formulation in equation (2.10), where the weighting function is the same as the residual $|W(\mathbf{x})| = |R(u_{apx}(\mathbf{x}))| \rightarrow WRF = \int_{\Omega} |R(u_{apx}(\mathbf{x}))|^2 dx$. The integral is again approximated using a numerical integration scheme. They find that the PSO is slightly better at producing low error solutions, however WCA is better at satisfying the boundary condition.

In their paper Chaquet and Carmona 2019 describe an algorithm that approximates a solution with a linear combination of Gaussian Radial Basis Function (RBF) as kernels:

$$u(\mathbf{x})_{apx} = \sum_{i=1}^{N} \omega_i e^{\gamma_i(||\mathbf{x}-\mathbf{c}_i||^2)} \tag{2.13}$$

The approximated function $u(\mathbf{x})_{apx}$ can be fully determined by a finite number of parameters: $\omega_i, \gamma_i, \mathbf{c}_i$. These are stacked together into a vector $\mathbf{p_{apx}}$ and called the decision variables which are optimised by the algorithm. The objective function can

be seen in equation (2.14). This is an update of the objective function in 2.9 where the inner collocation points also get scaled by a weighting function $\xi(\mathbf{x}_i)$.

$$F(u_{apx}(\mathbf{x})) = \frac{\sum_{i=1}^{n_C} \xi(\mathbf{x}_i)||\mathbf{L}u_{apx}(\mathbf{x}_i) - f(\mathbf{x}_i)||^2 + \phi \sum_{j=1}^{n_B} ||\mathbf{B}u_{apx}(\mathbf{x}_j) - g(\mathbf{x}_j)||^2}{m(n_C + n_B)} \tag{2.14}$$

The multipliers $\xi(\mathbf{x}_i)$ and ϕ are weighting factors for either the inner or the boundary term. The whole term is normalised with the number of collocation points. The parameters of the kernels are determined via a Covariance Matrix Adaption Evolution Strategy (CMA-ES) (Hansen, Müller, and Koumoutsakos 2003). To further improve the solution, the evolutionary algorithm is coupled with a DS method to carry out the local search. The authors show empirically that the local search significantly improves the performance by testing the algorithm on a set of 32 differential equations.

Fateh et al. 2019 use a simple variant of DE where candidates are represented as discrete function value points within the domain. The function values between the grid points are linearly interpolated. This is a radical brute force approach that results in a massive search space dimension. Yet, the main advantage is that the solution is not limited to a decomposition of kernel functions and thus, even non-smooth functions can be approximated. Since this approach does not produce an analytical solution, the differential equation and the boundary condition is incorporated into the fitness function by taking the sum of squared residuals at every grid point, as seen in equation (2.15). The derivatives within the residual are calculated between two neighbouring points by the difference quotient.

$$F(\mathbf{x}) = \sqrt{\sum_{i=0}^{n} R(\mathbf{x}_i)^2} \tag{2.15}$$

Paper	Algorithm	Representation	Problems
Howard and Roberts 2001	GP	polynomial of arbitrary length	one-dimensional steady-state model of convection-diffusion equation
Kirstukas, Bryden, and Ashlock 2005	GP	algebraic expression	heating of thin rod heating by current
Tsoulos and Lagaris 2006	GE	algebraic term	set of ODEs system of ODEs and PDEs
Mastorakis 2006	GA (global); DS (local)	5th order polynomial	unstable ODEs
Sobester, Nair, and Keane 2008	GP and RBF-NN	algebraic term for inner; RBF for boundary	elliptic PDEs
Howard, Brezulianu, and Kolibal 2011	GP	function value grid	convection–diffusion equation at different Peclet numbers
Chaquet and Carmona 2012	ES	partial sum of Fourier series	testbench of ODEs system of ODEs and PDEs
Babaei 2013	PSO	partial sum of Fourier series	integro-differential equation system of linear ODEs Brachistochrone nonlinear Bernoulli
Panagant and Bureerat 2014	DE	polynomial of unspecified order	set of 6 different PDEs
Sadollah et al. 2017	PSO HS WCA	partial sum of Fourier series	singular BVP
Chaquet and Carmona 2019	CMA-ES (global); DS (local)	linear combination of Gaussian kernels	testbench of ODEs system of ODEs and PDEs
Fateh et al. 2019	DE	function value grid	elliptic PDEs

Table 2.1: Literature research on the general topic of stochastic solver and their application. The papers are sorted by date of release.

2.3 Differential Evolution

The differential evolution framework was first introduced in Storn and Price 1997. Due to its simple and flexible structure, it quickly became one of the most successful evolutionary algorithm. Over the years, several adaptations to the original framework have been proposed and some of them currently count to the best performing algorithms, as the 100-Digit Challenge at GECCO 2019 (Suganthan 2020) shows.

The main DE framework consists of three necessary steps that continuously update a population of possible solutions. The population can be interpreted as a matrix, where each row-vector $\mathbf{x}_i$, also called individual, represents a point within the search domain and has a fitness value corresponding to the fitness function $f(\mathbf{x}_i) : \mathbb{R}^n \to \mathbb{R}$. The goal is to minimise the fitness function. These steps are performed in a loop until a predefined termination condition is reached. Each individual step is controlled by a user-defined parameter:

- Mutation:
  Mutation strength parameter F;
  The mutation uses the information from within the population to create a trial vector v_i. This is done by scaling the difference between some vectors in the population - hence the name *differential* evolution. The */current-to-pbest/1* mutation operator can be seen in equation (2.16) where x_i is the current individual, x^p_{best} is one random vector of the p% top vectors, x_{r1} is a random vector from the population while $\tilde{x}_{r2}$ is randomly chosen from the population and the archive. x_{r1} and $\tilde{x}_{r2}$ must not describe the same individual.

$$v_i = x_i + F_i(x^p_{best} - x_i) + F_i(x_{r1} - \tilde{x}_{r2}) \tag{2.16}$$

- Crossover:
  Crossover probability parameter CR;
  The crossover procedure randomly mixes the information between the trial vector v_i and a random candidate from the population x_i to create a new trial vector u_i. The binomial crossover from equation (2.17) randomly takes elements from both vectors, where K is a random index to ensure that at least one element from the trial vector v_i is taken.

$$u_{ij} = \begin{cases} v_{ij}, & \text{if } j = K \vee rand[0,1] \leq CR \\ x_{ij}, & \text{otherwise} \end{cases} \tag{2.17}$$

- Selection:
  Population size N;
  The selection replaces the old candidate x_i if the trial candidate u_i is better as measured by the fitness function. This is performed for every individual in the population, then the next generation is started.

In modern DE variants, these parameters are self-adapted during the evolutionary process. This means that the algorithms can balance out between exploration of the search-space and exploitation of promising locations.

A prominent example of a modern DE with self-adaption is JADE, which was developed by Zhang and Sanderson 2009. The adaption is performed by taking successful F and CR values of the last generation into account. If a certain setting is successful in generating better candidates, newly selected F and CR gravitate towards that setting. The pseudocode is presented in the appendix A.1.

This idea was later refined by Tanabe and A. Fukunaga 2013. They propose a similar self-adaptive scheme but extend the "memory" for good F and CR parameters over multiple generations. This idea improves the robustness as compared to JADE. The pseudocode in appendix A.2 shows the outline of this so called SHADE algorithm.

The latest iteration of SHADE is called L-SHADE (Tanabe and A. S. Fukunaga 2014), which improves the performance by including a deterministic adaptive concept for the population size. At first, L-SHADE starts with a big population size, and reduces the number of individuals in a linear fashion by deleting bad candidates. This has the effect of reducing the number of unnecessary function evaluations. The code is displayed in the appendix A.3.

3 Problem Definition

This chapter describes the broader idea of the WRM, which is used to reformulate any differential equation into an optimisation problem, and its application in the field of spectral methods (Shen, Tang, and Wang 2011). The fitness function originates from these approaches. Further, the different approximation schemes and numerical solution representation are depicted.

3.1 Theoretical Foundation

The most general description of a linear PDE is displayed in equation (3.1).

$$\begin{aligned} \mathbf{L}u(\mathbf{x}) &= f(\mathbf{x}) \\ \text{subjected to: } \mathbf{B}u(\mathbf{x}) &= g(\mathbf{x}) \end{aligned} \tag{3.1}$$

This is similar to the formulation of the strong form in equation (2.1), but not limited to a Dirichlet boundary problem. The matrix $\mathbf{B}$ can include differentiation, effectively allowing Neumann boundary conditions.

An approximate solution to this problem is expressed as a finite sum of basis functions $\phi_k(\mathbf{x})$, as denoted in equation (3.2). The coefficients a_k need to be determined. In classical approximation schemes, the basis functions are orthogonal, such as trigonometric functions or Lagrange basis polynomials.

$$u(\mathbf{x}) \approx u_{apx}(\mathbf{x}) = \sum_{k=0}^{N} a_k \phi_k(\mathbf{x}) \tag{3.2}$$

The residual of a PDE, as shown in equation (3.3), is formulated as the difference between the left and the right side of the differential equation. The residual of a solved PDE is zero. This is only possible for the analytical solution, further denoted as $u_{ext}(x, y)$. For a numerical approximation $u_{apx}(x, y)$, the residual should be small enough for the context of the approximation.

$$R(\mathbf{x}) = \mathbf{L}u_{apx}(\mathbf{x}) - f(\mathbf{x}) \tag{3.3}$$

The WRM (Shen, Tang, and Wang 2011) tries to minimise this residual of a numerical candidate solution over the whole domain Ω. Therefore, R at every $\mathbf{x} \in \Omega$ is evaluated and added up, resulting in the following integral of equation (3.4). The residual at every $\mathbf{x}$ can be scaled by a weighting function over the domain as denoted with $W(\mathbf{x})$, which is needed for numerical stability and is linked to the Gauss Quadrature integration scheme. The choice of the test function $\psi(\mathbf{x})$ is distinct for different methods. The actual optimum does not change, since the zero-product property holds. The WRM builds the basis for many solving strategies, including FEM.

$$WRF = \int_{\Omega} R(\mathbf{x})\psi(\mathbf{x})W(\mathbf{x})dx \tag{3.4}$$

This integral must be evaluated numerically. There are many different integration schemes available, but typically they are computational expensive. A less extensive approach is to evaluate the integral argument at different "collocation points". This can be seen in equation (3.5). Although it is not an integral per se, it does assign a numerical "score" to the residual.

$$\sum_{k=0}^{N} R(\mathbf{x}_k)\psi(\mathbf{x}_k)W(\mathbf{x}_k) \tag{3.5}$$

To ensure that negative and positive residuals do not cancel each other out, a common choice in heuristic methods from table 5.1 is to choose $\psi(\mathbf{x}_k)$ as the residual itself, effectively squaring it. The resulting "sum of squared residuals" forms the basis for nearly all fitness functions in the current literature, as represented in equation (3.6).

$$\sum_{k=0}^{N} R(\mathbf{x}_k)^2 W(\mathbf{x}_k) \tag{3.6}$$

These methods are often called "spectral methods" (Shen, Tang, and Wang 2011). Their main advantage over finite difference methods is that they take the whole domain into account. The derivative of the function at one point is influenced by the function at every other point in the domain. This global approach can lead to a higher accuracy.

3.2 Fitness Function

As mentioned above, the basis of the fitness function used in Chaquet and Carmona 2019 is the squared weighted residual in equation (3.6). They split the summation over the collocation points into two parts: the points on the boundary (n_B) and the points on the inner domain (n_C). Further, they divide the fitness value by the

number of points used. This fitness function, as seen in equation (2.14), is adopted in this thesis. Because here, systems of differential equations are not considered, the denominator changes to $m = 1$ resulting in the fitness function (3.7) below. The norm of the residual is not necessary for this thesis, since the fitness function does not have to work for system of PDEs.

$$F(u_{apx}(\mathbf{x})) = \frac{\sum_{i=1}^{n_C} \xi(\mathbf{x}_i) \left[\mathbf{L}u_{apx}(\mathbf{x}_i) - f(\mathbf{x}_i)\right]^2 + \phi \sum_{j=1}^{n_B} \left[\mathbf{B}u_{apx}(\mathbf{x}_j) - g(\mathbf{x}_j)\right]^2}{(n_C + n_B)} \tag{3.7}$$

A notable property of the fitness function is that it can not drop below 0. A solution, that satisfies the residual at every n_C and n_B, results in a fitness of 0. This is true for the analytical solution $u_{ext}(\mathbf{x})$. It is also important to notice that aliasing errors (as described in the chapter 4.3.3) can occur with this fitness function.

The weighting function is also split into two parts: ξ for the inner collocation points and ϕ as penalty factor for the boundary points. The weighting function ξ can be adapted by a parameter κ. For a $\kappa > 0$, ξ assigns larger values for collocation points closer to the boundary, effectively shifting the relative importance towards the boundary. These weights can be calculated a priori, so no computational effort is added to the fitness function. Again, the weights and the fitness function are directly extracted from Chaquet and Carmona 2019.

$$\xi(\mathbf{x}_i) = \frac{1 + \kappa \left(1 - \frac{min_{\forall \mathbf{x}_j \in n_B} ||\mathbf{x}_i - \mathbf{x}_j||}{max_{\forall \mathbf{x}_k \in n_C} (min_{\forall \mathbf{x}_j \in n_B} ||\mathbf{x}_k - \mathbf{x}_j||)}\right)}{1 + \kappa} \tag{3.8}$$

3.3 Candidate Representation

As Chaquet and Carmona 2019 suggest, an approximate solution should be represented as a summation of N scaled and shifted radial basis functions ϕ, as stated in equation (3.2). Gauss kernels have frequently been used for the approximation of functions. A solid foundation on the approximation theorem can be seen in Park and Sandberg 1991. RBF are functions that are point symmetric to a centre c and their function value only depends on the radius r.

$$r = ||\mathbf{x} - \mathbf{c}|| \tag{3.9}$$

This thesis mainly works with two different types of RBF. The first one is the classical Gauss RBF, also denoted as GaK. The second one, further called Gauss Sine RBF, or GSK, is more complex. A candidate solution is represented as the parameters that shift and deform these RBF.

3.3.1 Gauss Kernel

In general, a GaK is the classical choice to approximate functions. It was first introduced in Broomhead and Lowe 1988. Equation (3.10) shows the formulation of such a kernel. One kernel has 4 parameters that change its shape and location. ω is a scaling factor for each kernel and γ describes how sharp the e-function is. Depending on the space the solution is defined in, the number of values in the vector $\mathbf{c}$ could change - one for each dimension. However, in this work only $\mathbb{R}^2$ is of interest, thus $\mathbf{c}$ always includes 2 values. In figure 3.1 a single standard GaK is plotted.

$$gak(\mathbf{x}) = \omega e^{-\gamma||\mathbf{x}-\mathbf{c}||^2} \tag{3.10}$$

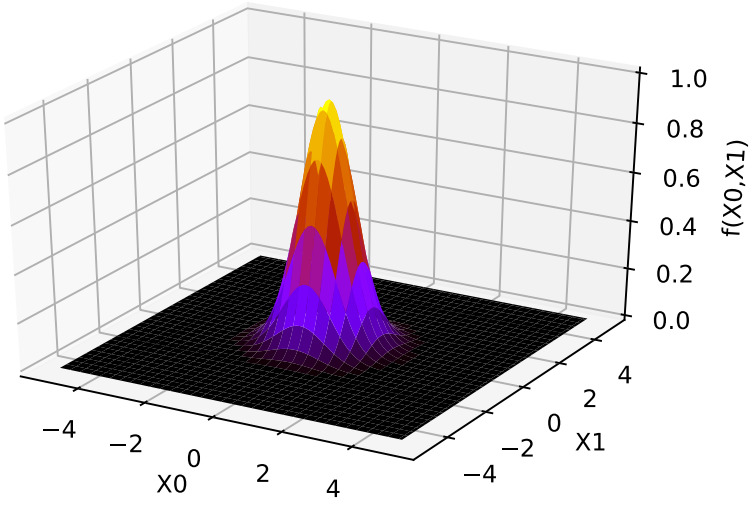

Figure 3.1: 3D plot of a single Gauss kernel with the parameters $\omega = 1$, $\gamma = 1$, $c_0 = 0$ and $c_1 = 0$

An approximate solution to the PDE in question is described as the superposition of N kernels as shown in equation (3.11).

$$u_{apx}(\mathbf{x}) = \sum_{i=0}^{N} \omega_i e^{-\gamma_i r_i^2} \tag{3.11}$$

A solution is encoded as a vector of these $4 \cdot N$ parameters stacked together. This is shown in equation (3.12).

$$\mathbf{p_{apx}} = \Big[\underbrace{\omega_0, \gamma_0, c_{00}, c_{01}}_{\text{kernel 0}}, \cdots \underbrace{\omega_i, \gamma_i, c_{i0}, c_{i1}}_{\text{kernel i}}, \cdots \underbrace{\omega_N, \gamma_N, c_{N0}, c_{N1}}_{\text{kernel N}}\Big]^T \tag{3.12}$$

To evaluate the residual of a PDE, the derivatives must be known. To that extend, the derivative of u_{apx} from equation (3.2) is calculated. The first order derivative with respect to x_0 is seen in equation (3.13). To solve the proposed testbed, also the second order derivatives are needed, as described in equation (3.14). Although the mixed term derivative is not used in this work, for the sake of completeness it is displayed in equation (3.15).

$$\frac{\partial u_{apx}(\mathbf{x})}{\partial x_j} = -2\sum_{i=0}^{N} \omega_i \gamma_i (x_j - c_{ij}) e^{-\gamma_i r_i^2} \tag{3.13}$$

$$\frac{\partial^2 u_{apx}(\mathbf{x})}{\partial x_j^2} = \sum_{i=0}^{N} \omega_i \gamma_i \left[4\gamma_i (x_j - c_{ij})^2 - 2\right] e^{-\gamma_i r_i^2} \tag{3.14}$$

$$\frac{\partial^2 u_{apx}(\mathbf{x})}{\partial x_j x_k} = 4\sum_{i=0}^{N} \omega_i \gamma_i^2 (x_j - c_{ij})(x_k - c_{ik}) e^{-\gamma_i r_i^2} \tag{3.15}$$

3.3.2 Gauss Sine Kernel

Additional to the Gauss kernel, a "Gauss Sine" kernel, further also abbreviated as GSK, is proposed. In essence, this is a multiplication of a GaK with a sine function, as seen in equation (3.16). It can be thought of as a sine function, where its influence declines with the radius r. The plot in figure 3.2 shows how the first half period is much larger than the second half. Both "sub-functions" are centred at the same $\mathbf{c}$. As shown in chapter 10.1, the universal approximation theorem for the GSK holds true. With the sine, two new parameters are introduced: f for the frequency of the sine wave and φ for the phase shift.

$$gsk(\mathbf{x}) = \omega e^{-\gamma ||\mathbf{x}-\mathbf{c}||^2} sin(f||\mathbf{x} - \mathbf{c}||^2 - \varphi) \tag{3.16}$$

It is important to notice that, with the correct parameter choice, both traits - the sine and the e-function - can be retrieved. When $\gamma = 0$ the e-function evaluates to 1 and leaves the sine on its own. By setting $f = 0$ and $\varphi = -\frac{\pi}{2}$, the sine resolves to 1 and the e-function part is obtained. Thus, with this kernel it should be possible to approximate more functions than the GaK.

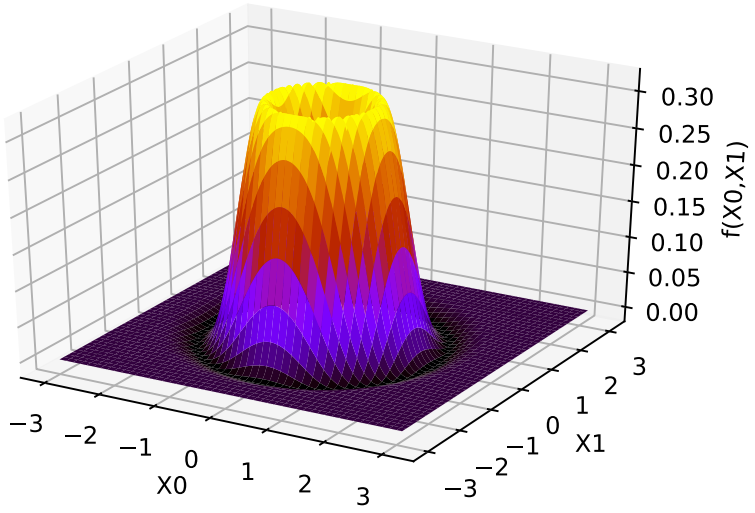

Figure 3.2: 3D plot of a single Gauss Sine kernel with the parameters $\omega = 1$, $\gamma = 1$, $c_0 = 0$, $c_1 = 0$, $f = 1$, $\varphi = 0$

Similar to the Gauss kernel, the approximate solution is described as the superposition of N GSK, as seen in equation (3.17).

$$u_{apx}(\mathbf{x}) = \sum_{i=0}^{N} \omega_i e^{\gamma_i r_i^2} sin(f_i r_i^2 - \varphi_i) \tag{3.17}$$

Equation (3.18) shows the solution representation in stacked vector notation, including the two new parameters f and φ.

$$\mathbf{p_{apx}} = \Big[\underbrace{\omega_0, \gamma_0, c_{00}, c_{01}, f_0, \varphi_0}_{\text{kernel 0}}, \cdots \underbrace{\omega_i, \gamma_i, c_{i0}, c_{i1}, f_i, \varphi_i}_{\text{kernel i}}, \cdots \underbrace{\omega_N, \gamma_N, c_{N0}, c_{N1}, f_N, \varphi_N}_{\text{kernel N}}\Big]^T \tag{3.18}$$

Again, the derivatives of the solution are needed, which are shown in the equations (3.19) through (3.21).

$$\frac{\partial u_{apx}(\mathbf{x})}{\partial x_j} = \sum_{i=0}^{N} 2\omega_i(x_j - c_{ij})e^{-\gamma_i r_i^2}(f_i cos(f_i r_i^2 - \varphi_i) - \gamma_i sin(f_i r_i^2 - \varphi_i)) \tag{3.19}$$

$$\frac{\partial^2 u_{apx}(\mathbf{x})}{\partial x_j^2} = \sum_{i=0}^{N} 2\omega_i e^{-\gamma_i r_i^2}$$
$$[-(2(f_i^2 - \gamma_i^2)(x_j - c_{ij})^2 + \gamma_i)sin(f_i r_i^2 - \varphi_i) - (4f_i\gamma_i(x_j - c_{ij})^2 - f_i)cos(f_i r_i^2 - \varphi_i)] \tag{3.20}$$

$$\frac{\partial^2 u_{apx}(\mathbf{x})}{\partial x_j x_k} = \sum_{i=0}^{N} -4\omega_i(c_{ij} - x_j)(c_{ik} - x_k)e^{-\gamma_i r_i^2}$$
$$\left[(f_i^2 - \gamma_i^2)sin(f_i r_i^2 - \varphi_i) + 2f_i\gamma_i cos(f_i r_i^2 - \varphi_i)\right] \tag{3.21}$$

4 Experimental Design

This chapter gives an overview on how the subsequent experiments are conducted. An integral part of solver comparison is to define a testbed that holds example problems with a known analytical solution. Further, a quality measurement must be defined that compares the numerical to the analytical solution. Since the memory consumption and the solving time is of interest, a robust method to measure these characteristics is needed. The baseline for all experiments is the FEM solver NGSolve (Schöberl, Lackner, and Hochsteger 2020).

4.1 Testbed

The testbed is a collection of multiple two-dimensional scalar PDEs that are analytically solved such that $u_{ext}(\mathbf{x}) : \mathbb{R}^2 \to \mathbb{R}$ is a solution to the underlying PDE. These can be used to demonstrate the correct implementation of a solver. The testbed can also be used to compare the performance of the classical FEM solver (NGSolve) with the Computational Intelligence (CI) solver. The equations and graphs are displayed in the appendix B. The equations used here are a mixture of different testbeds. Specifically, the equations PDE 2 and PDE 3 are picked from the testbed in Chaquet and Carmona 2019. These problems were also used by Tsoulos and Lagaris 2006 and Panagant and Bureerat 2014. Preliminary tests have shown that the equations used in these papers are rather simple to approximate. Thus, more complicate equations are added to test the solvability over a wider variety of functions. The more complex equations are taken from the National Institute of Standards and Technology (NIST) website (Mitchell 2018) that provides benchmarking problems for FEM solvers with adaptive mesh refinement methods. The other equations 0A, 0B and 8 are specially created to show different properties of the solver.

PDE 0A: Gauss Kernel
Equation Reference: (B.1)
Characteristics: sum of 5 GaK, thus can be approximated arbitrarily close; is designed to show convergence towards analytical solution;
Difficulty: not especially difficult;
Boundary: function value of solution;

PDE 0B: Gauss Sine Kernel
Equation Reference: (B.3)
Characteristics: can be approximated arbitrarily close by 3 GSK; 3 kernels are used to keep the minimal necessary dimension of the representation similar to PDE 0A;
Difficulty: the contrast between a dominant wave with a steep gradient in the middle and small waves with little influence on the boundary; simple approximations lay the focus on the middle, while good approximations also match the small waves;
Boundary: function value of solution;

PDE 1: Polynomial 2D
Equation Reference: (B.5)
Characteristics: polynomial of order 20
Difficulty: global structure similar to a GaK; thus, it is simple to approximate;
Boundary: homogeneous boundary condition;
Reference: Mitchell 2018;

PDE 2: Chaquet PDE 1
Equation Reference: (B.7)
Characteristics: compare the performance to other solvers;
Difficulty: rather simple; slight curvature and no steep gradient;
Boundary: function value on boundary;
Reference: Chaquet and Carmona 2019, Chaquet and Carmona 2012, Tsoulos and Lagaris 2006, Sobester, Nair, and Keane 2008, Panagant and Bureerat 2014;

PDE 3: Chaquet PDE 3
Equation Reference: (B.9)
Characteristics: compare the performance to other solvers; polynomial of order 2;
Difficulty: well behaved, no steep gradient;
Boundary: function value on boundary;
Reference: Chaquet and Carmona 2019, Chaquet and Carmona 2012, Tsoulos and Lagaris 2006, Panagant and Bureerat 2014;

PDE 4: Sine Bump 2D
Equation Reference: (B.11)
Characteristics: this PDE is used in both, the work of Chaquet and Carmona 2019 and Mitchell 2018 with slightly different boundary condition; preliminary tests have shown that the Chaquet and Carmona 2019 PDE is easier to solve, thus this formulation is disregarded;
Difficulty: sharp boundary condition on the corners of Ω;
Boundary: homogeneous boundary condition;
Reference: Mitchell 2018;

PDE 5: Arctan Circular Wave Front
Equation Reference: (B.13)
Characteristics: quarter section of slightly shifted arctan;
Difficulty: transition from the flat plateaus to the steep gradient of the circular wave front; preliminary tests have shown that this problem is especially hard;
Boundary: function value on boundary;
Reference: Mitchell 2018;

PDE 6: Peak 2D
Equation Reference: (B.15)
Characteristics: solution is a single but sharp Gaussian "peak" at $(0.5, 0.5)$;
Difficulty: large negative exponent in e-function results in a steep gradient and small region of interest;
Boundary: function value on boundary;
Reference: Mitchell 2018;

PDE 7: Boundary Line Singularity
Equation Reference: (B.17)
Characteristics: the solution to this problem is a root function that is only defined on $x \in \mathbb{R}^+$;
Difficulty: line singularity on boundary with increasing gradient;
Boundary: function value with singularity on boundary $x_0 = 0$;
Reference: Mitchell 2018;

PDE 8: Interior Point Singularity
Equation Reference: (B.19)
Characteristics: root function; a singularity within the domain;
Difficulty: not defined at $(0.5, 0.5)$ which results in numerical inaccuracies;
Boundary: function value on boundary;

PDE 9: Arctan Wave Front Homogeneous Boundary Conditions 2D
Equation Reference: (B.21)
Characteristics: arctan oscillation diagonal to the domain;
Difficulty: steep gradient on the transition between wave peak and trough; sharp corners on the boundary;
Boundary: homogeneous boundary condition;
Reference: Mitchell 2018;

4.2 Software Architecture

To simplify the preparation, execution and evaluation of the experiments, a comprehensive software architecture is defined. The UML class diagram can be seen in the appendix C. The limited class diagram, without any methods and attributes is shown in the figure 4.1 below. The architecture is organised in four main segments.

Optimisation Algorithm
The `IOptAlgoBase` interface must be implemented by every `OptAlgo` class to ensure the compatibility with `CiPdeBase` class of the testbed. A nice side-effect is that it reduces the number of user-defined parameters. An optimisation algorithm of this class must only take an initial guess (e.g. the starting population) as well as two stopping criteria: the maximum number of function evaluation or a minimum error to reach. Also a fitness function (i.e. the function to be optimised) must be provided. Four lists of the same length are returned: the optimum-guess, the function value, the crossover probability and the scale factor per each generation. The actual implementation of the algorithm is not predefined.

Kernels
As described in chapter 3.3, a candidate solution is defined as a sum of RBF. In order to test different candidate representations, different classes must be implemented. Again, to ensure compatibility with the `CiPdeBase` class, all representations must implement the `IKernelBase` interface. This assures that all classes have a method that can calculate the solution as well as the first and the second order derivatives. Here, only two kernels are implemented. A typical Gauss kernel as described in chapter 3.3.1 and a so called Gauss Sine kernel shown in chapter 3.3.2.

Testbed
The testbed holds the 11 differential equations used in all experiments. The testbed is abstracted in such a way that an experiment is as simple as creating an PDE object and calling its solve method. All testbed classes must implement the `ITestbenchBase` interface. This ensures the minimal functionality of every subsequent class. Currently two classes implement this interface, the `FemPdeBase` and the `CiPdeBase`. These are the base classes that provide the specific attributes and methods needed for the FEM solver and the CI solver. The actual PDE problems are implemented in the classes `FemPdeN` or `CiPdeN` which inherit from the `FemPdeBase` and the `CiPdeBase`, respectively. The number N in their name is representative for all different testbench problems and every PDE has its own class. Since all PDE classes have the same methods/attributes and only differ in their implementation and name, they do not have to be displayed separately. Therefore, they are symbolised together by a "stacked notation" used in the class diagram. Some methods in these

classes must be overridden and adapted to the current PDE problem, which is indicated by the $\wedge$ character.

Post Processing
Although the post processing block is not actually a class, it is still represented in this diagram. This module provides functions that take `FemPdeN` or `CiPdeN` objects and perform actions with them. The methods are used in the experiments chapters to interpret the results. A detailed description of the implementation is given in the appendix D.

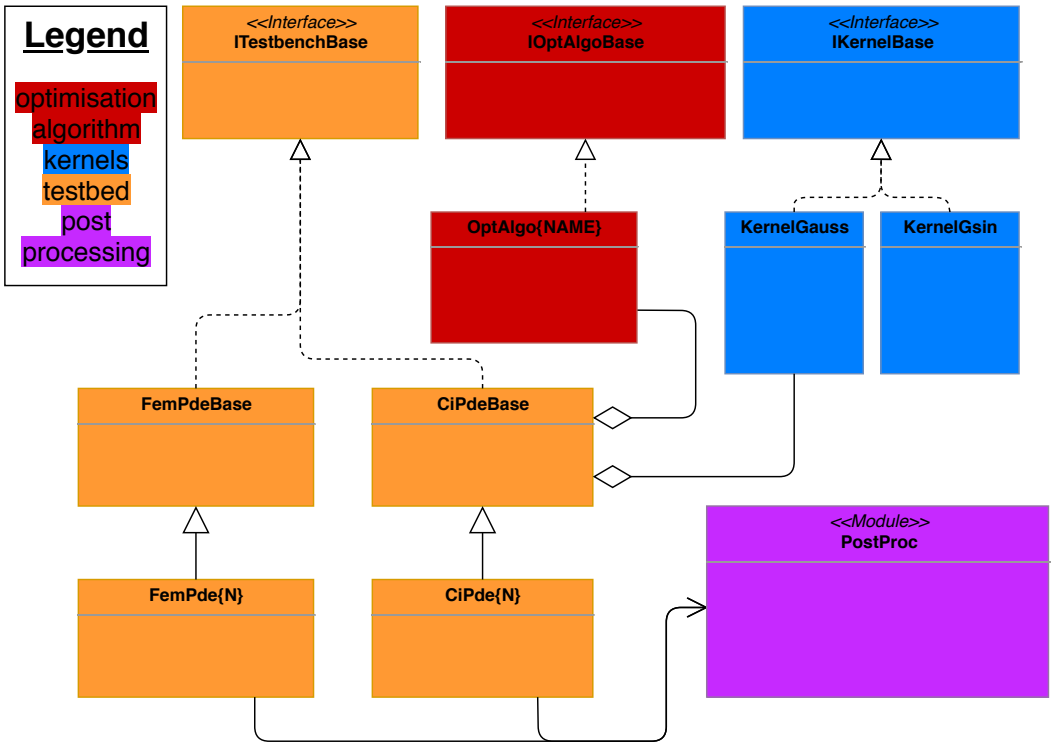

Figure 4.1: This reduced UML class diagram gives an overview of the testbed design and its interfaces and classes.

4.3 Performance Metric

In order to scientifically compare the results produced by the different solvers, some metrics are necessary. Three important solver-properties are measured: the execution time, the memory usage and the quality of the numerical solution. The following chapters describe the measurement process in greater detail.

4.3.1 Solving Time

The solving time is measured within the `solve()` method of either class. The time module of the T. P. S. Library 2020 is used to interact with the system clock. The resolution, that the time module can access, depends on the system it is running on. Specifically, on the machine used in all further experiments, `time.time()` returns a 24 byte float that represents the time passed since 1st of January 1970. Usually, consecutive calls of this function return increasing values - changing the system time could interfere with the correctness of this value.

As the execution time of a program depends on many other factors, such as the current system load, the CPU temperature and the process scheduler, it is necessary to view it as a random variable. Thus, multiple replications have to be done before trying to interpret the results. To make for a fair comparison, the same machine with a similar work-load must be used. The replications are not done within the `solve()` function and must be applied during the experiment. To reduce the random effects and prevent possible outlier, the Python garbage collector is switched off during the time measurement. For a step-by-step description, the pseudocode is shown in the appendix E.

4.3.2 Memory Usage

Similar to the solving time measurement, the memory usage is determined within the `solve()` method. The *psutil* module (Rodola 2020) provides the functionality to read the amount of memory attached to a process at a given time. The function call `process.memory_info()` returns an object with multiple attributes about the current state of the process. Of special interest is the Virtual Memory Size (VMS) field. This includes the Resident Set Size (RSS), the memory that is currently held within the main memory, and the memory that is currently swapped out to the hard drive.

Without assuming anything about the inner workings of the process, the memory usage is also a random variable. Thus, similar to the time measurement, replications have to be performed. The same pseudocode as for the time measurement (appendix E) also applies here. To remove outliers, it is helpful to create and solve one testbed object before recording the experiment. This sets up the necessary references to libraries and modules. Thus they are not mingled into the actual experiments. This should be done for both, the FEM and the CI solver.

4.3.3 Quality Measurement

Although the fitness function is the criterion that is optimised, it is not applicable as an objective quality measure. As Chaquet and Carmona 2019 describe, it depends on multiple factors:

- user-defined parameters ξ and ϕ
- the formulation of the PDE
- number of collocation points used
- number of kernels used

Thus, Chaquet and Carmona 2019 define a new quality measurement based on the Root-Mean-Square Error (RMSE) over the collocation points as seen in equation (4.1).

$$RMSE^2 = \frac{\sum_{i=1,\mathbf{x}_i \in C}^{n_C} ||u(\mathbf{x}_i) - u_{ext}(\mathbf{x}_i)||^2 + \sum_{j=1,\mathbf{x}_j \in B}^{n_B} ||u(\mathbf{x}_j) - u_{ext}(\mathbf{x}_j)||^2}{(n_C + n_B)} \tag{4.1}$$

This quality criterion has three inherent issues. At first, it firmly depends on the number of collocation points used. In an algorithm that uses self-adaptive collocation points, where the distribution of the points depends on random variables, subsequent measures of similar solutions could result in different quality values. Especially in solutions with high condition numbers, the RMSE measurement would be rendered useless since a small deviation of the point results in a large difference of the function value.

Further with the RMSE, the quality is only measured on the collocation points and not in between. However, a good solution fits not only these discrete points, but the whole domain. This is called an aliasing error. An approximation can fit the points, without correctly representing the space between them. This is shown in the following figure 4.2.

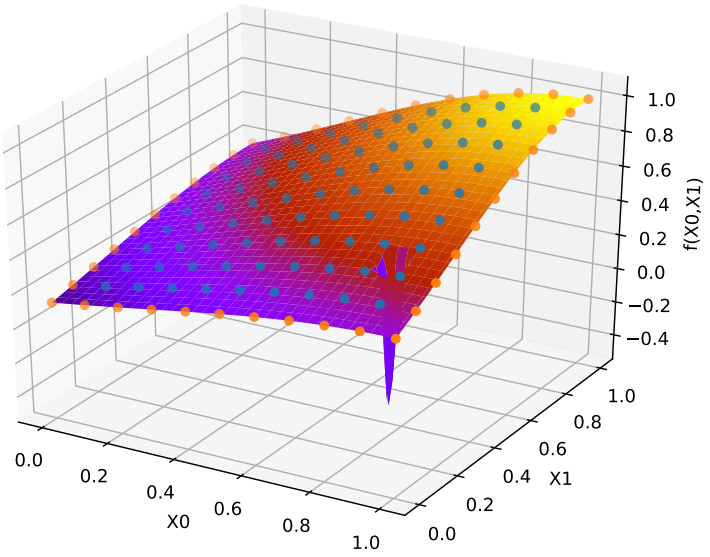

Figure 4.2: Aliasing Error: sharp inaccuracies in between collocation points

Finally, the FEM method doesn't use collocation points, so this quality measurement could not be calculated. A good quality measurement tool only uses the numerical and analytical solution, independently of the solving method.

This leads to the quality measurement formulation used in this thesis: the L2 norm defined for functions as denoted in equation (4.2). This actually measures the distance between the analytical solution and the numerical approximation.

$$||u_{ext} - u_{apx}|| = \sqrt{\int_{\Omega} (u_{ext}(\mathbf{x}) - u_{apx}(\mathbf{x}))^2 dx} \tag{4.2}$$

Although this integral is numerically evaluated, the discretisation is much finer than the resolution of the collocation points used in the fitness function - thus also taking the areas between these points into account.

4.4 Baseline: NGSolve

As mentioned above, the NGSolve framework (Schöberl, Lackner, and Hochsteger 2020) is used as the baseline for all experiments. NGSolve is a state of the art FEM solver that is in part developed and maintained by numerous well-known institutes such as the Vienna University of Technology, the University of Göttingen and the Portland State University. This chapter describes the

results obtained by running NGSolve on the testbed. The metrics from chapter 4.3 are applied.

4.4.1 Setup

At first the PDEs must be transformed into their corresponding weak form. As all testbed problems are Poisson equations and only differ in their algebraic sign and inhomogeneous part, the weak form is similar for all problems. Referring to equation (2.3), the terms $\vec{b} = 0$ and $c = 0$, thus these parts vanish. The matrix A is either $\left[\begin{smallmatrix} 1 & 0 \\ 0 & 1 \end{smallmatrix}\right]$ or with a negative sign $\left[\begin{smallmatrix} -1 & 0 \\ 0 & -1 \end{smallmatrix}\right]$ as only the non-mixed second order derivatives occur in the equations. This results in the weak form as presented in equation (4.3), where f is the inhomogeneous part of the PDE.

$$\int_{\Omega} \nabla u^T \nabla v dV = \int_{\Omega} f v dV \tag{4.3}$$

To enhance the performance of NGSolve, static condensation is turned on. Further, a multigrid preconditioner is used. All problems are approximated by second order polynomials. The automatic mesh refinement is performed until a maximum of $5 \cdot 10^4$ DOF is reached. To properly interpret the results, 20 replications for each problem are performed. This is only needed for time and memory usage, the solution itself is not a random variable. To further reduce memory usage, the GUI of NGSolve is switched off.

4.4.2 Result

With the parameters described above, the following results are produced. The solving time as well as the memory usage are displayed in the boxplots 4.3 and 4.4, respectively. These datasets provide a reference point for the performance of the CI solver. In general, the solving time ranges from 2.5 to 5.0 seconds at about 50 to 80 Mbyte of memory. Only problem 3 stands out as a notable exception. To keep the diagram within a readable scale, this PDE is omitted and plotted in a separate figure.

Table 4.1 presents the achieved distances between the exact and the approximated solutions. On PDE 3 the best numerical quality is achieved.

The problem PDE 7 only needs around 2.5 seconds to be solved. A reason could be that the solution only depends on one variable and the derivative with respect to y evaluate to zero $\frac{\partial u}{\partial y} = 0$ and thus vanishes. This does not effect the memory usage, since all $5 \cdot 10^4$ DOF must be created to terminate.

Problem PDE	L2 Norm
0A	$2.967 \cdot 10^{-5}$
0B	$1.071 \cdot 10^{-5}$
1	$8.004 \cdot 10^{-7}$
2	$3.501 \cdot 10^{-8}$
3	$1.680 \cdot 10^{-9}$
4	$4.764 \cdot 10^{-7}$
5	$6.057 \cdot 10^{-6}$
6	$1.908 \cdot 10^{-7}$
7	$5.203 \cdot 10^{-5}$
8	$3.237 \cdot 10^{-7}$
9	$2.366 \cdot 10^{-7}$

Table 4.1: These are the results obtained by the FEM solver in terms of distance to the analytical solution. The solver achieves the smallest deviation in PDE 3.

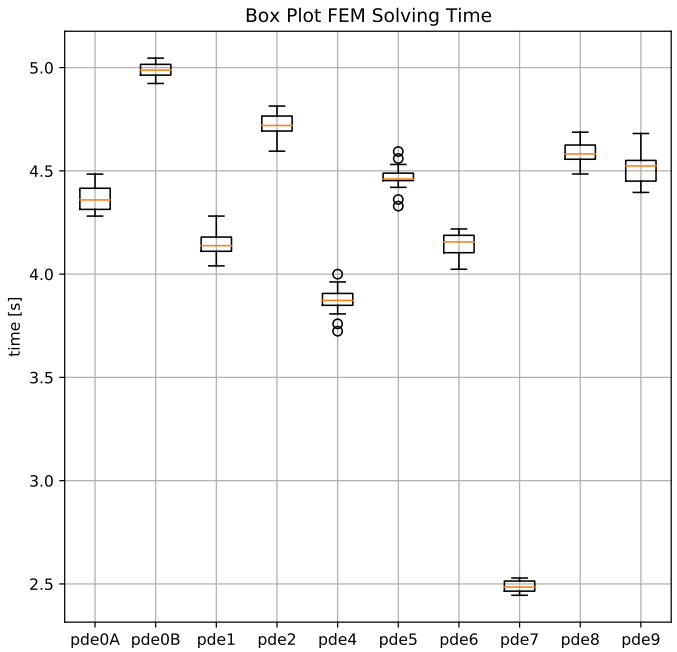

Figure 4.3: Boxplot: time (in seconds) needed to solve the testbed PDE (without PDE3)

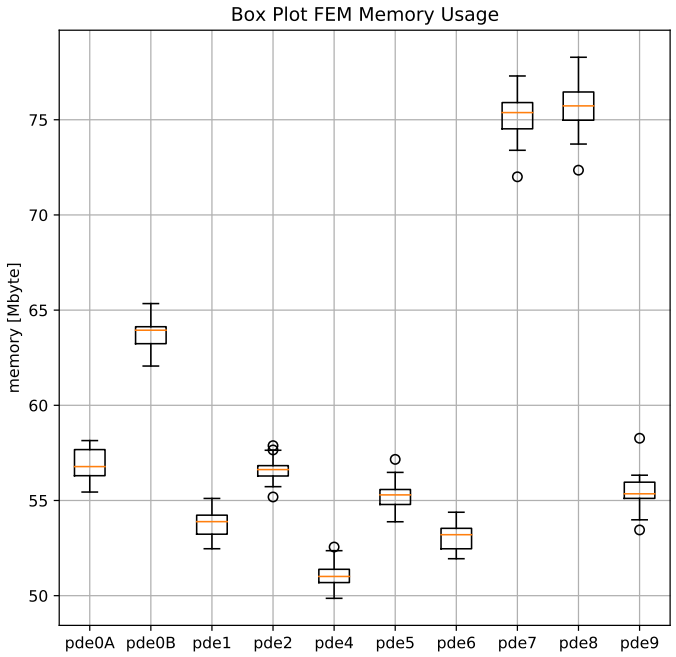

Figure 4.4: Boxplot: memory (in Mbyte) needed to solve the testbed PDE (without PDE3)

The following figures 4.6a and 4.6b show the boxplot of the time and memory consumption for the testbed PDE 3 with $5 \cdot 10^4$ DOF. Compared to the other equations, this problem takes longer to solve while also needing more memory: somewhere around 65.2 seconds at about 130 Mbyte. One possible explanation for that is the fundamental structure of the PDE. As described in equation (B.10), the exact solution to this problem is a polynomial of second order. This can be approximated perfectly by the FEM solver, since it also uses second order polynomials as basis functions. The mesh-refinement step takes more iterations to produce the $5 \cdot 10^4$ DOF as compared to the other testbed problems. In fact, since the numerical errors per finite element accumulate, more DOF should result in a larger approximation error. Figure 4.5 shows the performance metrics at different DOF budgets. The plot supports this hypothesis that less DOF take less time and memory to solve the PDE and still end up with a better quality.

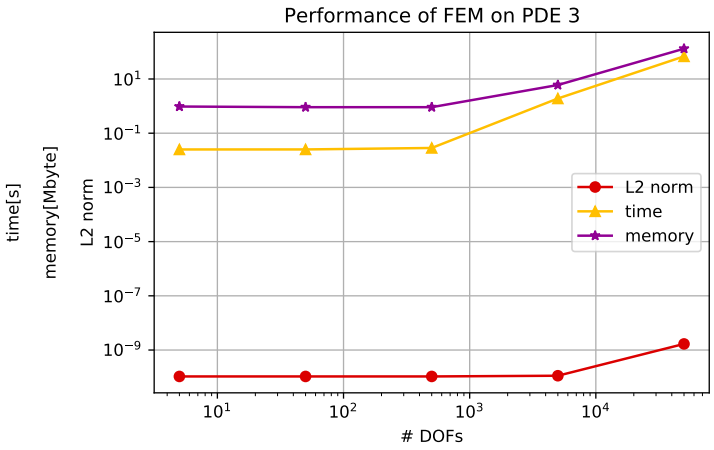

Figure 4.5: PDE 3 performance metrics at different DOF budgets.

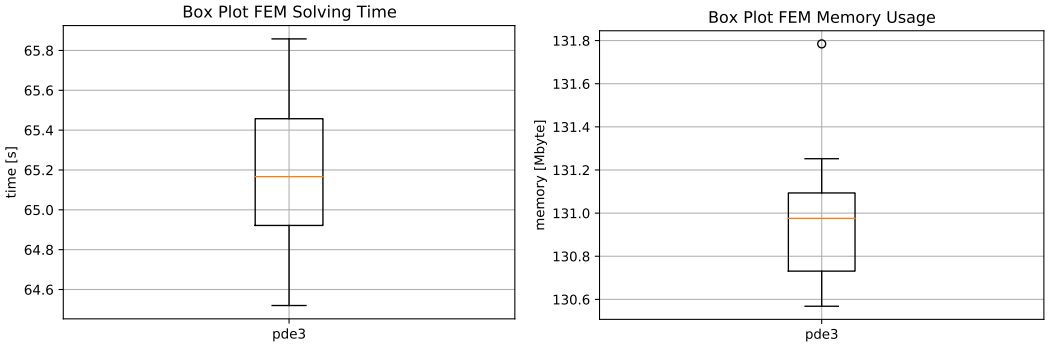

(a) Boxplot: time to solve testbed PDE3 at $5 \cdot 10^4$ DOF.

(b) Boxplot: memory to solve testbed PDE3 at $5 \cdot 10^4$ DOF.

Figure 4.6: Comparison of time and memory effort on PDE 3 at $5 \cdot 10^4$ DOF.

4.5 Default CI Parameter

Typically, the performance of heuristic optimisation algorithms can be adjusted to specific testbed problems by tuning its parameters. For all further experiments the JADE algorithm, as described with pseudocode A.1, is used. Similarly, the reported CI solver has many parameters that could be adapted. However, adjusting every parameter in order to find the best combination is not an option, since that would take an extensive amount of computation time. Some parameters that might not have a great effect on the performance can be predefined. These values are determined by preliminary tests. If not stated

otherwise, the following parameters from table 4.2 are used in the subsequent experiments.

Parameter	JADE	CMA-ES (Chaquet and Carmona 2019)
φ	100	300
κ	1	3
population size	$2 \cdot dim$	$\frac{3}{2}(4 + \lfloor 3 \cdot ln(dim) \rfloor)$
min error	0	-
p	0.3	-
c	0.5	-
replication	20	50
nb nc	40 81 121 = 11x11	100 equally spaced points over the domain
initialisation	$\vec{u_{apx}} \in \mathcal{N}(0,1)$	$\omega_i \in \mathcal{U}[-0.01, 0.01]$ $\gamma_i \in \mathcal{U}(0,1]$ $c_{ik} \in \mathcal{U}[2\Omega]$

Table 4.2: These predefined parameters are used for the following numerical experiments.

The parameters φ and κ are used in the fitness function (equation (3.7)) for changing the relative importance of the boundary and the interior. Chaquet and Carmona 2019 take similar values. However, preliminary tests have shown, that the current values perform slightly better on the present testbed. Figure 4.7 shows the values of ξ and φ. It further describes how the weighting factor emphasises the areas closer to the boundary.

The population size used by Chaquet and Carmona 2019 is based on the original formulation of the CMA-ES. However, they observed a better convergence when scaling the recommended population size by three. Typically, DE uses larger population sizes. Mallipeddi and Suganthan 2008 describe an empirical study on choosing this parameter. They discuss the trade-off between premature convergence and computational effort. The results suggest that population sizes of $2 \cdot dim$ are more likely to stagnate, but also converge faster. Since time is a critical resource for the CI-solver, this population size is chosen.

The termination condition for DE is either a maximum number of function evaluation, or a minimal function value to reach. Since the fitness function (equation (3.7)) has its optimum at 0, this value is used as the termination condition. A helpful side-effect is that it ensures the same amount of function

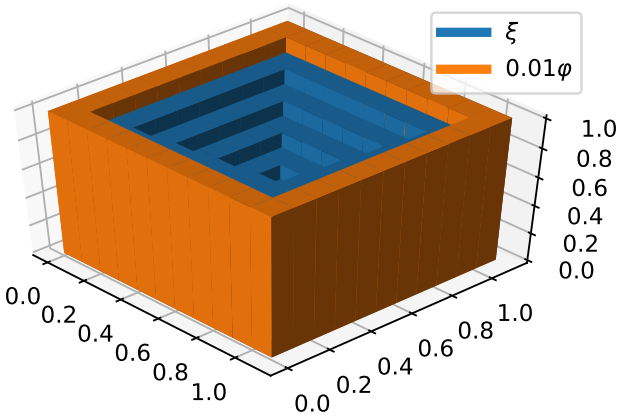

Figure 4.7: Weighting factor φ and ξ on every collocation point

evaluation in every run, without early termination. This prevents outliers in the time and memory measurement.

The parameters p and c are specific to JADE (algorithm A.1). The mutation operator `mutationCurrentToPBest1` uses p to select the best individuals and c weights the parameter adaption mechanism. For all experiments these values are set at $p = 0.3$ and $c = 0.5$.

To account for the statistical influence, every setup is reevaluated by 20 replications where each replication starts with independent initial guesses.

The FEM solver terminates after it surpasses $5 \cdot 10^4$ DOF. The whole number of collocation points $(n_B + n_C)$ is the equivalent for the CI solver. Typically, fewer collocation points are used, since the evaluation time of the fitness function scales poorly with more points. Chaquet and Carmona 2019 use 100 equally spaced collocation points over the domain to solve the PDE. Here, 121 points are created, as seen in figure 4.8.

The initialisation is done by a standard normal distribution. This means that every value in the $\mathbf{p_{apx}}$ vector is drawn from a normal distribution. On the contrary, Chaquet and Carmona 2019 initialise the values specifically tailored to each parameter of the kernel. This process assumes a priori information about the solution. In the typical application, this knowledge is not available and thus it should not be used.

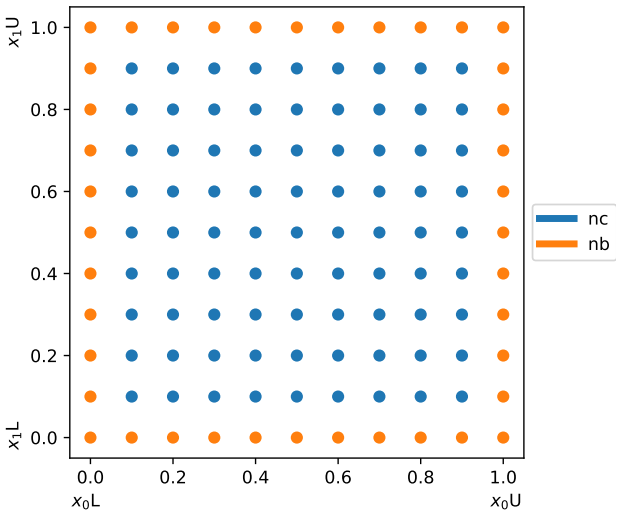

Figure 4.8: Collocation points used in the testbed. For the PDEs 0A and 0B with the larger domain, the lower limits x_0L and x_1L are replaced with -2 and the upper limits x_0U and x_1U are replaced with 2. The points are still equally spaced.

4.6 Hardware Infrastructure

To increase the experimental throughput, two machines are used: a personal computer (machine 1) and a server in the cloud (machine 2). It is important that any time or memory usage comparisons must be performed between experiments on the same machine. In the experiments chapter it is separately denoted which comparisons are allowed. The following table 4.3 shows the properties of both machines. It is important to note that these information are only a reference point. This is probably not enough to actually recreate the exact time or memory data presented in this work.

Property	Machine 1	Machine 2
Operating System	Windows 10 Home 1909 18363.900	CentOS Linux release 7.3.1611
Python	Anaconda version 2019.03	Anaconda version 2020.02
Processor	Intel Core i7-4790K CPU @ 4.00GHz	Intel Xeon CPU E5-2630 v3 @ 2.40GHz
Cores	4 Cores + 4 logical	32 Cores

Table 4.3: Comparison of the machines used for the experiments.

Due to the Python incompatibilities, NGSolve can only be installed on machine 1. Thus, any time or memory usage comparisons between the CI solver and the FEM solver must be conducted on machine 1.

5 Experiment 0: Serial Memetic JADE

This chapter describes the results obtained by the most basic adaption of JADE for solving PDEs. The algorithm used here builds on the concepts described in Chaquet and Carmona 2019. Aside from substituting some parameters, the only main difference is the usage of JADE instead of a CMA-ES.

5.1 Hypotheses

A memetic algorithm was first mentioned by Moscato 2000. In essence, it is a hybridisation of a population-based evolutionary algorithm and a deterministic direct or local search. The pseudocode 5.1 below shows the implementation of such a memetic JADE. At first, JADE performs the global search and places its population around the optimum. Then the Downhill Simplex (DS) exploits this area. The budget of #FE is split into two parts: JADE takes nearly all #FE and leaves $2 \cdot dim$ #FE for the DS. The SciPy implementation of the DS is used (SciPy 2020a).

Algorithm 5.1: Pseudocode of memetic JADE

```
1 Function memeticJADE(X, funct, minErr, maxFE):
2     dim, popsize ← size(X)
3     p ← 0.3
4     c ← 0.5
5     pop, FE, F, CR ← JADE(X, p, c, funct, minErr, maxFE − 2dim )
6     bestIndex = argmin(FE)
7     bestSol = pop[bestIndex]
8     pop, FE = downhill simplex(funct, bestSol, minErr, 2dim)
9     return pop, FE, F, CR
```

This experiment provides a first insight into the performance of the proposed algorithm. It tries to answer the question if JADE is a suitable surrogate algorithm for a CMA-ES. Further, the memory usage and solving time is compared to the FEM results obtained in chapter 4.4.

5.2 Experiment Setup

The standard parameters from table 4.2 are taken. The memetic JADE is limited to either 10^4 #FE or 10^6 #FE. The experiment is done on two different machines. The first try with 10^4 #FE is run on the same machine ($\rightarrow$ machine 1) as the FEM experiment. This allows a fair memory and solving time comparison. This comparison can not be performed with the data obtained by using 10^6 #FE ($\rightarrow$ machine 2). Further, 5 GaK are used which results in a dimension of 20 parameters. Thus, the population consists of 40 individuals.

To validate the results, a statistical significance test is performed. The test function is based on the Wilcoxon test. The Wilcoxon test checks for significance at $\alpha = 0.05$. To decide if the results are better or worse, the mean and the median are compared. If both are smaller, the results are better. Contrary, if both are larger, the results are worse. If only one of the values is smaller, the results are undecided. The implementation is further explained in appendix D.

5.3 Results

Table 5.1 compares the obtained results with results from previous research papers. Therefore, the common testbed functions PDE 2 and PDE 3 are used. It is important to notice that the parameters used to obtain the results might not coincide. Tsoulos and Lagaris 2006 also use these two PDEs, but their paper did not provide any usable error metric.

Paper	Parameter	RMSE PDE 2	RMSE PDE 3
Chaquet and Carmona 2019	4 kernel max #FE=10^6 50 replications	$(1.75 \pm 1.14)10^{-4}$	$(1.09 \pm 0.846)10^{-5}$
Chaquet and Carmona 2012	10 harmonics max #FE = $G \cdot \lambda = 1.2 \cdot 10^6$ 10 replications	$(6.37 \pm 0.733)10^{-3}$	$(5.90 \pm 0.799)10^{-3}$
Sobester, Nair, and Keane 2008	50 max tree length 12 generations 20 replications	$(6.9 \pm 8.3)10^{-4}$	N/A
Panagant and Bureerat 2014	unknowns: N/A #FE=$5 \cdot 10^5$ replications: N/A	7.25610^{-4}	9.48910^{-6}
serial memetic JADE	5 kernel max #FE = 10^6 20 replications	$(2.9798 \pm 1.5541)10^{-2}$	$(3.8225 \pm 1.9438)10^{-2}$

Table 5.1: This table compares the results obtained with the serial memetic JADE to the numerical results obtained by similar work in literature. The same metric must be used, thus the RMSE as defined in equation (4.1) is calculated.

The following table 5.2 lists the smallest L2 norm reached after 10^4 #FE and 10^6 #FE, respectively. A standard Wilcoxon test, as described in the appendix D, is performed. Remarkable is that the results on PDE 5 get significantly worse when more #FE are used.

#FE	10^4		10^6		
stat	mean	median	mean	median	Wilcoxon Test
PDE 0A	1.9415 ± 0.3321	1.8844	0.6596 ± 0.5510	0.9285	sig. better
PDE 0B	0.7137 ± 0.1979	0.6354	0.2027 ± 0.1302	0.1516	sig. better
PDE 1	0.1874 ± 0.0408	0.1938	0.0149 ± 0.0049	0.0151	sig. better
PDE 2	0.0890 ± 0.0334	0.0760	0.0257 ± 0.0140	0.0224	sig. better
PDE 3	0.2409 ± 0.1051	0.2309	0.0328 ± 0.0169	0.0285	sig. better
PDE 4	0.1102 ± 0.0367	0.0985	0.0378 ± 0.0083	0.0352	sig. better
PDE 5	0.6645 ± 0.1930	0.6263	1.1968 ± 0.0286	1.2056	sig. worse
PDE 6	1.9660 ± 1.3845	1.6540	0.4135 ± 1.2133	0.0018	sig. better
PDE 7	0.0457 ± 0.0137	0.0452	0.0221 ± 0.0019	0.0223	sig. better
PDE 8	0.2186 ± 0.0045	0.2191	0.2170 ± 0.0019	0.2175	unsig. better
PDE 9	0.0525 ± 0.0147	0.0516	0.0451 ± 0.0119	0.0459	unsig. better

Table 5.2: L2 norm reached with serial JADE at 10^4 #FE and 10^6 #FE

The following two images 5.1 and 5.2 show the time and memory usage for solving the testbed with 10^4 #FE in relation to the FEM solver. The images highlight the varying complexity of the testbed-PDEs and their corresponding fitness function. Although these results are not obtained for 10^6 #FE, they provide insight on how the solver scales with more #FE.

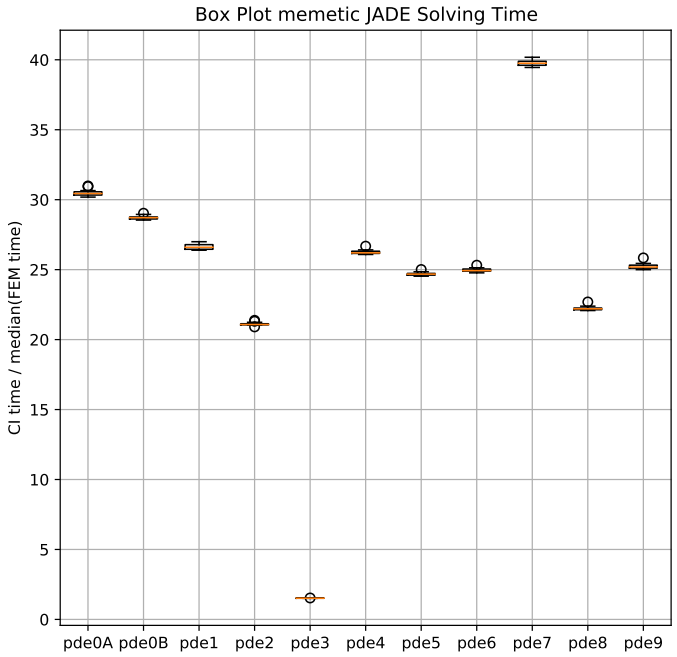

Figure 5.1: Relative solving time results of memetic JADE after 10^4 #FE.

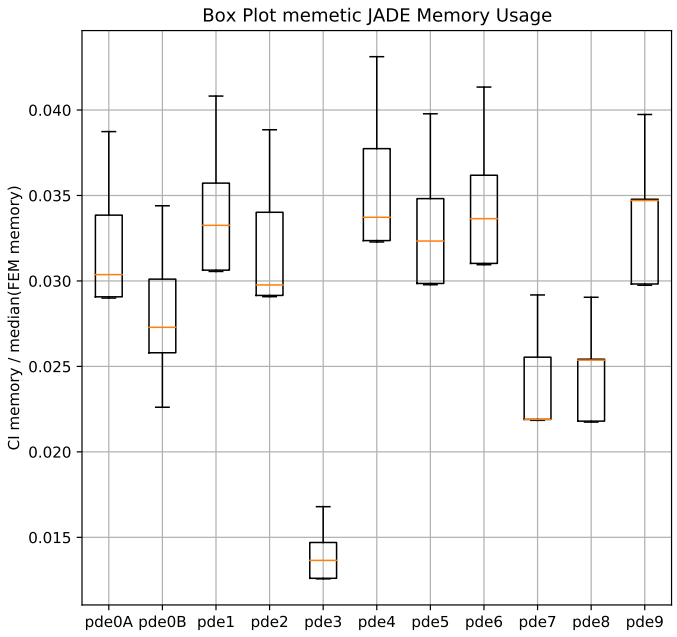

Figure 5.2: Relative memory usage results of memetic JADE after 10^4 #FE.

5.4 Discussion

The results presented in chapter 5.3 above are discussed on the following pages. A comparison to the current literature is drawn. The solving time and memory consumption in relation to the FEM solver NGSolve is examined. Especially interesting are the results obtained on PDE 0A and PDE 5.

5.4.1 Comparison to Literature

The RMSE reached on the PDE 2 and 3, are clearly not as good as the results obtained in previous papers, especially the results presented in Chaquet and Carmona 2019. There might be a few reasons for that:

- As stated in the previous table 4.2, the penalty and weighting factor on the collocation points are different. These settings have been chosen on the basis of preliminary experiments, but there is no guarantee that the choice of these parameters is optimal. Setting these values is not a trivial task and must be tailored to the optimisation algorithm and the differential equation.
- Since PDE 0A is defined as a combination of 5 GaK, at least that many kernels must be provided to the solver. This setup results in a greater search dimension, as compared in table 5.1. In general, more kernels result in a better solution, which is confirmed by experiments in Chaquet and Carmona 2019 and in chapter 7.4.4. To reduce the computational effort per generation, and thus allow JADE to adapt the internal parameters for a longer period, the population size is set to $2 \cdot dim$. According to Mallipeddi and Suganthan 2008, the population size should not be lower than that. Again, choosing these parameters is not necessarily simple. The combination of larger problem dimension and smaller population size could influence the convergence to the worse.
- Compared to Chaquet and Carmona 2019, the #FE-budget for the local DS search is smaller. Thus, the algorithm puts more emphasis on the exploration. However, due to the internal parameter-adaption JADE can perform both - exploration and exploitation. Preliminary experiments have shown that the direct search converges fast with very little progress after more than 100 #FE.
- JADE might simply be not as well suited for the problem as e.g. a CMA-ES.

5.4.2 Solving Time/Memory Usage

The results from table 5.2 show that the CI solver can not nearly compete with the results obtained by the FEM solver from table 4.1. However, more interesting is the comparison of time and memory usage. In the current implementation, the population and the corresponding function values as well as the F and the CR history

are recorded at every generation. Therefore, the memory usage scales linearly with the number of function evaluations used. This information is not necessary for the actual algorithm, but helpful for evaluating the results. In later implementations, this could be disregarded in order to even further reduce the memory consumption. Depending on the testbed PDE, only 1.5 to 4.0 percent of the memory used by the FEM solver is needed. The CI solver uses less memory on all problems (figure 5.2).

The CI solver takes between 3 and 40 times as long as the FEM solver (figure 5.1) to perform 10^4 #FE. Since the solving time scales linearly, 10^6 #FE take about 10 times longer. An interesting observation is the distribution of the solving time within the testbed. The more operations a fitness function needs, the more expensive is one function evaluation and thus the longer is its solving time. However, this does not necessarily correspond with the quality of the solutions. For example, PDE 0B requires the longest absolute evaluation time ($29 \cdot 5$ s ≈ 145 s), compared to the other PDEs, it reaches a "fairly" good quality.

5.4.3 PDE 0A

The purpose of this PDE is to show that the solver would converge globally towards the analytical solution, if it can be represented by a finite number of kernels. However, his can not be confirmed with the current implementation. While more function evaluations do tend to generate better results (as confirmed by the Wilcoxon test in table 5.2), it is common for the CI solver to result in different functions. A typical phenomenon is that the obtained approximation has some of its Gauss "bumps" outside of the domain Ω. The comparison of two solutions with 10^4 #FE and 10^6 #FE in figure 5.3 shows this behaviour. Since the results improve from 10^4 to 10^6, it is possible that the results from 10^6 #FE can be refined with an even larger #FE budget. However, this is not tested due to the already extensive computational effort.

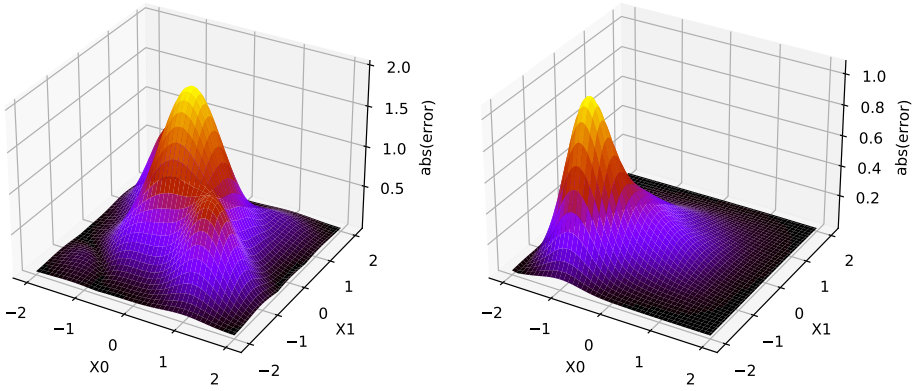

(a) PDE 0A error; 10^4 #FE:
L2 norm: 2.5075
FE value: 4.4129
RMSE: 0.5699

(b) PDE 0A error; 10^6 #FE:
L2 norm: 0.9281
FE value: 1.3762
RMSE: 0.2111

Figure 5.3: Comparison of two typical PDE 0A solutions.

5.4.4 PDE 5

A fascinating property of PDE 5 is observed: more function evaluations (from 10^4 to 10^6) result in a significantly worse solution quality. This is confirmed by a Wilcoxon test, as seen in table 5.2. This property can even be concluded from a visual perspective. A comparison between the best solution after 10^4 #FE and the best solution after 10^6 #FE is shown in figure 5.4. The solution after 10^4 #FE describes the global structure more accurately. It seems that the correct description of the boundary points gets lost with more #FE.

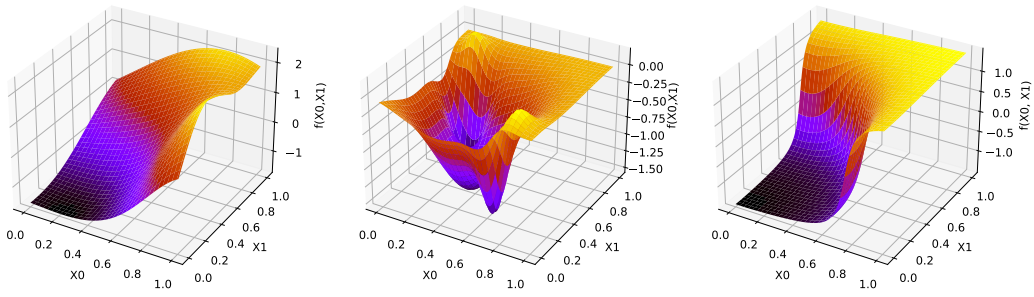

(a) best solution 10^4 #FE
L2 norm: 0.4283
FE value: 2980.96

(b) best solution 10^6 #FE
L2 norm: 1.1095
FE value: 1007.44

(c) analytical solution
to testbed
PDE 5.

Figure 5.4: Comparison of best solution after 10^4 and 10^6 #FE.

The distributions of the achieved fitness value after 10^4 and 10^6 #FE is shown in figure 5.5a. They are clearly separated with distinct mean and median. As expected, both the mean and the median after 10^6 #FE are significantly smaller than these values after 10^4 #FE. The corresponding L2 norm distributions are plotted in figure 5.5b. As described by the Wilcoxon test, the results are inverted. The mean and the median of the L2 norm after 10^4 #FE are smaller than the ones after 10^6 #FE.

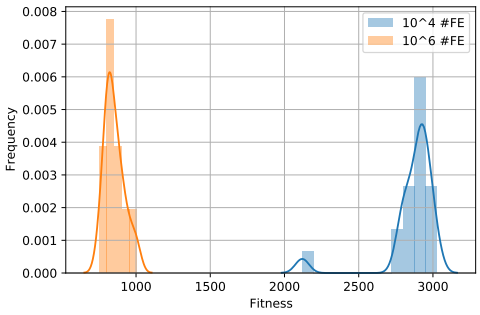

(a) Histogram of the fitness value reached on PDE 5.

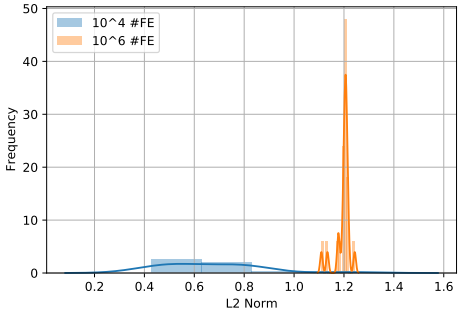

(b) Histogram of the L2 norm reached on PDE 5.

Figure 5.5: Histograms of the fitness and the L2 norm reached with 10^4 #FE and 10^6 #FE on PDE 5.

This phenomenon can be explained by the structural difference between the fitness function and the L2 norm. The fitness of a candidate solution can only decrease or stay the same, due to the greedy selection used in JADE (line 15 in the pseudocode A.1). The monotonically decreasing fitness value at every generation of an exemplary individual within the population is plotted in figure 5.6. Because the L2 norm is not the property that gets optimised, the quality of an individual at every generation is not necessarily monotonically decreasing. The L2 norm and the fitness at every generation of one individual from the population is plotted in figure 5.6.

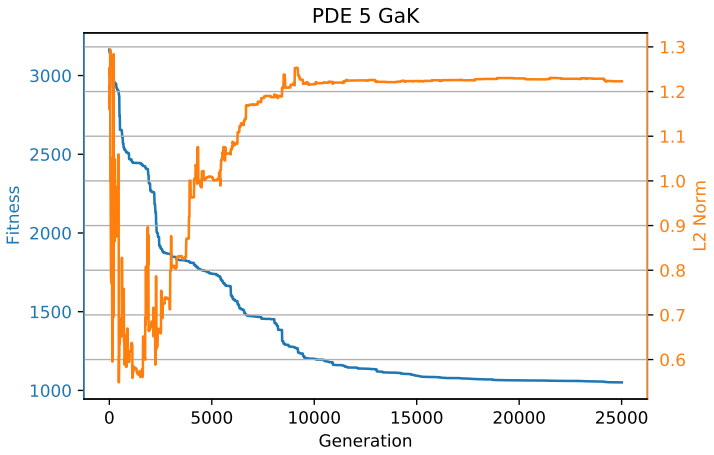

Figure 5.6: Fitness value and L2 Norm of one individual at every generation on PDE 5.

This indicates that the current fitness function does not fully describe the optimisation problem. Some possible solutions to this problem could be:

- An adaptive number of kernels reduces the dimensionality of the problem and only increases the kernel number if necessary.
- A different kernel type that better resembles the structure of the solution could be used.
- A denser grid of collocation points alters the fitness function. This introduces more points that might sit at more interesting positions within the domain. However, this also increases the computational effort to evaluate the fitness function. Alternatively, a scheme that adapts the collocation points during the optimisation process could balance out the computational effort and interesting probing locations.

An adaptive kernel scheme is proposed in chapter 7. The GSK kernel type is examined in chapter 8.

6 Experiment 1: Parallel Population JADE

With the serial algorithm from the chapter above, evaluating a PDE takes way to long to be practically relevant (beyond $14.5 \cdot 10^3$ seconds at 10^6 #FE). To reduce the solving time and speed up all further experiments, a parallel JADE is implemented. This chapter describes the benefits and drawbacks of the new algorithm.

6.1 Hypotheses

The actual parallel JADE algorithm is shown in appendix F. The pseudocode F.1 is very similar to the JADE algorithm A.1. The main differences are laid out in the code-lines 11 to 17. The mutation, the crossover, the parameter adaption and the fitness evaluation are done in parallel for each individual in the population. The parallelism is based on the Python module multiprocessing (M. P. S. Library 2020), in particular the `multiprocessing.Pool.apply_async(func, *args)` method. This method takes a function, in this case an adapted version of the for-loop from code-line 11 to 17, and automatically maps it to a number of preallocated processes. After this is done for every individual in the population, the processes are synchronised and the results get returned to the main process. Therein lies the actual difference to the serial JADE. In the parallel algorithm new individuals are only available after each generation, whereas with the serial algorithm, the individuals are constantly updated before the next generation starts. This means that in the parallel algorithm information is withheld until the next generation - the same information can spread faster in the serial algorithm.

For the sake of completeness, the memetic parallel JADE pseudocode is shown in the algorithm 6.1 below. The only difference compared to the serial memetic JADE 5.1 is the usage of the pJADE in code-line 5.

This chapter discusses the question if the explained distinctions actually influence the results, to the better or the worse. Further, the time-benefits of this strategy are examined and assessed.

Algorithm 6.1: Pseudocode of memetic parallel JADE

```
1 Function memeticJADE(X, funct, minErr, maxFE):
2     dim, popsize ← size(X)
3     p ← 0.3
4     c ← 0.5
5     pop, FE, F, CR ← pJADE(X, p, c, funct, minErr, maxFE − 2dim )
6     bestIndex = argmin(FE)
7     bestSol = pop[bestIndex]
8     pop, FE = downhill simplex(funct, bestSol, minErr, 2dim)
9     return pop, FE, F, CR
```

6.2 Experiment Setup

Similar to the experiment 0 before, the standard parameters from table 4.2 are used. Again, two different machines with either 10^4 #FE ($\rightarrow$ machine 1) or 10^6 #FE ($\rightarrow$ machine 2) are used, whereby the time comparison is only allowed on machine 1. Also, 5 GaK are used, meaning the problem dimension is 20 and the population size is 40. The standard Wilcoxon test (explained in appendix D) is used to proof statistical significance.

Additionally, a new parameter is introduced: the number of allocated parallel processes. Typically, this parameter is set to the number of available processors, but this also depends on the general workload of the machine. When using too many processes, the system might be overwhelmed, effectively slowing down the task and resulting in an even longer solving time. On machine 1, 5 processes are implemented, while machine 2 is capable of handling 30 processes. With other machines, it might be possible to introduce even more processes, potentially increasing the speed-up even further.

6.3 Results

The two images 6.1 and 6.2 display a boxplot of the time- and memory usage. To ensure comparability with the results obtained for the serial JADE, these images represent the results at 10^4 #FE on machine 1.

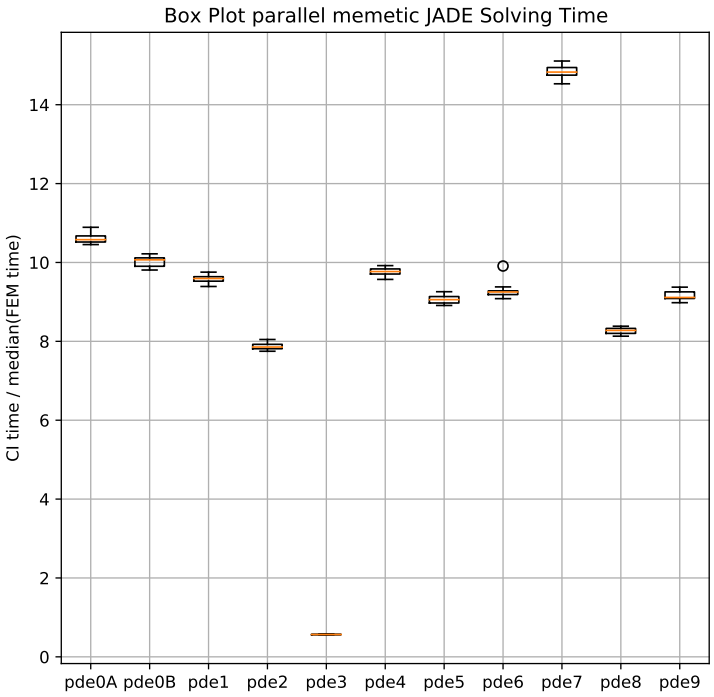

Figure 6.1: Relative solving time results of parallel memetic JADE after 10^4 #FE.

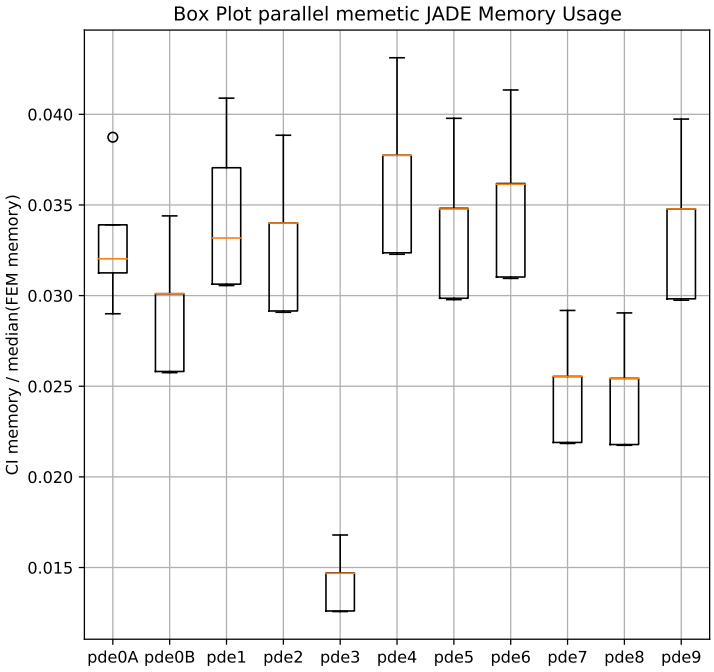

Figure 6.2: Relative memory usage results of parallel memetic JADE after 10^4 #FE.

Table 6.1 shows the mean and the median L2 norm reached on the testbed by both the serial and the parallel algorithm. This is completed with a Wilcoxon test, to identify the difference in the performance. The term "undecided" in this context means that the mean and the median paint different pictures: one of those values is smaller while the other one is larger. Most notably, on PDE 4 the parallel JADE performs significantly worse than the serial JADE.

Algorithm	serial JADE		parallel JADE		
stat	mean	median	mean	median	Wilcoxon Test
PDE 0A	0.6596 ± 0.5510	0.9285	0.6939 ± 0.6635	0.9243	unsig. undecided
PDE 0B	0.2027 ± 0.1302	0.1516	0.2809 ± 0.3071	0.2035	unsig. worse
PDE 1	0.0149 ± 0.0049	0.0151	0.0239 ± 0.0467	0.0146	unsig. undecided
PDE 2	0.0257 ± 0.0140	0.0224	0.0300 ± 0.0157	0.0255	unsig. worse
PDE 3	0.0328 ± 0.0169	0.0285	0.0371 ± 0.0206	0.0295	unsig. worse
PDE 4	0.0378 ± 0.0083	0.0352	0.0505 ± 0.0121	0.0481	sig. worse
PDE 5	1.1968 ± 0.0286	1.2056	1.2030 ± 0.0465	1.2053	unsig. undecided
PDE 6	0.4135 ± 1.2133	0.0018	0.5814 ± 1.3550	1.266E-17	unsig. undecided
PDE 7	0.0221 ± 0.0019	0.0223	0.0228 ± 0.0025	0.0226	unsig. worse
PDE 8	0.2170 ± 0.0019	0.2175	0.2167 ± 0.0017	0.2169	unsig. better
PDE 9	0.0451 ± 0.0119	0.0459	0.0426 ± 0.0115	0.0463	unsig. undecided

Table 6.1: This table compares the results obtained by the parallel and the serial JADE. All results are obtained at 10^6 #FE. The serial data is the same as already presented in table 5.2.

6.4 Discussion

The results from above are analysed in this chapter. The time and memory usage as well as the speed-up for every testbed function is discussed. Further, the significant worse results on PDE 4 are investigated. Finally, the usage of the parallel JADE in all further experiments is justified.

6.4.1 Memory Usage

As the boxplot 6.2 shows, the memory usage is roughly at the same level, somewhere between 1.5 to 4.0 percent of FEM solver. The memory usage is very similar to the serial experiment. This is expected, since memory-wise no integral changes have been performed.

6.4.2 Solving Time

The main purpose of the parallelisation is to cut down the solving time and accelerate all further experiments. To that extent, the population is evaluated in parallel. As the solving time boxplot in figure 6.1 shows, this goal was achieved. The execution time after 10^4 #FE now ranks between the 8 and 15-fold of the FEM solver. This is unquestionably faster than the solving time of the serial algorithm. Remarkable is that on PDE 3, the CI solver is even faster than NGSolve and takes only about $0.56 \cdot 65.2\ \text{s} \approx 36.5\ \text{s}$. Of course, to compete with the solution quality, more #FE are needed, which increases the execution time.

Image 6.3 shows the calculated mean Speed-Up (sp) over 20 replications that is accomplished by substituting the serial JADE with the parallel version. The sp is calculated by dividing the serial solving time with the parallel solving time. The 95% confidence interval is shown in yellow.

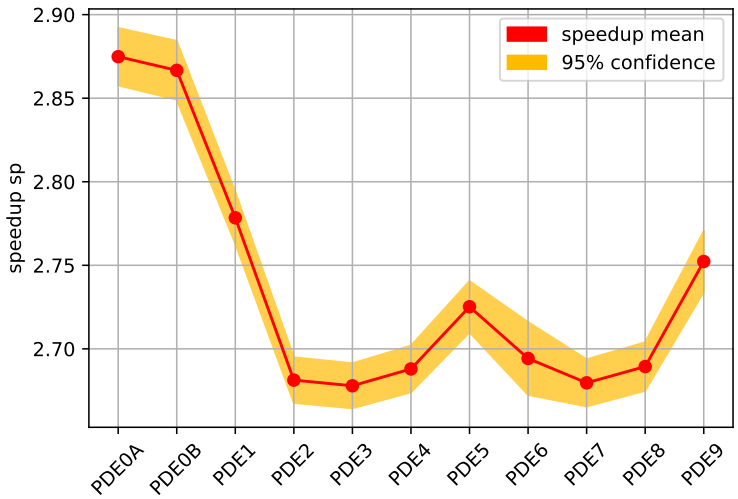

Figure 6.3: Mean speed-up of parallel JADE with 95% confidence interval.

Plot 6.3 shows that the speed-up varies by testbed function. This can be directly linked to the number of operations needed to construct the fitness function, which is primarily determined by the Right Hand Side (RHS) of the PDE. The longer the fitness function takes to evaluate, the greater is the speed-up that can be achieved ($time(fit\ evaln) \uparrow \rightarrow sp \uparrow$). One would expect the same correlation for the size of the population: the larger a population, the better is the speed-up ($pop\ size \uparrow \rightarrow sp \uparrow$). However, this is not experientially verified. Larger fitness functions are needed by the testbed PDEs 0A, 0B, 1, 5, and 9. Looking at the definition of these equations in appendix B, it is notable that the RHS are constructed of more terms compared to the other equations.

6.4.3 PDE 4

Table 6.1 shows that the L2 norm achieved on PDE 4 is significantly worse when the parallel JADE is used. This is not expected and hinders the justification of substituting the serial JADE with the parallel version. It is of interest to confirm the hypothesis and allow the usage of the parallel JADE in all further experiments.

The absolute error (calculated by $E_{abs} = |u_{apx}(x_0, x_1) - u_{ext}(x_0, x_1)|$) of the worst solution generated either by the serial or the parallel algorithm can be seen in the plot from figure 6.4. The plot suggests that the underlying structure of the error is similar in both cases. Although, the L2 norm, the fitness value and the RMSE are lower with the serial JADE, the absolute error values from the plot are similar. Only on the boundary $x_1 = 0, x_0 \in [0, 1]$, the serial JADE generates a visually smaller error.

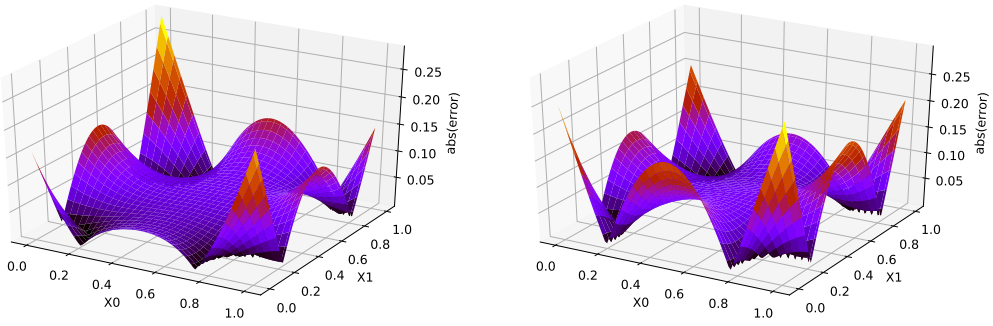

(a) Absolute error, serial JADE
L2 norm: 0.0608
FE value: 0.4632
RMSE: 0.0752

(b) Absolute error, parallel JADE
L2 norm: 0.0733
FE value: 0.6976
RMSE: 0.0895

Figure 6.4: Comparison of the absolute error of the worst solution on PDE 4 by a parallel and a serial memetic JADE at 10^6 #FE

In order to make the results easier to interpret, the histogram from figure 6.5 shows the L2 norm data from table 6.1. The best solutions of both algorithms are at a similar quality level. The parallel sample introduces more results with a worse quality. The absolute numerical range of the quality is visualised in the boxplot 6.6. The Wilcoxon test asserts that the two shown distributions are significantly different. While this can be confirmed visually, it can also be seen that the differences are only marginal.

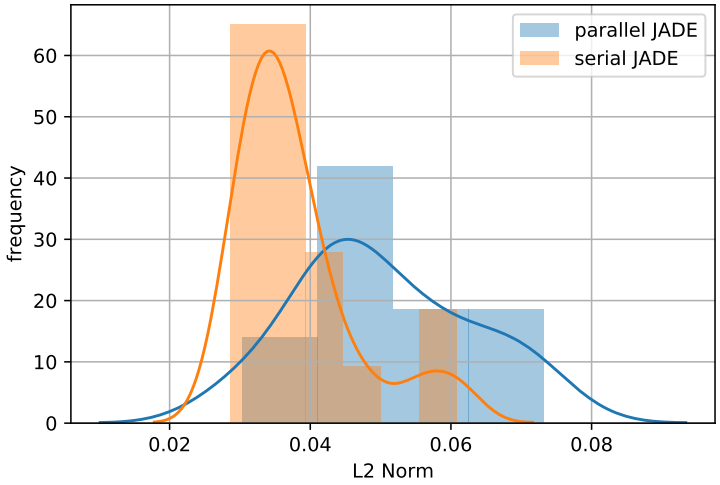

Figure 6.5: Histogram of the L2 norm data obtained by the serial and the parallel JADE on PDE 4 from table 6.1.

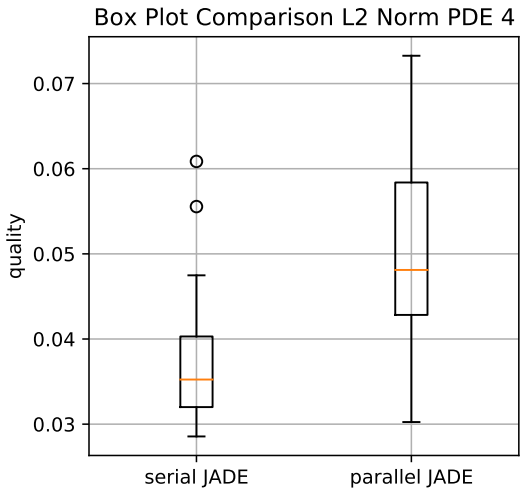

Figure 6.6: Boxplot of the L2 norm data from table 6.1 on PDE 4.

Increasing the number of independent replications could provide further clues to that matter. Considering that quality-wise the parallel JADE makes no significant difference on 10 of 11 tested PDEs and the compelling speed-up on all test problems, the parallel JADE is applied in all further experiments. At the very worst, the algorithm is faster by a factor of 2.5 and results in a minor decrease of the solution quality. This trade-off is acceptable.

7 Experiment 2: Adaptive Number of Kernels

Although the parallel algorithm is effectively faster, the quality of the achieved solution is still not good enough. A common inaccuracy, especially with the testbed PDE 0A is that not all Gauss "bumps" are represented in the approximation, as described in chapter 5.4.3. A possible method to compensate that could be to adapt the number of kernels along the solving process, instead of arbitrarily using 5 kernels.

7.1 Hypotheses

The idea tested in this chapter is an adaptive scheme for the number of kernels used, which is directly linked to the search dimensionality of the optimisation problem.

This new concept requires a convergence based halting criterion in the JADE algorithm, which is not included in the algorithm before. The pseudocode G.1 in the appendix G is extended by a so called "state detector". Ideally, the state detector (code-lines 37 to 40) should stop the overall optimisation loop as soon as the algorithm has converged and before the function evaluation budget is exceeded. Generally, this is done by checking if the function value has not changed for a certain amount of generations. The state detector introduces a new parameter. The Delay Time (dT) represents the number of generations over which the best function value must remain unchanged. It can also be thought of as a buffer-time that allows the DE parameters F and CR to self-adapt. Further, the minError parameter has a new purpose. This is the minimal difference that the function value is allowed to change over dT generations, without resetting the counter for dT.

The new paJADE is wrapped into the memetic framework, already used in the chapters before. A flowchart of the process in shown in figure 7.1. The corresponding pseudocode H.1 in the appendix describes the implementation.

The algorithm always starts with one kernel. From there on, the number of kernels is increased. After the "state detector" has stopped the paJADE, the DS is employed on the best individual of the last population. If the last JADE/DS cycle was able to improve the function value, it is assumed that the best solution for that dimensionality is found. Thus, to further improve the approximation quality, the number of kernels must be increased. If the function value could not be decreased, a restart around

the previous best population is performed. Since the number of kernels is always increased by one, the previous best population must have one kernel less.

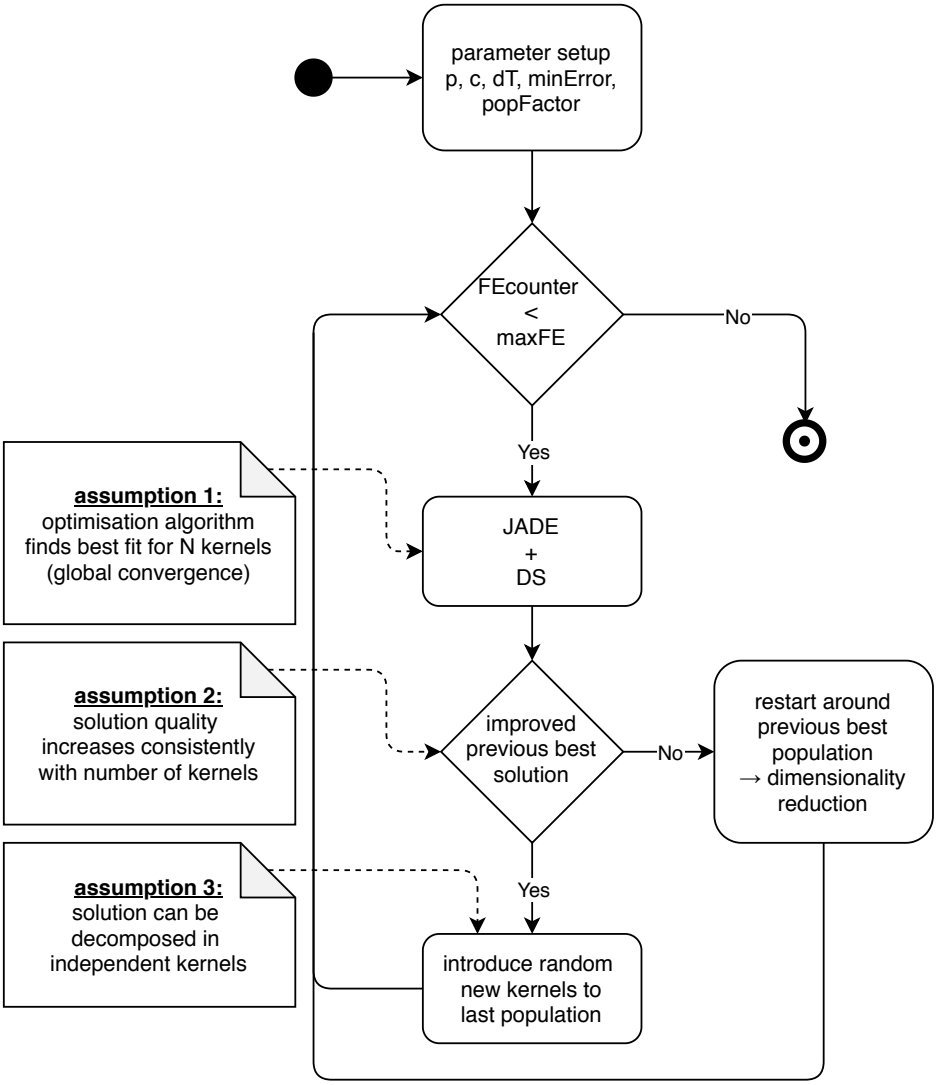

Figure 7.1: Flowchart of the adaptive kernel scheme.

This adaptive scheme operates under 3 strong assumptions. To reduce their possible negative impact, corresponding counter-strategies are implemented.

- **Assumption 1:** The optimisation algorithm (JADE + DS) finds (a close approximation to) the global optimum. This would be the best approximation of the solution by N kernels. Obviously, this property is not necessarily true. Currently, only a very limited amount of research papers exist that discuss global convergence properties of DE (Hu et al. 2013, Opara and Arabas 2019). To counteract this assumption, restarts are performed.

- **Assumption 2:** The theoretically best achievable solution quality increases with the number of kernels. After a maximum number of kernels is reached, the quality can not be surpassed. Based on this assumption, the algorithm starts with one kernel and the dimensionality increases by only one kernel at a time. To catch the point after which too many kernels are used, the dimensionality reduction step is introduced. Generally, the maximum number of kernels is not known except for PDE 0A and PDE 6.
- **Assumption 3:** The best approximation of e.g. 3 kernels to a particular problem is independent of the best approximation by 4 kernels. This means that from 3 to 4 kernels simply a new kernel is introduced while not altering the other 3. Again, this is not true for every PDE. Preliminary experiments on PDE 0A have confirmed this assumption, while on other PDEs, like PDE 2, the solution can not simply be decomposed into independent kernels.

  The concept is similar to the one explained in Chaquet and Carmona 2012. They start the approximation process by optimising the first harmonic. During the search for the second harmonic, the first one is fixed in place.

  In this algorithm, the first kernels are allowed to change. When introducing a new random kernel, it is simply appended to the ever evolving $\mathbf{p_{apx}}$ vector. Thus, the search for the 4th kernel starts where the best approximation for 3 kernels was found, but since the earlier kernels are allowed to readapt, other solutions can be retrieved.

This chapter discusses the question if this strategy is an effective method to increase the quality of obtained solutions. Also, the time and memory aspects are investigated.

7.2 Experiment Setup

Again, as in the experiments before, machine 1 runs at 10^4 #FE and machine 2 performs 10^6 #FE. The time- and memory-comparison are done on machine 1. The number of kernels is adapted, but the algorithm starts with 1 GaK. Thus, the dimension is 4 and the population size is 8. The population size gets corrected if the number of kernels changes. The Wilcoxon test from appendix D investigates the statistical significance.

The two new parameters dT and minError must be set. The minError is again set to 0. The delay time dT is set to 100. When the function value could not be improved over the course of 100 consecutive generations, a new kernel is introduced. This choice is rather arbitrary and depending on the PDE, different values might be more successful. However, this property is not analysed in the current experiment.

7.3 Results

Similar to the experiments before, the two images 7.2 and 7.3 illustrate the time and memory usage of the described kernel adaptive JADE. The data to both plots is obtained on machine 1 at 10^4 #FE. PDE 7 takes the longest to solve, about 8.5 times longer than the FEM solver. Contrary, PDE 3 is solved the fastest, where the CI solver only needs about a quarter of the time used by FEM solver. The memory effort of the CI solver over all testbed problems is between 0.5 and 2.5 percent of the memory needed by the FEM solver.

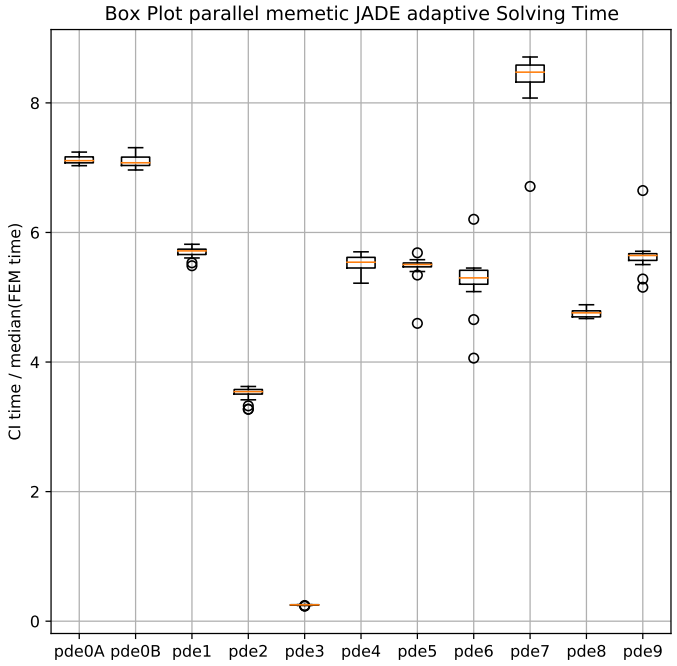

Figure 7.2: Relative solving time results of parallel memetic JADE with adaptive kernels after 10^4 #FE.

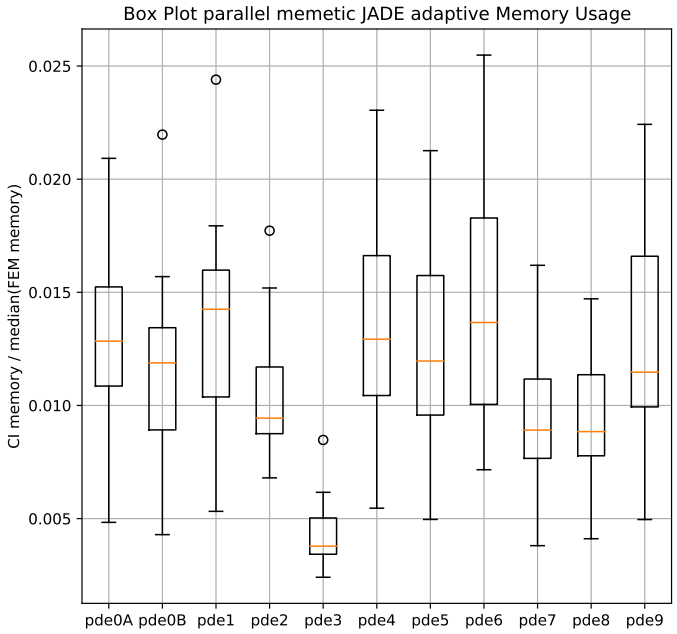

Figure 7.3: Relative memory usage results of parallel memetic JADE with adaptive kernels after 10^4 #FE.

The table 7.1 shows the L2 norm data obtained by the adaptive JADE and compares them against the results from the parallel JADE. The Wilcoxon test indicates mixed results. The adaptive kernel scheme works fine on the PDE 0A, but it also produces significantly worse results on the problems PDE 2, 3, 4 and 7.

Algorithm	parallel JADE 10^6 #FE		adaptive JADE 10^6 #FE		
stat	mean	median	mean	median	Wilcoxon Test
PDE 0A	0.6939 ± 0.6635	0.9243	9.694E-16 ± 1.486E-16	9.255E-16	sig. better
PDE 0B	0.2809 ± 0.3071	0.2035	0.2380 ± 0.0572	0.2607	unsig. undecided
PDE 1	0.0239 ± 0.0467	0.0146	0.0116 ± 0.0061	0.0084	unsig. better
PDE 2	0.0300 ± 0.0157	0.0255	0.0735 ± 0.0358	0.1034	sig. worse
PDE 3	0.0371 ± 0.0206	0.0295	0.1731 ± 0.0395	0.1822	sig. worse
PDE 4	0.0505 ± 0.0121	0.0481	0.0707 ± 0.0053	0.0720	sig. worse
PDE 5	1.2030 ± 0.0465	1.2053	122.6312 ± 372.5676	1.1643	unsig. undecided
PDE 6	0.5814 ± 1.3550	1.266E-17	0.4428 ± 1.0980	1.266E-17	unsig. undecided
PDE 7	0.0228 ± 0.0025	0.0226	0.0513 ± 0.0442	0.0231	sig. worse
PDE 8	0.2167 ± 0.0017	0.2169	0.2144 ± 0.0044	0.2128	unsig. better
PDE 9	0.0426 ± 0.0115	0.0463	0.0483 ± 0.0149	0.0468	unsig. worse

Table 7.1: Comparison of the achieved L2 norm by the pJADE and the paJADE at 10^6 #FE. The pJADE data is directly taken from table 6.1.

Since the number of kernels is not predefined, the resulting solution may have any amount of kernels. This is also a random variable, and the results are shown in the boxplot 7.4 below. As expected, this varies between different testbed problems, but it can not be less than 1 kernel.

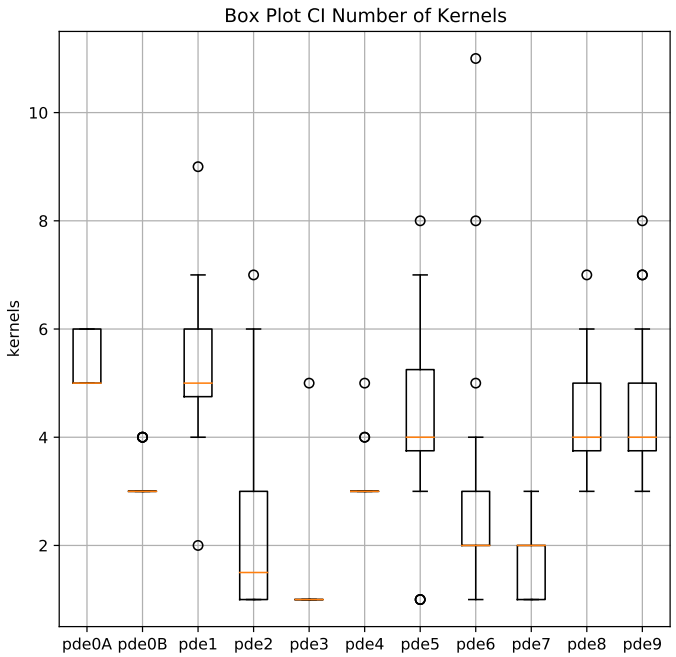

Figure 7.4: Number of kernels of the proposed solution by the paJADE per PDE at 10^6 #FE

7.4 Discussion

This chapter analyses the presented results from section 7.3. The time and memory usage is discussed. The significantly better results on PDE 0A are investigated. The adaptive kernel scheme performs significantly worse on the testbed problems PDE 2, 3, 4, and 7. Therefore the *minError* parameter is adapted and the results are critically examined.

7.4.1 Solving Time

This new adaptive strategy can significantly decrease the time that is necessary to solve any PDE of the testbed. This follows from the solving time box plot in figure 7.2. This effect can be explained by the reduction of the dimension and the adaptive population size. Depending on the number of kernels, the population can

grow. It always starts with 1 kernel and therefore the size of the population is 8. The boxplot shows that this breaks the pattern of simpler and more complex PDEs that is exhibited in the previous experiments.

7.4.2 Memory Usage

The adaptive approach also leads to a reduction in the memory usage, as described by the memory boxplot in figure 7.3. The same explanation that describes the solving time reduction can be applied here: smaller populations need less memory to be stored. Since not all PDEs result in the same dimension, the memory consumption over all testbed problems is not the same. Further, the adaptive scheme dismantles the linear scaling of memory usage with increasing #FE.

7.4.3 PDE 0A

As noted before, the testbed PDE is especially designed to be solved by 5 GaK. The common problem, that not all kernels are established, is solved by the adaptive strategy. The kernel boxplot in figure 7.4 shows that all 20 replications generate at least 5 kernels. However, some solutions are composed of 6 kernels, but this has only a limited effect on the numerical value of the solution quality. Generally, 6 kernels tend to produce worse solutions. The results by the CI solver can even compete with the FEM solver results from table 4.1.

There are mainly three things that can happen to the unnecessary kernel:

- Put the kernel far outside of Ω with c_0 and c_1, so that the influence within the domain is negligible.
- Reduce the scaling factor φ to near 0, therefore the kernel has a small influence compared to the others.
- Increase the exponent γ so that the kernel is very sharp and the influence dies out rapidly with r.

Figure 7.5 shows the 3D plot of two separate unnecessary kernels produced by the adaptive memetic pJADE. A kernel with increased γ is not included in the dataset.

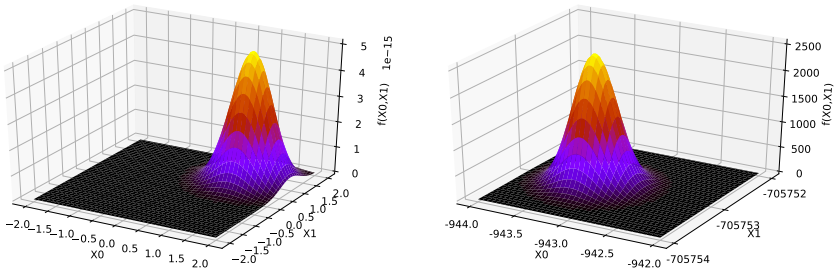

(a) small scaling factor
$\varphi = 5.066 \cdot 10^{-15}$
$f(c_0, c_1) = 5 \cdot 10^{-15}$

(b) outside the domain Ω
$c_0 = -943.237$
$c_1 = -705753.067$.

Figure 7.5: 3D plot and comparison of unnecessary 6^{th} kernels on PDE 0A.

7.4.4 Significantly Worse Quality

The Wilcoxon significance test of table 7.1 shows that the adaptive scheme is worse for the PDEs 2, 3, 4 and 7. The boxplot 7.4 shows that on these test problems the solver frequently results in a smaller number of kernels, where the majority of runs even produce less than 5 GaK. This phenomenon points towards a shared problem where the solver does not increase the number of kernels consistently.

Figure 7.6 plots the solution quality against its number of kernels. It is clearly shown that on these PDEs, more kernels strongly correlate with a better quality.

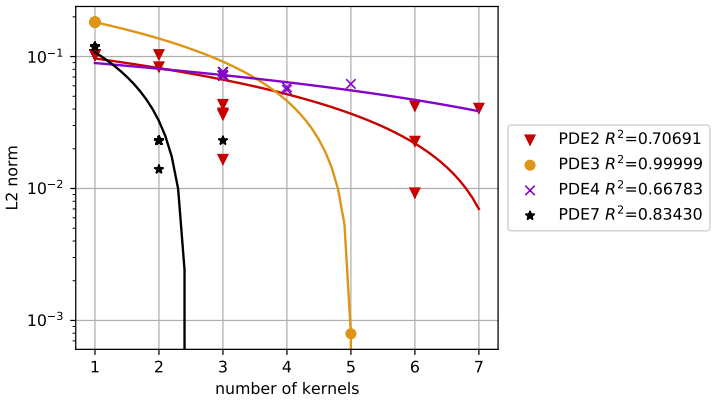

Figure 7.6: Semi-logarithmic plot of the correlation between the L2 norm and the number of kernels. The results are taken at 10^6 #FE on the PDEs 2, 3, 4 and 7. The corresponding R^2 values of the linear regression are denoted.

It seems that JADE exploits some areas long enough so that it does not terminate due to convergence. Thus, the number of kernels is not increased, which leads to a

poor approximation quality. The kernel bar plot of the best and the worst replication for these 4 PDEs is shown in the appendix I and confirms this hypothesis. A simple solution to mitigate this issue might be to adjust the parameters of the "state-detector". In this experiment, $minError = 0$ is used, however it might be beneficial to allow small changes in the function value and still terminate.

Parameter Adaption: *minError*

In this "sub-experiment" the effect of increasing the *minError* parameter is examined. Therefore, the same algorithm is rerun on the PDEs 2, 3, 4 and 7 at four different *minError* levels. Again, 20 replications are done. It is expected that the average number of kernels is increased. Simultaneously, the approximation quality should become better.

As expected, the average number of kernels in the solution gets increased. This is confirmed by the plot in figure 7.7a. Figure 7.7b shows the connection between the median L2 norm and the *minError*. The distance to the analytical solution decreases on PDE 2 and 3. However, this does not improve the results of PDE 4 and 7, where the quality stays roughly on the same level. This is supported statistically by the Wilcoxon test in table 7.2.

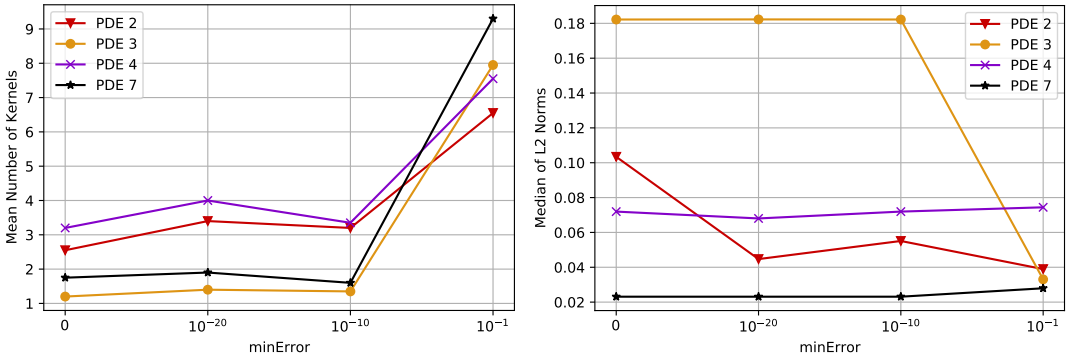

(a) Plot of the mean number of kernels against the *minError*.

(b) Plot of the median L2 norm against the *minError*.

Figure 7.7: Comparison of *minError* against the number of kernels and the achieved solution quality.

Setup	$minError = 0$; 10^6 #FE		$minError = 10^{-1}$; 10^6 #FE		
stat	mean	median	mean	median	Wilcoxon Test
PDE 2	0.0735 ± 0.0358	0.1034	0.0418 ± 0.0156	0.0389	sig. better
PDE 3	0.1731 ± 0.0395	0.1822	0.0455 ± 0.0406	0.0331	sig. better
PDE 4	0.0707 ± 0.0053	0.0720	0.0726 ± 0.0080	0.0744	unsig. worse
PDE 7	0.0513 ± 0.0442	0.0231	0.0287 ± 0.0045	0.0279	unsig. undecided

Table 7.2: Statistical comparison of the achieved L2 norm by paJADE with $minError = 0$ and $minError = 10^{-1}$ after 10^6 #FE. The data with $minError = 0$ is directly taken from table 7.1.

Although the results on PDE 2 and 3 do get significantly better, the adaptive process with greater *minError* introduces a larger spread of the results - both in the number of kernels and in the reached L2 norm. This can be seen in figure 7.8. Compared to the same plot at $minError = 0$ (figure 7.6), the coefficient of determination R^2 is smaller, indicating a poor correlation.

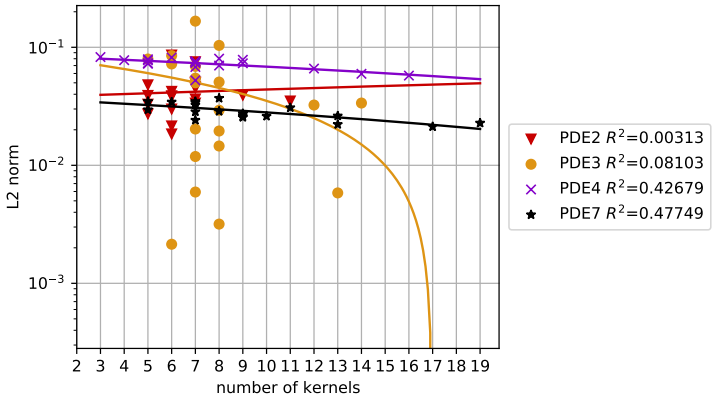

Figure 7.8: Semi-logarithmic plot of the correlation between the L2 norm and the number of kernels. The results are produced with a $minError = 10^-1$ after 10^6 #FE.

Because JADE is terminated earlier, the exploitation is not as progressed. This trade-off needs to be managed by setting the "state-detector"-parameters. A small *minError* ensures that the exploitation is progressed sufficiently, but it exceeds the #FE budget before the number of kernels is increased. Contrary, larger *minError*-values terminate faster and increase the number of kernels, but the solution is not fully exploited.

7.4.5 PDE 5

The results presented in table 7.1 show an interesting observation for the testbed problem 5. The mean L2 norm of the adaptive scheme is very large, but the median is slightly smaller than the median of the non-adaptive JADE. The Wilcoxon test reveals an insignificant difference, which hints that the adaptive scheme includes some very large outliers. This is demonstrated by comparing the box plots of both L2 norm distributions in figure 7.9a. The same data is shown twice, with and without the outlier.

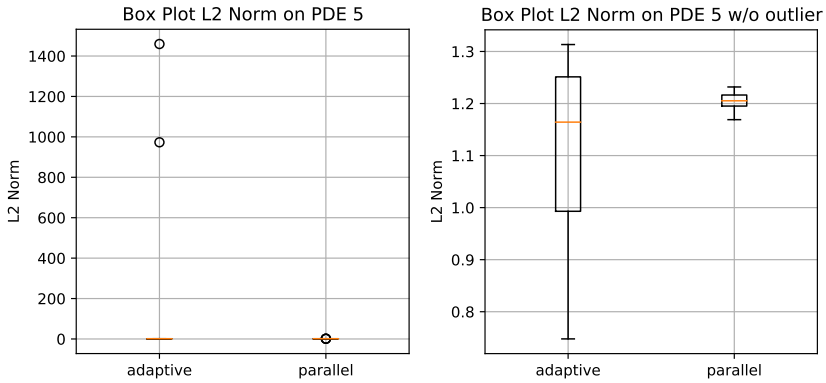

(a) Boxplot of PDE 5 solution quality with outlier.

(b) Boxplot of PDE 5 solution quality without outlier.

Figure 7.9: Boxplot of solution quality on PDE 5 with a budget of 10^6 #FE. Comparison of distribution with and without outliers.

The approximate solution of the outlier is shown in the two 3D plots in figure 7.10 below. Evidently, both results have nothing in common with the actual solution from figure 7.10c. In general, it can be said that the adaptive scheme exhibits a greater spread in the quality of the solution.

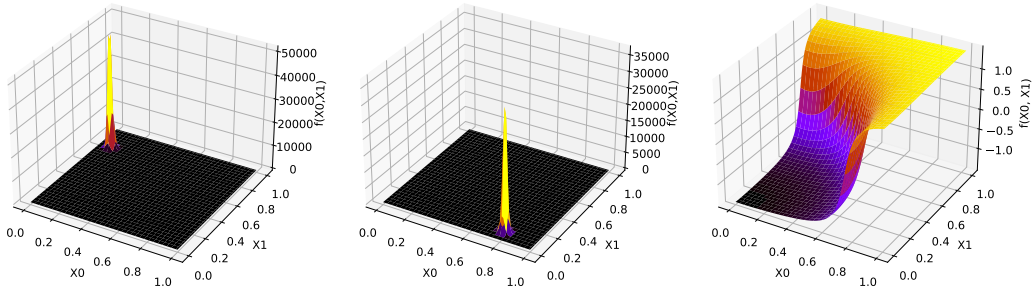

(a) 3D plot of first outlier on PDE 5

(b) 3D plot of second outlier on PDE 5

(c) analytical solution to PDE 5.

Figure 7.10: 3D plot of the outlier solution produced by the adaptive kernel scheme on PDE 5 after 10^6 #FE.

Both outliers have a very similar structure. This might indicate that JADE diverges to areas where the fitness function does not give a proper signal towards the optimum. The adaptive strategy can not improve the results on PDE 5. A second possibility would be to use a different kernel type.

7.4.6 PDE 6

The testbed PDE 6 could theoretically be solved exactly by a single GaK. As the Wilcoxon test shows, the adaptive kernel method does not improve the results significantly. This is confirmed in the subsequent boxplot of figure 7.11. Even good solutions are made of more than one kernel, as the boxplot in 7.4 indicates. This means that the adaptive kernel strategy is not successful on PDE 6. JADE terminates to early and introduces more kernels. The influence of these unnecessary kernels must be minimised by the same strategies as with PDE 0A as presented in chapter 7.4.3.

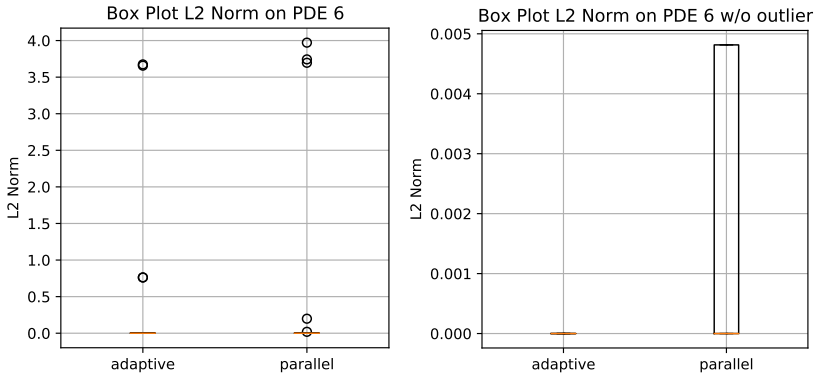

(a) Boxplot of PDE 6 L2 norm results with fliers.

(b) Boxplot of PDE 6 L2 norm results without fliers.

Figure 7.11: Comparison of the L2 norm reached by the paJADE and a non-adaptive pJADE on PDE 6 after 10^6 #FE.

Besides the good results, there are two recurring bad solutions as seen in figure 7.12. Their 3D plot shows no resemblance with the actual solution from figure 7.12c. The fact that these obviously bad approximations happen multiple times indicates that JADE converges to these local optima.

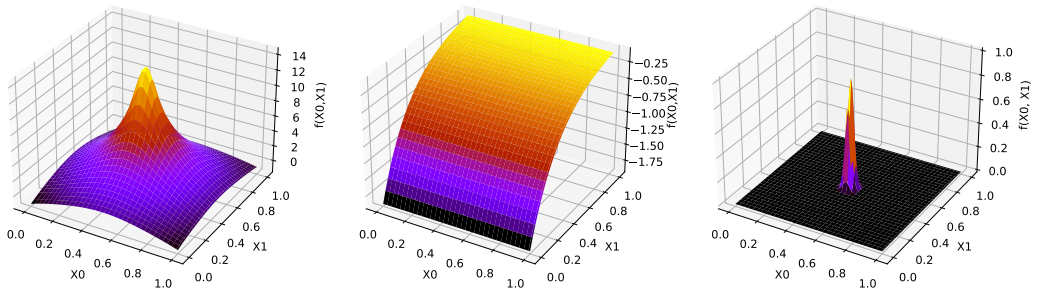

(a) outlier 8 GaK kernel bar plot figure 7.13

(b) outlier 1 GaK kernel bar plot figure 7.14

(c) Analytical solution to PDE 6.

Figure 7.12: These wrong solutions are generated with paJADE after 10^6 #FE and represent local optima where JADE gets stuck.

Corresponding to these 3D plots, the kernel bar plot is depicted in figure 7.13 and 7.14. The kernel bar plot connects the decline of the fitness value with the adaption of the kernel number. Darker areas show a strong decline of the best fitness value over generations, lighter areas represent stagnation. A green bar indicates an increment by one kernel. Contrary, the red bar expresses a decrement by one kernel. This shows how figure 7.12a is created by increasing the kernel count, although one kernel should

be sufficient. Similar, figure 7.12b consists of a single kernel, where a local optimum is exploited. Both false solutions occur twice within the 20 replications.

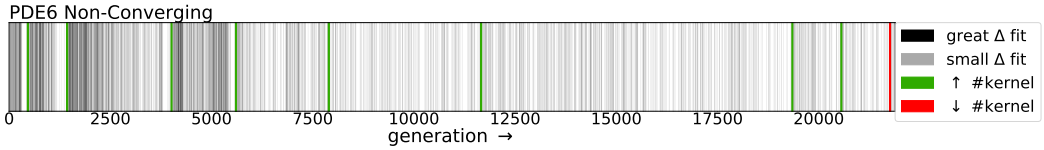

Figure 7.13: Kernel bar plot of the false solution, represented in figure 7.12a

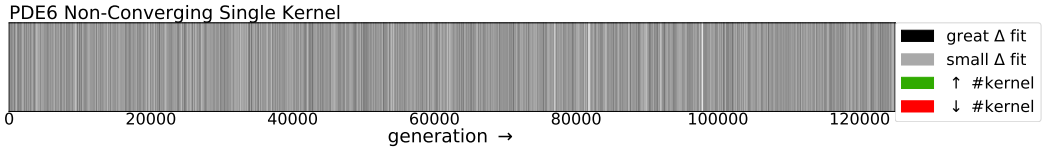

Figure 7.14: Kernel bar plot of the false solution, represented in figure 7.12b

8 Experiment 3: Gauss-Sinus Kernel

Up until now, the results on PDE 5 were always considerably worse than on all other testbed functions. The idea discussed in this chapter is the usage of a new kernel. The Gauss-Sinus Kernel, also abbreviated with GSK, is introduced in chapter 3.3.2. Theoretically, the kernel should be able to solve the testbed PDEs 0A and 0B exactly.

8.1 Hypotheses

As stated in chapter 5.4.4 attempting to solve PDE 5 with more #FE results in a worse solution quality. The adaptive kernel scheme could not improve the results. This means that the fitness function must be reconsidered. A simple approach to change the fitness function is by introducing a new kernel type. The GSK has the features of a Gauss kernel and a sine function and is potentially able to approximate more PDE solutions. The idea of the sine function is to help with the circular features of the wave front.

This experiment tries to answer the question if the new GSK kernel type can effectively improve the results on PDE 5. Further, it should at least maintain the solution quality on all other testbed PDEs.

8.2 Experiment Setup

As stated in the experiments chapters before, machine 1 performs the time and memory experiments at 10^4 #FE. Similar, machine 2 runs the experiment at the full computational budget of 10^6 #FE. The Wilcoxon test from appendix D is used to show statistical significance. Because the last experiment was not entirely conclusive, only a memetic pJADE without kernel-adaption is tested. Since the new kernel has 6 parameters, the dimension and the population size change. To ensure that the algorithm is able to solve PDE 0A, 5 GSK are used. This results in a dimension of 30 parameters and a population size of 60. All other parameters for the experiments are taken from table 4.2.

8.3 Results

The box plots in figure 8.1 compares the relative execution time of the memetic pJADE with the FEM solver. The results seen in this graph are obtained after 10^4 #FE on machine 1. Similar, the data in figure 8.2 compares the memory usage of both algorithms.

The memory usage boxplot exhibits many outliers, where some even indicate a memory usage of 0 Mbyte. This is not expected and might result from technical difficulties. Thus, when comparing these specific results, only the median should be considered.

The following table shows the statistical test. The comparison between the GSK and the GaK on the memetic parallel JADE is shown in table 8.1. The comparison is done with a budget of 10^6 #FE.

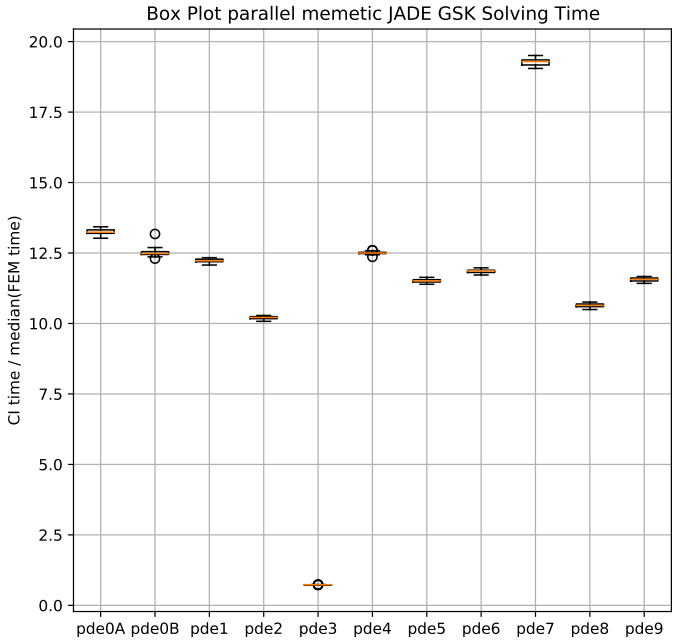

Figure 8.1: Relative solving time results of parallel memetic JADE with GSK after 10^4 #FE.

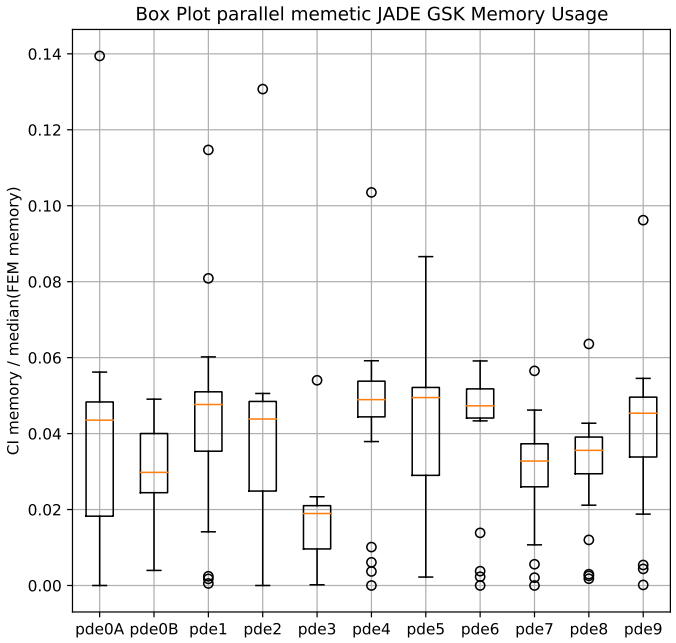

Figure 8.2: Relative memory usage results of parallel memetic JADE with GSK after 10^4 #FE.

Algorithm	parallel JADE GaK 10^6 #FE		parallel JADE GSK 10^6 #FE		
stat	mean	median	mean	median	Wilcoxon Test
PDE 0A	0.6939 ± 0.6635	0.9243	0.8106 ± 0.7929	0.6765	unsig. undecided
PDE 0B	0.2809 ± 0.3071	0.2035	0.0667 ± 0.0470	0.0614	sig. better
PDE 1	0.0239 ± 0.0467	0.0146	0.1665 ± 0.1015	0.1952	sig. worse
PDE 2	0.0300 ± 0.0157	0.0255	0.0448 ± 0.0224	0.0416	unsig. worse
PDE 3	0.0371 ± 0.0206	0.0295	0.0263 ± 0.0111	0.0269	unsig. better
PDE 4	0.0505 ± 0.0121	0.0481	0.0470 ± 0.0078	0.0458	unsig. better
PDE 5	1.2030 ± 0.0465	1.2053	0.5860 ± 0.2149	0.6841	sig. better
PDE 6	0.5814 ± 1.3550	0.0000	3.7321 ± 0.6397	3.9079	sig. worse
PDE 7	0.0228 ± 0.0025	0.0226	0.0243 ± 0.0046	0.0241	unsig. worse
PDE 8	0.2167 ± 0.0017	0.2169	0.2154 ± 0.0018	0.2150	sig. better
PDE 9	0.0426 ± 0.0115	0.0463	0.0351 ± 0.0099	0.0333	unsig. better

Table 8.1: Statistical comparison of the the parallel JADE using the GaK and the GSK.

8.4 Discussion

This chapter discusses the results obtained above with the GSK kernel. It is compared to the memetic parallel JADE using a GaK from experiment 1 in chapter 6. At first, the time and memory consumption comparison is done. The performance on the PDEs 0A and 6 are discussed. The PDE 0B can be perfectly modelled with 3 GSK, thus the performance on this PDE is interesting. Finally, the behaviour of the GSK on PDE 5 is observed.

8.4.1 Solving Time

The solving time for the memetic pJADE with GSK forms the same pattern as the time consumption by the GaK from figure 7.2. The solving time depends on the testbed problem. On PDE 7 the CI solver takes 20 times as long as the FEM solver. This is longer than for the GaK, which can be explained by the larger dimension and the greater population size.

8.4.2 Memory Usage

As mentioned above, the memory measurement includes many outliers. However, the median is quite stable. The CI solver needs only 2 to 5 percent of the memory used by the FEM solver. This is more than the corresponding GaK results from figure 6.2. The greater memory usage can be explained by the larger search dimension and the greater population size.

8.4.3 PDE 0A and PDE 6

Theoretically, PDEs 0A and 6 could be approximated perfectly by the GaK and the GSK. To that extend, the parameters of the GSK must evaluate to $f = 0$ and $\varphi = -\frac{\pi}{2}$. Since the optimisation algorithm will always produce numerical inaccuracies and never actually result in these values, the solution quality is expected to be worse. As table 8.1 shows, the GSK results are not significantly different on PDE 0A.

However, the approximation quality for PDE 6 degrades by a lot. The mean as well as the median of the L2 norm is beyond 3.5. When looking at the data, a common theme is observed: one kernel is adapted quite well, but JADE fails to minimise the influence of the other 4 kernels. Thus, artefacts introduced by these kernels distort the function. A possible solution could be the adaptive kernel scheme.

8.4.4 PDE 0B

Using a GSK produces significantly better solution qualities on PDE 0B. This is expected, since the variation generated by the sine in the actual analytical solution can not be portrayed by the GaK.

The following comparison from figure 8.3 confirms this assumption. The left plot shows the absolute error to the analytical solution of the best result with a GaK. In contrast, the right figure shows the absolute error of best solution with a GSK. Remarkable is the structure of the error with the GaK: the error is clearly dominated by a domain-centred oscillation. This oscillation can not be portrayed by the GaK.

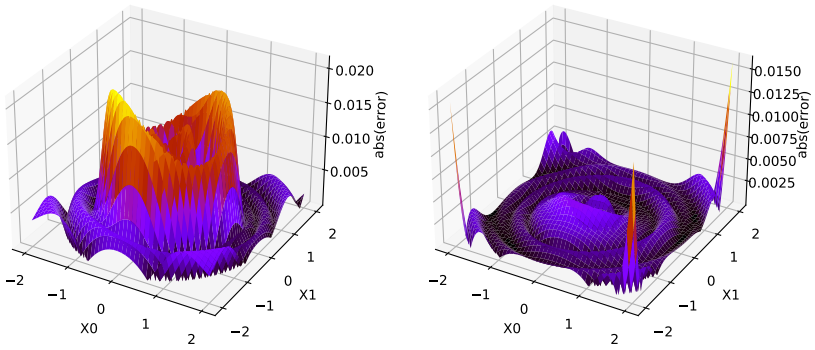

(a) Absolute error best result using GaK.

(b) Absolute error best result using GSK.

Figure 8.3: Comparisons of best solution absolute error by memetic parallel JADE using GaK and GSK after 10^6 #FE.

8.4.5 PDE 5

The hypothesis of the GSK is that it significantly increases the approximation quality of PDE 5. Further, it should overcome the phenomenon where the L2 norm increases with more #FE.

As table 8.1 shows, the results are indeed significantly better. Again, this can be confirmed from a visual perspective by looking at the 3D plot of the approximation. Figure 8.4 depicts the best and the worst approximation of the 20 replications. Although the results are clearly better and the global structure is described more accurately, the CI solver can not compete with the FEM solver.

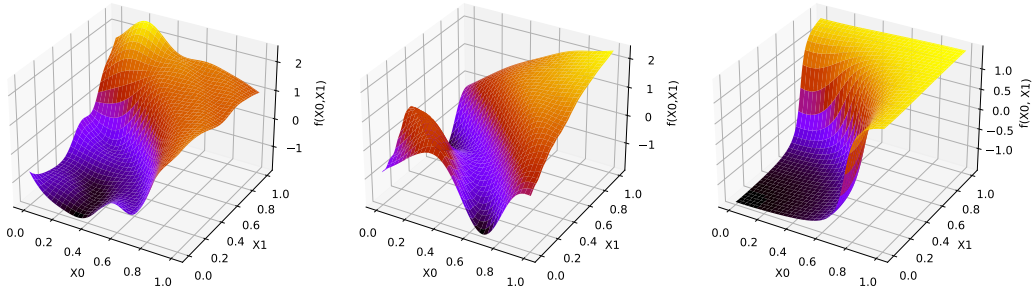

(a) best run GSK
L2 norm: 0.252574

(b) worst run GSK
L2 norm: 0.883869

(c) analytical solution
to PDE 5.

Figure 8.4: Comparison of the best and the worst result generated by memetic pJADE with GSK after 10^6 #FE.

The following histograms in figure 8.5b compare the experimental distribution of the L2 norm with the GaK and the GSK. As inferred from the Wilcoxon test, the distributions are significantly different. Further, the mean and the median of the "GSK-data" are smaller than the same statistical indicators of the "GaK-data".

The histogram of the fitness values is shown in figure 8.5a. Contrary, the fitness values of the GaK are smaller than the fitness values of the GSK. Because the fitness function changes with the usage of the GSK, the numerical values can not be compared directly.

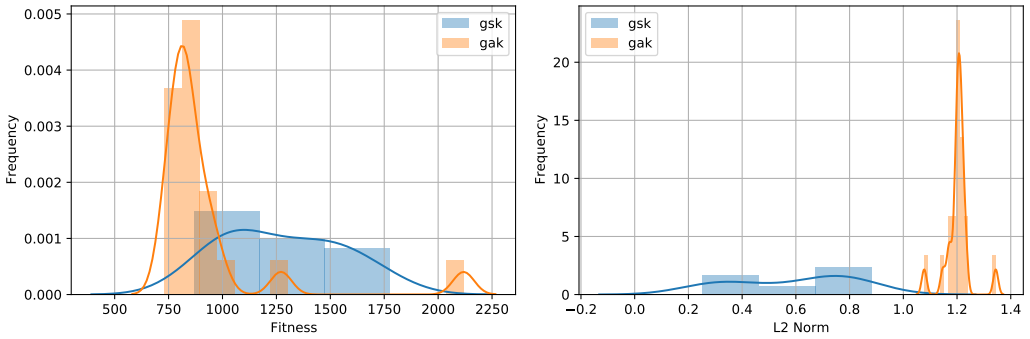

(a) Histogram of fitness value using GSK and GaK.

(b) Histogram of L2 norm using GSK and GaK.

Figure 8.5: Histograms of GSK and GaK L2 norm and fitness value on PDE 5 after 10^6 #FE.

Similar to the plot in chapter 5.4.4, figure 8.6 connects the L2 norm of one individual with its fitness value at every generation. Although the effect of a raising L2 norm with increasing #FE is mitigated, it can be seen that the best quality is not reached

after 10^6 #FE. After generation 5000, the L2 norm settles in at around 0.4, while the fitness value continues to decrease.

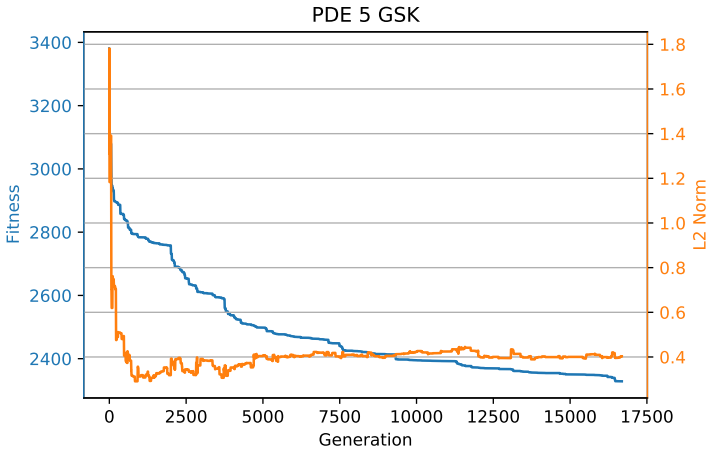

Figure 8.6: Fitness value and L2 Norm of an exemplary individual at every generation on PDE 5 using a GSK.

This again shows that a good fitness value does not necessarily indicate a good approximation quality. Although this property is only shown on PDE 5, it might also be true on other PDEs. This issue demonstrates that the fitness function suffers from a fundamental problem, but currently this is the best indicator for good solutions that only use the information posed in the original problem definition. It can be concluded that choosing an appropriate kernel is not trivial, especially in the common case where the analytical solution to the PDE is not known.

9 Limitations

This work and its proposed solver suffer from several limiting factors. At first, the testbed only includes one type of equation. Further, the treatment of the boundary condition is critically examined. Finally, the achieved quality is strictly limited by the #FE-budget. Thus, the different algorithms are compared with their computational effort.

9.1 Testbed

Contrary to the testbed used by other authors, the test-equations used here are only second order PDEs in $\mathbb{R}^2$. In particular, for all test-PDEs the Laplace operator Δ is applied to a solution function $u(\mathbf{x})$, resulting in various types of Poisson equations. Further, only Dirichlet type boundary conditions are used. This means that the testbed is not very diverse. Especially compared to Chaquet and Carmona 2019, the testbed falls short of ODE and systems of differential equations. However, the results presented in the experiment chapters already indicate mixed performances on different testbed PDEs. Thus, starting with a manageable variety of problems helps with assessing the performance on a particular subset of differential equations.

9.2 Fulfilment of Boundary Condition

Contrary to the FEM solver, the described CI solver does not guarantee the boundary-condition fulfilment. There are ways to counteract the deviation on the boundary.

A simple possibility is to increase the penalty factor φ on the boundary collocation points n_B. This sets an emphasis on the boundary, however it still does not assure the fulfilment of the boundary condition.

Similarly, the number of collocation points on the boundary n_B could be increased. This would shift the relative importance of the fitness function to the boundary, however it would also increase the computational effort. More experiments must be done to evaluate the performance of these ideas.

As described in the literature overview, Kirstukas, Bryden, and Ashlock 2005 propose a strategy that repairs the boundary condition after the solver supposed an

approximation to the interior domain. The same strategy could also be applied to the present solver, which could potentially increase the quality of the approximation.

As discussed in chapter 4.1, PDE 4 is used in the testbed by Chaquet and Carmona 2019 and Mitchell 2018. Since preliminary experiments have shown that the CI solver produced worse results on the Mitchell 2018 implementation, this version is adopted for the current testbed. The main difference between these variants of PDE 4 is the definition of the boundary condition:

- **Mitchell 2018**:

  Homogeneous Dirichlet Boundary Condition:
  $$u(x,0) = 0$$
  $$u(x,1) = 0$$
  $$u(0,y) = 0$$
  $$u(1,y) = 0$$

- **Chaquet and Carmona 2019**:

  Mixed Boundary Condition:
  $$u(x,0) = 0$$
  $$\frac{\partial u}{\partial y}(x,0) = \pi sin(\pi x)$$
  $$u(0,y) = 0$$
  $$u(1,y) = 0$$

Experiment 1 investigates the error behaviour of PDE 4. As seen in figure 6.4, the error is large on the boundary of the domain $\partial\Omega$, while the interior suffers of a relatively small error. Thus, improvements on the boundary can be achieved more easily. Therefore, it makes sense that the solver is sensitive to the implementation of the boundary condition. However, in the typical application the boundary condition can not be rewritten. Thus, better methods for ensuring the boundary condition are needed.

9.3 Computational Effort

The greatest limiting factor for the solver is the extensive computational effort. This is best measured by the Empirical Runtime Distribution (ERD). The ERD calculates the performance of heuristic optimisation algorithms and makes them comparable. ERD plots are often used in Black Box Optimisation Benchmarking (BBOB) contests,

such as the annual Comparing Continuous Optimisers (COCO) workshop (Hansen, Brockhoff, et al. 2019).

The ERD plot from figure 9.1 shows the correlation between the #FE and the percentage of the solved functions in the testbed. Therefore, the #FE is increased from 10^3 to 10^6. The testbed consists of 11 PDEs. Further, different target values in the L2 norm are inspected: $5 \cdot 10^{-2}$, $1 \cdot 10^{-2}$, $5 \cdot 10^{-3}$ and $1 \cdot 10^{-3}$. Thus, the vertical axis indicates how often an algorithm reaches these $4 \cdot 11 = 44$ target values.

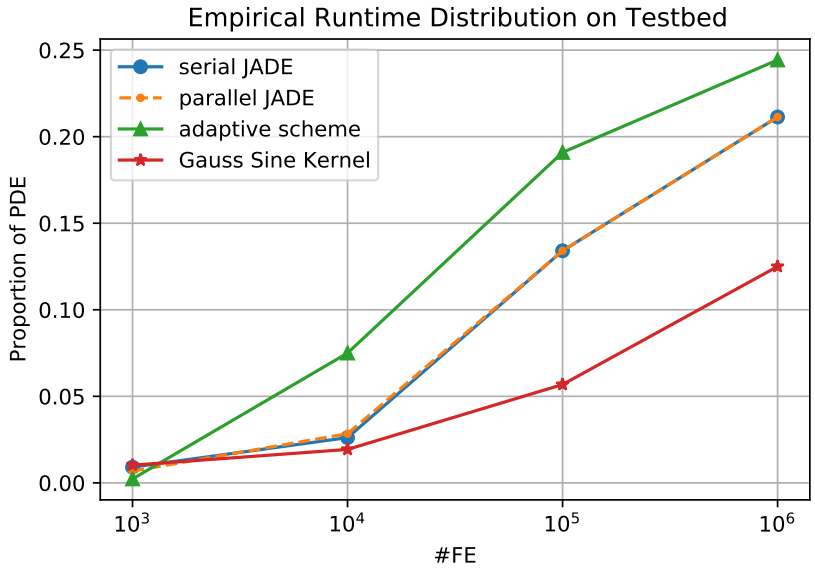

Figure 9.1: Empirical Runtime Distribution of all algorithms on the 11 testbed PDEs at target values $5 \cdot 10^{-2}$, $1 \cdot 10^{-2}$, $5 \cdot 10^{-3}$ and $1 \cdot 10^{-3}$.

Remarkable is the virtually non-existing performance difference between the serial and the parallel memetic JADE. Since "performance" in this graph does not mean "time-consumption", this is expected.

The adaptive JADE scores continuously best and solves up to a quarter of the target values. This is largely thanks to the good performance on PDE 0A, which contributes 9 percent $\left(\frac{1}{11}\right)$ to the whole testbed.

Extrapolating the ERD plots indicates a further performance increase with more #FE. Due to the already expensive algorithm, this is not tested.

In further experiments the same ERD plot should be calculated for other algorithms, like the CMA-ES. Thus, the performance could be directly compared and better converging algorithms can be identified.

10 Theoretical Notes

This chapter deals with a few theoretical notes. At first, the universal approximation theorem for the GSK is shown. Further, the multimodality of the fitness function is proven. Thereby, a symmetry is observed that could lead to the design of better variation operators.

10.1 Universial Approximation Theorem

The Gauss kernel is able to approximate all functions that are part of the Lebesgue space $f(\mathbf{x}) \in L^1(\mathbb{R}^n)$ arbitrarily close. This has been proven by various works (Park and Sandberg 1991, Hangelbroek and Ron 2010). In particular, Park and Sandberg 1991 extends the universal approximation theorem to other kernels. The following paragraphs show that the GSK fulfils the posed conditions and thus can benefit from the approximation theorem.

The Gauss-Sine kernel, as defined in equation (10.1), is a multiplication of the Gauss kernel with a sine function. Its main purpose is described in the experiment chapter 8.

$$gsk(\mathbf{x}) = \omega e^{-\gamma||\mathbf{x}-\mathbf{c}||^2} sin(f||\mathbf{x}-\mathbf{c}||^2 - \varphi) \tag{10.1}$$

To prove that the universal approximation theorem is also applicable to the GSK, it must comply with the conditions placed by Park and Sandberg 1991. At first, a kernel, in this case the $gsk(\mathbf{x})$, must be continuous and bounded. This already restricts $\gamma > 0$. However, Chaquet and Carmona 2019 found that not placing any limits on the parameters results in a better performance. Thus, this constraint is not implemented in the current version of the algorithm. Secondly, the integral over the whole domain of the kernel $K(\mathbf{x})$ must not be 0. Thus, it needs to be shown that

$$\int_{\mathbf{x}=-\infty}^{\infty} gsk(\mathbf{x})\ d\mathbf{x} \neq 0 \tag{10.2}$$

Intuitively, the next restriction on $\omega \neq 0$ is found.

To simplify the following calculations, the GSK is rewritten into polar coordinates. Further, the offsets by c_0 and c_1 are accounted for by an appropriate coordinate transformation. This results in

$$\lim_{t\to\infty}\int_{r=0}^{t}\int_{\theta=0}^{2\pi} e^{-\gamma(r^2)}sin(fr^2-\varphi)r\ dr\ d\theta \tag{10.3}$$

Since the kernel is radial symmetric and thus has no dependency on θ, the respective integral can be solved immediately which results in a multiplicative factor of 2π. The integral can be further simplified by substituting $r^2 = u$. The resulting expression can be solved with "integration by part" $\int f(u)\frac{g(u)}{du} = f(u)g(u) - \int g(u)\frac{f(u)}{du}$. The formula has to be applied twice.

$$\begin{aligned} &2\pi\lim_{t\to\infty}\int_{r=0}^{t} e^{-\gamma(r^2)}sin(fr^2-\varphi)r\ dr \\ =&\pi\lim_{t\to\infty}\int_{u=0}^{t}\underbrace{e^{-\gamma u}}_{\frac{g(u)}{du}}\underbrace{sin(fu-\varphi)}_{f(u)}\ du \\ =&-\frac{sin(fu-\varphi)e^{-\gamma u}}{\gamma}+\frac{f}{\gamma}\left[-cos(fu-\varphi)\frac{e^{-\gamma u}}{\gamma}-\frac{f}{\gamma}\int e^{-\gamma u}sin(fu-\varphi)du\right] \end{aligned} \tag{10.4}$$

The same integral is retrieved. Thus, the equation can be rearranged and solved for the integral. Considering the constant factors and the integral limits gives

$$\lim_{t\to\infty}\frac{\pi e^{-\gamma r^2}(-\gamma sin(fr^2-\varphi)-fcos(fr^2-\varphi))}{\gamma^2+f^2}+C\Bigg|_{r=0}^{t}. \tag{10.5}$$

To resolve the limit of the function towards ∞, the function value must be bounded. Therefore, γ must be positive, which is already required. Finally, this results in

$$\frac{-\pi(\gamma sin(\varphi)+fcos(\varphi))}{\gamma^2+f^2}\neq 0. \tag{10.6}$$

This places more constraints on the parameter of the GSK as seen in the equation (10.7) below.

$$\begin{aligned} &\gamma > 0 \\ &\omega \neq 0 \\ &\gamma sin(\varphi)+fcos(\varphi)\neq 0 \end{aligned} \tag{10.7}$$

These restrictions on the parameters could be enforced during the optimisation process. They could further be used to limit the search dimension. Thus, other optimisation algorithms that are good at handling constraints must be used.

10.2 Multimodality and Symmetry

The optimisation algorithm tries to find the best approximation of N kernels to the solution of a differential equation. Assume, that a kernel K is fully defined by a vector of parameters $\mathbf{p}$. The best fit is defined as

$$\hat{\mathbf{p}}_{\mathbf{apx}} = \left[\underbrace{[\hat{\mathbf{p}}_{K_0}]}_{\text{kernel 0}}, \cdots \underbrace{[\hat{\mathbf{p}}_{K_i}]}_{\text{kernel i}}, \cdots \underbrace{[\hat{\mathbf{p}}_{K_N}]}_{\text{kernel N}} \right]^T \tag{10.8}$$

where the parameters $\hat{\mathbf{p}}$ of every kernel are chosen optimally. The optimal kernel functions $K(\hat{\mathbf{p}}_{K_i}, \mathbf{x})$ are summed up to form the optimal approximation $\hat{u}_{apx}(\mathbf{x})$.

$$\hat{u}_{apx}(\mathbf{x}) = \sum_{i=0}^{N} K(\hat{\mathbf{p}}_{K_i}, \mathbf{x}) \tag{10.9}$$

Since the order of the summation is irrelevant, any kernel-wise permutation describes an optimal solution $\hat{\mathbf{p}}_{\mathbf{apx}}$. Thus, the fitness function $F(u_{apx}(\mathbf{x}))$ has at least $N!$ number of local optima and all of them share the same function value.

Further, a symmetry in the location of the optima is observed. All optima lay on the surface of the hypersphere that is centred at the origin and has a radius of $r = ||\hat{\mathbf{p}}_{\mathbf{apx}}||$.

The following 3D plot in figure 10.1 shows an exemplary distribution of optima on the fitness function. For the sake of simplicity, a kernel now consists of only one parameter. As an example, the vector $\hat{\mathbf{p}}_{\mathbf{apx}} = [2, 1, -1]^T$ describes an optimal solution that consists of 3 kernels. Any permutation of these three coordinates is itself a perfect fit.

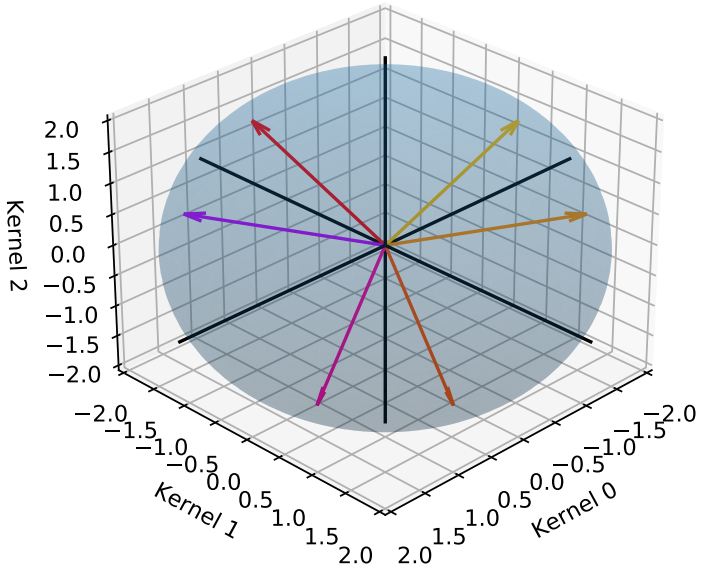

Figure 10.1: Distribution of exemplary optima on the fitness function in 3D space.

This symmetry is independent of the kernel type. Large parts of the fitness function, such as the weighting and penalty factors or the number of collocation points, have no influence on the actual radial arrangement of the optima. The symmetry is a fundamental property of the sum of RBF. Thus, it could even be applied in other fields that use this kind of representation. One of these could be non-linear function approximation.

Obviously, the order of summation is not only true for the optimum, but also for every other point in between. Thus, the entire fitness function exhibits this radial symmetry. More work investigating the structure of the fitness function must be done. With more knowledge about the features of this function, it might be possible to design algorithms specifically to that problem.

11 Conclusion

This chapter summarises what has been learnt about the performance of the algorithms during the experiments. Further, remarks on advantages and disadvantages of the proposed strategy are briefly stated.

Using JADE could not replicate the objectively good performance observed with CMA-ES in Chaquet and Carmona 2019 and other related work. The reason for this is not completely apparent. The poor convergence might be due to some bad parameter choices. Otherwise, JADE might not be as well suited for that sort of fitness function as a CMA-ES is.

To speed up the optimisation process, the parallel JADE is implemented. Thus, the already present parallel hardware structure can be used. Depending on the problem PDE, evaluating the population in parallel significantly speeds up the solving time by at least a factor of 2.6. The parallel JADE works as expected, however it does not reduce the computational effort. Since nowadays, single-core machines do not exist any more, a parallel structure should be the standard for all newly created software. At the very least, new algorithms should be designed with the possibility for parallelisation in mind.

The purpose of the adaptive kernels scheme is to reduce the search dimension and increase the number of kernels only when necessary. It works very well on the testbed PDE 0A. This PDE fulfils the assumptions that have been made for this algorithm. Mixed results have been observed on all other testbed problems. The experiments suggest that the problems could be overcome with an algorithm that converges faster.

The present fitness function might not be the perfect formulation of the problem. Ideally, the quality of the approximation should be tightly linked to the fitness value. However, experiments have shown that this might not always be the case. Specifically, on PDE 5 more #FE result in a significantly worse approximation quality. Thus, a new kernel called GSK is created. The goal for this kernel is to alter the fitness function and thus enhance the correlation between fitness function and quality. The idea works as intended and the results on that PDE do get significantly better. Although the GSK exhibits all the features of the Gauss kernel, the quality of the results for all other PDEs are mixed. This might be due to the larger search space that comes with the new kernel. More experiments investigating the connection of the adaptive scheme with the GSK could provide more insight into that subject.

Obviously, this CI approach to solve PDEs is not as effective as the FEM method. FEM is specifically designed to work on elliptic PDEs and convergence is proven. However, the CI method is a universal approach that should be able to solve all sorts of differential equations.

Contrary, the "universal solver" attribute might also be the greatest disadvantage of this strategy. Currently, there is no guarantee for convergence. The simple implementation and the relatively straight forward approach could misguide the user into applying this strategy, although there might exist better solvers for the problem at hand.

Since there is no guarantee on the quality of the solution, it is potentially risky to apply the CI strategy. The method should work best for problems, where a vague idea on the structure of the solution is already present. A perfect example for such a field of application could be image processing, specifically "shape from shading" (Horn 1970). With this method, the shape of an object can be computed directly from one image. This is done by using the shadows cast by a single light source. At the core of the problem stands a PDE that needs to be solved. Since the image of the object is available to the user, additional quality checks on the approximation can be performed. Surely, there are other applications that could benefit from this solver strategy.

12 Further Work

Many improvements on the current implementation could be performed to reduce the time consumption and potentially increase the accuracy. They can be grouped into three major topics.

Technology:
At the moment, the solver is implemented in Python. Since Python is an interpreted scripting language it is easy to use but it is also slow. Pre-compiling the optimisation algorithm and the fitness function could decrease the time consumption. This would also mean that the #FE could be increased, which could even enhance the accuracy.

Theory:
The described symmetry should be further investigated. This could lead to the design of an algorithm that is explicitly tailored to this optimisation problem. It might even be a starting point for further theoretical advances.

Generally, more mathematical rigour should be applied to this solver strategy. Users are rightfully reluctant to apply a solver to their problem if no convergence properties are proven.

Algorithm:
It seems that JADE can not successfully substitute the CMA-ES. To explore the limitations of a CMA-ES, it should be applied on the current testbed - especially the hard problems like PDE 5.

In a next step the CMA-ES could be tested in combination with the newly defined concept of the kernel adaption scheme. Faster convergence could effectively overcome the problems exhibited with JADE. Further, the CMA-ES and the new GSK could be tied together. It is possible that the CMA-ES is better at handling the higher dimensions of the GSK.

The CMA-ES is the backbone of many ES based optimisation techniques. However, the bare CMA-ES is already a few years old and many new iterations are proposed. It might be possible to increase the performance by using one of these newer algorithms.

In FEM, the adaptive mesh refinement is used to increase the accuracy at certain areas of the PDE. Similarly, the collocation points of the CI solver could be adapted. Where the fitness value is greater, new collocation points could be included. This would set the emphasis on these areas which would then be subjected to refinement.

Acronyms

AB Adams–Bashforth. 1

BBOB Black Box Optimisation Benchmarking. 72

CI Computational Intelligence. 19, 22, 24, 27, 30–33, 39, 40, 47, 53, 56, 67, 68, 71, 72, 79, 80

CMA-ES Covariance Matrix Adaption Evolution Strategy. 8, 9, 31, 34, 39, 73, 78, 80

COCO Comparing Continuous Optimisers. 73

DE Differential Evolution. 1, 2, 7–11, 31, 50, 51

DOF Degree of Freedom. VII, 27, 29, 30, 32

DS Downhill-Simplex. 5, 8, 9, 34, 39, 50, 51

dT Delay Time. 50, 52

ERD Empirical Runtime Distribution. 72, 73

ES Evolution Strategy. 6, 9, 80

FE Forward-Euler. 1

FEM Finite Element Method. X, 2, 3, 13, 19, 22, 24, 26, 28, 29, 32–35, 37–39, 46, 47, 53, 56, 65, 67, 68, 71, 79, 80

GA Genetic Algorithm. 5, 9

GaK Gauss Kernel. IX, X, 14–16, 19, 20, 35, 38, 44, 52, 56, 57, 61, 62, 65–69

GE Grammatical Evolution. 5, 9

GP Genetic Programming. 5, 6, 9

GSK Gauss Sine Kernel. IX, X, 14, 16, 17, 20, 42, 64–70, 74, 75, 78, 80

#FE	Number of Function Evaluation. VII–X, 34–41, 43–48, 52–57, 59–62, 64–66, 68–71, 73, 78, 80
HS	Harmony Search. 7, 9
JSON	JavaScript Object Notation. 100
ODE	Ordinary Differential Equation. 5, 71
PDE	Partial Differential Equation. VII–IX, 2, 3, 5, 12, 14–16, 19, 20, 22, 23, 25, 27–30, 32–43, 46–50, 52–62, 64, 66–73, 78–80, 100, 101, 110, 111
PSO	Particle Swarm Optimisation. 6, 7, 9
RBF	Radial Basis Function. 7, 14, 22, 77
RHS	Right Hand Side. 47
RMSE	Root-Mean-Square Error. 25, 38, 48, 100
RSS	Resident Set Size. 24
sp	Speed-Up. 47
UML	Unified Modeling Language. VII, IX, 22, 23, 99
VMS	Virtual Memory Size. 24
WCA	Water Cycle Algorithm. 7, 9
WRM	Weighted Residual Method. 4, 7, 12, 13

Bibliography

Babaei, M. (July 2013): "A general approach to approximate solutions of nonlinear differential equations using particle swarm optimization". en. In: *Applied Soft Computing* 13.7, pp. 3354–3365. ISSN: 1568-4946. DOI: 10.1016/j.asoc.2013.02.005. URL: http://www.sciencedirect.com/science/article/pii/S1568494613000598 (visited on 02/27/2020) (cit. on pp. 6, 9).

Broomhead, David S. and Lowe, David (1988): "Multivariable Functional Interpolation and Adaptive Networks". In: *Complex Systems* (cit. on p. 15).

Chaquet, Jose M. and Carmona, Enrique J. (Sept. 2012): "Solving differential equations with Fourier series and Evolution Strategies". en. In: *Applied Soft Computing* 12.9, pp. 3051–3062. ISSN: 1568-4946. DOI: 10.1016/j.asoc.2012.05.014. URL: http://www.sciencedirect.com/science/article/pii/S1568494612002505 (visited on 03/02/2020) (cit. on pp. 6, 9, 20, 35, 52).

Chaquet, Jose M. and Carmona, Enrique J. (Mar. 2019): "Using Covariance Matrix Adaptation Evolution Strategies for solving different types of differential equations". en. In: *Soft Computing* 23.5, pp. 1643–1666. ISSN: 1433-7479. DOI: 10.1007/s00500-017-2888-9. URL: https://doi.org/10.1007/s00500-017-2888-9 (visited on 03/02/2020) (cit. on pp. 7, 9, 13, 14, 19, 20, 25, 31, 32, 34, 35, 38, 71, 72, 74, 78).

Eskandar, Hadi et al. (Nov. 2012): "Water cycle algorithm – A novel metaheuristic optimization method for solving constrained engineering optimization problems". en. In: *Computers & Structures* 110-111, pp. 151–166. ISSN: 0045-7949. DOI: 10.1016/j.compstruc.2012.07.010. URL: http://www.sciencedirect.com/science/article/pii/S0045794912001770 (visited on 05/05/2020) (cit. on p. 7).

Fateh, Muhammad Faisal et al. (Oct. 2019): "Differential evolution based computation intelligence solver for elliptic partial differential equations". en. In: *Frontiers of Information Technology & Electronic Engineering* 20.10, pp. 1445–1456. ISSN: 2095-9230. DOI: 10.1631/FITEE.1900221. URL: https://doi.org/10.1631/FITEE.1900221 (visited on 02/11/2020) (cit. on pp. 8, 9).

Geem, Zong Woo; Kim, Joong Hoon, and Loganathan, G.V. (Feb. 2001): "A New Heuristic Optimization Algorithm: Harmony Search". en. In: *SIMULATION* 76.2. Publisher: SAGE Publications Ltd STM, pp. 60–68. ISSN: 0037-5497. DOI: 10.1177/003754970107600201. URL: https://doi.org/10.1177/003754970107600201 (visited on 05/05/2020) (cit. on p. 7).

Guyan, R. J. (1965): "Reduction of stiffness and mass matrices". In: *AIAAJ Aeronautics / Astronautics*, p. 380. DOI: 10.2514/3.2874 (cit. on p. 4).

Hangelbroek, Thomas and Ron, Amos (July 2010): "Nonlinear approximation using Gaussian kernels". en. In: *Journal of Functional Analysis* 259.1, pp. 203–219. ISSN: 0022-1236. DOI: 10.1016/j.jfa.2010.02.001. URL: http://www.sciencedirect.com/science/article/pii/S0022123610000467 (visited on 02/28/2020) (cit. on p. 74).

Hansen, Nikolaus; Brockhoff, Dimo, et al. (Mar. 2019): *COmparing Continuous Optimizers: numbbo/COCO on Github*. Version v2.3. DOI: 10.5281/zenodo.2594848. URL: https://doi.org/10.5281/zenodo.2594848 (cit. on p. 73).

Hansen, Nikolaus; Müller, Sibylle D., and Koumoutsakos, Petros (Mar. 2003): "Reducing the Time Complexity of the Derandomized Evolution Strategy with Covariance Matrix Adaptation (CMA-ES)". In: *Evolutionary Computation* 11.1. Publisher: MIT Press, pp. 1–18. ISSN: 1063-6560. DOI: 10.1162/106365603321828970. URL: https://doi.org/10.1162/106365603321828970 (visited on 08/15/2020) (cit. on p. 8).

Heino, Henrik (May 2020): *henu/bigjson*. original-date: 2016-08-03T01:33:27Z. URL: https://github.com/henu/bigjson (visited on 06/13/2020) (cit. on p. 108).

Holland, John H. (July 1962): "Outline for a Logical Theory of Adaptive Systems". In: *Journal of the ACM* 9.3, pp. 297–314. ISSN: 0004-5411. DOI: 10.1145/321127.321128. URL: https://doi.org/10.1145/321127.321128 (visited on 05/29/2020) (cit. on p. 5).

Horn, Berthold K. P. (Nov. 1970): "Shape from Shading A Method for Obtaining the Shape of a Smooth Opaque Object from One View". en. In: URL: https://dspace.mit.edu/handle/1721.1/6885 (visited on 08/13/2020) (cit. on p. 79).

Howard, Daniel; Brezulianu, Adrian, and Kolibal, Joseph (Jan. 2011): "Genetic programming of the stochastic interpolation framework: convection–diffusion equation". en. In: *Soft Computing* 15.1, pp. 71–78. ISSN: 1433-7479. DOI: 10.1007/s00500-009-0520-3. URL: https://doi.org/10.1007/s00500-009-0520-3 (visited on 03/14/2020) (cit. on pp. 6, 9).

Howard, Daniel and Roberts, Simon C. (July 2001): "Genetic Programming solution of the convection-diffusion equation". In: *Proceedings of the 3rd Annual Conference on Genetic and Evolutionary Computation*. GECCO'01. San Francisco, California: Morgan Kaufmann Publishers Inc., pp. 34–41. ISBN: 978-1-55860-774-3. (Visited on 02/27/2020) (cit. on pp. 5, 9).

Hu, Zhongbo et al. (2013): *Sufficient Conditions for Global Convergence of Differential Evolution Algorithm*. en. Research Article. DOI: https://doi.org/10.1155/2013/193196. URL: https://www.hindawi.com/journals/jam/2013/193196/ (visited on 02/11/2020) (cit. on p. 51).

Kennedy, J. and Eberhart, R. (Nov. 1995): "Particle swarm optimization". In: *Proceedings of ICNN'95 - International Conference on Neural Networks*. Vol. 4, 1942–1948 vol.4. DOI: 10.1109/ICNN.1995.488968 (cit. on p. 6).

Kirstukas, Steven J.; Bryden, Kenneth M., and Ashlock, Daniel A. (June 2005): "A hybrid genetic programming approach for the analytical solution of differential equations". In: *International Journal of General Systems* 34.3. Publisher: Taylor & Francis _eprint: https://doi.org/10.1080/03081070500065676, pp. 279–299. ISSN: 0308-1079. DOI: 10.1080/03081070500065676. URL: https://doi.org/10.1080/03081070500065676 (visited on 03/02/2020) (cit. on pp. 5, 9, 71).

Koza, John R. (1992): *Genetic programming: on the programming of computers by means of natural selection*. Cambridge, MA, USA: MIT Press. ISBN: 978-0-262-11170-6 (cit. on p. 5).

Library, Multiprocessing Python Standard (July 2020): *multiprocessing — Process-based parallelism — Python 3.8.4rc1 documentation*. en. Documentation. URL: https://docs.python.org/3/library/multiprocessing.html (visited on 07/02/2020) (cit. on p. 43).

Library, Time Python Standard (May 2020): *time — Time access and conversions — Python 3.8.3 documentation*. en. Documentation. URL: https://docs.python.org/3/library/time.html (visited on 05/22/2020) (cit. on p. 24).

Mallipeddi and Suganthan (June 2008): "Empirical study on the effect of population size on Differential evolution Algorithm". In: *2008 IEEE Congress on Evolutionary Computation (IEEE World Congress on Computational Intelligence)*. ISSN: 1941-0026, pp. 3663–3670. DOI: 10.1109/CEC.2008.4631294 (cit. on pp. 31, 38).

Mastorakis, Nikos E (Aug. 2006): "Unstable Ordinary Differential Equations: Solution via Genetic Algorithms and the method of Nelder-Mead". en. In: Elounda, Greece, p. 7. URL: https://www.researchgate.net/profile/Nikos_Mastorakis2/publication/261859052_Unstable_ordinary_differential_equations_Solution_via_genetic_algorithms_and_the_method_of_Nelder-Mead/links/573b254e08ae9f741b2d7853.pdf (visited on 02/19/2020) (cit. on pp. 5, 9).

Mitchell, William F. (Mar. 2018): *NIST AMR Benchmarks*. en. URL: https://math.nist.gov/amr-benchmark/index.html (visited on 02/21/2020) (cit. on pp. 19–21, 72).

Moscato, Pablo (Oct. 2000): "On Evolution, Search, Optimization, Genetic Algorithms and Martial Arts - Towards Memetic Algorithms". In: *Caltech Concurrent Computation Program* (cit. on p. 34).

Nelder, J. A. and Mead, R. (Jan. 1965): "A Simplex Method for Function Minimization". en. In: *The Computer Journal* 7.4. Publisher: Oxford Academic, pp. 308–313. ISSN: 0010-4620. DOI: 10.1093/comjnl/7.4.308. URL: https://academic.oup.com/comjnl/article/7/4/308/354237 (visited on 05/05/2020) (cit. on p. 5).

Opara, Karol R. and Arabas, Jarosław (Feb. 2019): "Differential Evolution: A survey of theoretical analyses". en. In: *Swarm and Evolutionary Computation* 44, pp. 546–558. ISSN: 2210-6502. DOI: 10.1016/j.swevo.2018.06.010. URL: http://www.sciencedirect.com/science/article/pii/S2210650217304224 (visited on 03/04/2020) (cit. on p. 51).

Panagant, Natee and Bureerat, Sujin (2014): "Solving Partial Differential Equations Using a New Differential Evolution Algorithm". en. In: *Mathematical Problems in Engineering* 2014.2014. Publisher: Hindawi, e747490. ISSN: 1024-123X. DOI: https://doi.org/10.1155/2014/747490. URL: https://www.hindawi.com/journals/mpe/2014/747490/ (visited on 02/27/2020) (cit. on pp. 7, 9, 19, 20, 35).

Park, J. and Sandberg, I. W. (June 1991): "Universal Approximation Using Radial-Basis-Function Networks". In: *Neural Computation* 3.2. Publisher: MIT Press, pp. 246–257. ISSN: 0899-7667. DOI: 10.1162/neco.1991.3.2.246. URL: https://doi.org/10.1162/neco.1991.3.2.246 (visited on 08/11/2020) (cit. on pp. 14, 74).

Rajeev and Krishnamoorthy (May 1992): "Discrete Optimization of Structures Using Genetic Algorithms". In: *Journal of Structural Engineering* 118.5. Publisher: American Society of Civil Engineers, pp. 1233–1250. DOI: 10.1061/(ASCE)0733-9445(1992)118:5(1233). URL: https://ascelibrary.org/doi/abs/10.1061/(ASCE)0733-9445(1992)118:5(1233) (visited on 03/23/2020) (cit. on p. 7).

Rechenberg, I. (1978): "Evolutionsstrategien". de. In: Schneider, Berthold and Ranft, Ulrich (Eds.): *Simulationsmethoden in der Medizin und Biologie*. Medizinische Informatik und Statistik. Berlin, Heidelberg: Springer, pp. 83–114. ISBN: 978-3-642-81283-5. DOI: 10.1007/978-3-642-81283-5_8 (cit. on p. 6).

Rodola, Giampaolo (May 2020): *psutil documentation — psutil 5.7.1 documentation*. en. Documentation. https://github.com/giampaolo/psutil/blob/master/docs/index.rst. URL: https://psutil.readthedocs.io/en/latest/ (visited on 05/21/2020) (cit. on p. 24).

Ryan, Conor; Collins, JJ, and Neill, Michael O. (1998): "Grammatical evolution: Evolving programs for an arbitrary language". en. In: Banzhaf, Wolfgang et al. (Eds.): *Genetic Programming*. Lecture Notes in Computer Science. Berlin, Heidelberg: Springer, pp. 83–96. ISBN: 978-3-540-69758-9. DOI: 10.1007/BFb0055930 (cit. on p. 5).

Sadollah, Ali et al. (July 2017): "Metaheuristic optimisation methods for approximate solving of singular boundary value problems". In: *Journal of Experimental & Theoretical Artificial Intelligence* 29.4. Publisher: Taylor & Francis _eprint: https://doi.org/10.1080/0952813X.2016.1259271, pp. 823–842. ISSN: 0952-813X. DOI: 10.1080/0952813X.2016.1259271. URL: https://doi.org/10.1080/0952813X.2016.1259271 (visited on 03/02/2020) (cit. on pp. 7, 9).

Schöberl, Joachim; Lackner, Christopher, and Hochsteger, Matthias (Apr. 2020): *NGSolve/ngsolve*. original-date: 2017-07-18T08:47:19Z. URL: https://github.com/NGSolve/ngsolve (visited on 04/02/2020) (cit. on pp. 2, 19, 26).

Schwefel, Hans-Paul (1977): "Evolutionsstrategien für die numerische Optimierung". de. In: Schwefel, Hans-Paul (Ed.): *Numerische Optimierung von Computer-Modellen mittels der Evolutionsstrategie: Mit einer vergleichenden Einführung in die Hill-Climbing- und Zufallsstrategie*. Interdisciplinary Systems Research / Interdisziplinäre Systemforschung. Basel: Birkhäuser, pp. 123–176. ISBN: 978-3-0348-5927-1. DOI: 10.1007/978-3-0348-5927-1_5. URL: https://doi.org/10.1007/978-3-0348-5927-1_5 (visited on 05/29/2020) (cit. on p. 6).

SciPy, Reference Guide (Aug. 2020a): *scipy.optimize.fmin — SciPy v1.5.2 Reference Guide*. en. Documentation. URL: https://docs.scipy.org/doc/scipy/reference/generated/scipy.optimize.fmin.html (visited on 08/06/2020) (cit. on p. 34).

SciPy, Reference Guide (June 2020b): *scipy.stats.wilcoxon — SciPy v1.4.1 Reference Guide*. Documentation. URL: https://docs.scipy.org/doc/scipy/reference/generated/scipy.stats.wilcoxon.html#scipy.stats.wilcoxon (visited on 06/20/2020) (cit. on p. 109).

Shen, Jie; Tang, Tao, and Wang, Li-Lian (2011): *Spectral Methods: Algorithms, Analysis and Applications*. en. Springer Series in Computational Mathematics. Berlin Heidelberg: Springer-Verlag. ISBN: 978-3-540-71040-0. DOI: 10.1007/978-3-540-71041-7. URL: https://www.springer.com/de/book/9783540710400 (visited on 04/24/2020) (cit. on pp. 3, 12, 13).

Sobester, AndrÁs; Nair, Prasanth B., and Keane, Andy J. (Aug. 2008): "Genetic Programming Approaches for Solving Elliptic Partial Differential Equations". In: *IEEE Transactions on Evolutionary Computation* 12.4. Conference Name: IEEE Transactions on Evolutionary Computation, pp. 469–478. ISSN: 1941-0026. DOI: 10.1109/TEVC.2007.908467 (cit. on pp. 6, 9, 20, 35).

Storn, Rainer and Price, Kenneth (Dec. 1997): "Differential Evolution – A Simple and Efficient Heuristic for global Optimization over Continuous Spaces". en. In: *Journal of Global Optimization* 11.4, pp. 341–359. ISSN: 1573-2916. DOI: 10.1023/A:1008202821328. URL: https://doi.org/10.1023/A:1008202821328 (visited on 04/05/2019) (cit. on pp. 7, 10).

Suganthan (Jan. 2020): *Suganthan/CEC2019*. original-date: 2019-07-01T11:46:13Z. URL: https://github.com/P-N-Suganthan/CEC2019 (visited on 03/20/2020) (cit. on p. 10).

Tanabe, Ryoji and Fukunaga, Alex (June 2013): "Success-history based parameter adaptation for Differential Evolution". In: *2013 IEEE Congress on Evolutionary Computation*. ISSN: 1941-0026, pp. 71–78. DOI: 10.1109/CEC.2013.6557555 (cit. on p. 11).

Tanabe, Ryoji and Fukunaga, Alex S. (July 2014): "Improving the search performance of SHADE using linear population size reduction". In: *2014 IEEE Congress on Evolutionary Computation (CEC)*. ISSN: 1941-0026, pp. 1658–1665. DOI: 10.1109/CEC.2014.6900380 (cit. on p. 11).

Tsoulos, I. G. and Lagaris, I. E. (Mar. 2006): "Solving differential equations with genetic programming". en. In: *Genetic Programming and Evolvable Machines* 7.1, pp. 33–54. ISSN: 1573-7632. DOI: 10.1007/s10710-006-7009-y. URL: https://doi.org/10.1007/s10710-006-7009-y (visited on 02/15/2020) (cit. on pp. 5, 9, 19, 20, 35).

Zhang, Jingqiao and Sanderson, Arthur C. (Oct. 2009): "JADE: Adaptive Differential Evolution With Optional External Archive". In: *IEEE Transactions on Evolutionary Computation* 13.5. Conference Name: IEEE Transactions on Evolutionary Computation, pp. 945–958. ISSN: 1941-0026. DOI: 10.1109/TEVC.2009.2014613 (cit. on p. 11).

Appendices

A Differential Evolution Pseudocodes

A.1 JADE Pseudocode

Algorithm A.1: JADE Pseudocode

Function JADE($\mathbf{X}_{g=0}$, p, c, $function$, $minError$, $maxFE$):
  $fValue_{g=0} \leftarrow function(\mathbf{x}_{g=0})$
  $\mu_{CR} \leftarrow 0.5$
  $\mu_F \leftarrow 0.5$
  $A \leftarrow \emptyset$
  while $fe \leq maxFE$ **do**
    $g \leftarrow g + 1$
    $S_F \leftarrow \emptyset$
    $S_{CR} \leftarrow \emptyset$
    for $i = 1$ *to* NP **do**
      $F_i \leftarrow randc_i(\mu_F, 0.1)$
      $v_i \leftarrow mutationCurrentToPBest1(\mathbf{x}_{i,g}, A, fValue_g, F_i, p)$
      $CR_i \leftarrow randn_i(\mu_{CR}, 0.1)$
      $u_i \leftarrow crossoverBIN(\mathbf{x}_{i,g}, v_i, CR_i)$
      if $function(\mathbf{x}_{i,g}) \geq function(\mathbf{u}_{i,g})$ **then**
        $\mathbf{x}_{i,g+1} \leftarrow \mathbf{x}_{i,g}$
      end
      else
        $\mathbf{x}_{i,g+1} \leftarrow \mathbf{u}_{i,g}$
        $fValue_{i,g+1} \leftarrow function(\mathbf{u}_{i,g})$
        $\mathbf{x}_{i,g} \rightarrow \mathbf{A}$
        $CR_i \rightarrow S_{CR}$
        $F_i \rightarrow S_F$
      end
    end
    // resize A to size of $\mathbf{x}_g$
    if $|A| > NP$ **then**
      $A \leftarrow A \setminus A_{rand_i}$
    end
    $fe \leftarrow fe + size(\mathbf{X})$
    $\mu_{CR} \leftarrow (1 - c) \cdot \mu_{CR} + c \cdot arithmeticMean(S_{CR})$
    $\mu_F \leftarrow (1 - c) \cdot \mu_F + c \cdot lehmerMean(S_F)$
  end

A.2 SHADE Pseudocode

Algorithm A.2: SHADE Pseudocode

Function SHADE($\mathbf{x}_{G=0}$, p, H, $function$, $minError$, $maxFE$):
  $M_{CR} \leftarrow 0.5$; $M_F \leftarrow 0.5$; $A \leftarrow \emptyset$; $G \leftarrow 0$; $k \leftarrow 1$
  $fValue_{G=0} \leftarrow function(\mathbf{x}_{G=0})$
  while *termination condition not met* **do**
    $S_{CR} \leftarrow \emptyset$; $S_F \leftarrow \emptyset$
    for $i = 1$ *to* N **do**
      $r_i \leftarrow rand_{int}(1, H)$
      $CR_{i,G} \leftarrow randn_i(M_{CR,r_i}, 0.1)$; $F_{i,G} \leftarrow randc_i(M_{F,r_i}, 0.1)$
      $v_i \leftarrow mutationCurrentToPBest1(\mathbf{x}_{i,G}, A, fValue_G, F_i, p)$
      $u_i \leftarrow crossoverBIN(pop, v_i, CR)$
    end
    for $i = 1$ *to* N **do**
      if $function(u_{i,G}) \leq function(x_{i,G})$ **then**
        $x_{i,G+1} \leftarrow u_{i,G}$; $fValue_{i,G+1} \leftarrow function(\mathbf{u}_{i,G})$
      end
      else
        $x_{i,G+1} \leftarrow x_{i,G}$
      end
      if $function(u_{i,G}) < function(x_{i,G})$ **then**
        $x_{i,G} \rightarrow A$; $CR_{i,G} \rightarrow S_{CR}$; $F_{i,G} \rightarrow S_F$
      end
    end
    if $|A| > N$ **then**
      $A \leftarrow A \setminus A_{rand_i}$
    end
    if $S_{CR} \neq \emptyset \wedge S_F \neq \emptyset$ **then**
      $$M_{CR,k,G+1} = \begin{cases} arithmeticMean(S_{CR}) & \text{if } S_{CR} \neq \emptyset \\ M_{CR,k,G} & otherwise \end{cases}$$
      $$M_{F,k,G+1} = \begin{cases} lehmerMean(S_F) & \text{if } S_F \neq \emptyset \\ M_{F,k,G} & otherwise \end{cases}$$
      $k \leftarrow k + 1$
      if $k > H$ **then**
        $k \leftarrow 1$
      end
    end
    $G \leftarrow G + 1$
  end

A.3 L-SHADE Pseudocode

Algorithm A.3: L-SHADE Pseudocode

Function `LSHADE`($\mathbf{x}_{G=0}$, p, H, $function$, $minError$, $maxFE$)**:**
  $M_{CR} \leftarrow 0.5$; $M_F \leftarrow 0.5$; $A \leftarrow \emptyset$; $G \leftarrow 0$; $k \leftarrow 1$
  $fValue_{G=0} \leftarrow function(\mathbf{x}_{G=0})$; $NG_{init} \leftarrow size(\mathbf{x}_{G=0})$; $NG_{min} = \lceil 1/p \rceil$
  while *termination condition not met* **do**
    $S_{CR} \leftarrow \emptyset$; $S_F \leftarrow \emptyset$
    for $i = 1$ *to* N **do**
      $r_i \leftarrow rand_{int}(1, H)$
      $CR_{i,G} \leftarrow randn_i(M_{CR,r_i}, 0.1)$; $F_{i,G} \leftarrow randc_i(M_{F,r_i}, 0.1)$
      $v_i \leftarrow mutationCurrentToPBest1(\mathbf{x}_{i,G}, A, fValue_G, F_i, p)$
      $u_i \leftarrow crossoverBIN(pop, v_i, CR)$
    end
    for $i = 1$ *to* N **do**
      if $function(u_{i,G}) \leq function(x_{i,G})$ **then**
        $x_{i,G+1} \leftarrow u_{i,G}$; $fValue_{i,G+1} \leftarrow function(\mathbf{u}_{i,G})$
      end
      else
        $x_{i,G+1} \leftarrow x_{i,G}$
      end
      if $function(u_{i,G}) < function(x_{i,G})$ **then**
        $x_{i,G} \rightarrow A$; $CR_{i,G} \rightarrow S_{CR}$; $F_{i,G} \rightarrow S_F$
      end
    end
    if $|A| > N$ **then**
      $A \leftarrow A \setminus A_{rand_i}$
    end
    if $S_{CR} \neq \emptyset \wedge S_F \neq \emptyset$ **then**
      $$M_{CR,k,G+1} = \begin{cases} arithmeticMean(S_{CR}) & \text{if } S_{CR} \neq \emptyset \\ M_{CR,k,G} & otherwise \end{cases}$$
      $$M_{F,k,G+1} = \begin{cases} lehmerMean(S_F) & \text{if } S_F \neq \emptyset \\ M_{F,k,G} & otherwise \end{cases}$$
      $k \leftarrow k + 1$
      if $k > H$ **then**
        $k \leftarrow 1$
      end
    end
    $\mathbf{x}_{G+1} \leftarrow popSizeRed(\mathbf{x}_{G+1}, fValue, G, maxGen, NG_{init}, NGmin)$
    $G \leftarrow G + 1$
  end

B Testbed

The following pages describe the testbed that is used for all experiments. The problems are structured in these major points:

- differential equation
  - differential equation
  - domain Ω
  - Dirichlet bounday condition obtained by evaluating the solution on the boundary
- solution
- plot of the solution over the domain

PDE 0A: Gauss Kernel

Problem PDE:

$$\begin{aligned}
\frac{\partial^2 u}{\partial x^2} + \frac{\partial^2 u}{\partial y^2} &= (18x^2 - 6)e^{-1.5(x^2+y^2)} + (18y^2 - 6)e^{-1.5(x^2+y^2)} \\
&+6(6x^2 + 12x + 5)e^{-3((x+1)^2+(y+1)^2)} + 6(6y^2 + 12y + 5)e^{-3((x+1)^2+(y+1)^2)} \\
&+6(6x^2 - 12x + 5)e^{-3((x-1)^2+(y+1)^2)} + 6(6y^2 + 12y + 5)e^{-3((x-1)^2+(y+1)^2)} \\
&+6(6x^2 + 12x + 5)e^{-3((x+1)^2+(y-1)^2)} + 6(6y^2 - 12y + 5)e^{-3((x+1)^2+(y-1)^2)} \\
&+6(6x^2 - 12x + 5)e^{-3((x-1)^2+(y-1)^2)} + 6(6y^2 - 12y + 5)e^{-3((x-1)^2+(y-1)^2)} \\
&\text{on the domain } \Omega : x, y \in [-2, 2] \\
&\text{subjected to:} \\
u(x, 2) &= 2e^{-1.5(x^2+4)} + e^{-3((x+1)^2+9)} + e^{-3((x+1)^2+1)} + e^{-3((x-1)^2+9)} + e^{-3((x-1)^2+1)} \\
u(x, -2) &= 2e^{-1.5(x^2+4)} + e^{-3((x+1)^2+1)} + e^{-3((x+1)^2+9)} + e^{-3((x-1)^2+1)} + e^{-3((x-1)^2+9)} \\
u(2, y) &= 2e^{-1.5(4+y^2)} + e^{-3(9+(y+1)^2)} + e^{-3(9+(y-1)^2)} + e^{-3(1+(y+1)^2)} + e^{-3(1+(y-1)^2)} \\
u(-2, y) &= 2e^{-1.5(4+y^2)} + e^{-3(1+(y+1)^2)} + e^{-3(1+(y-1)^2)} + e^{-3(9+(y+1)^2)} + e^{-3(9+(y-1)^2)}
\end{aligned} \tag{B.1}$$

Solution:

$$\begin{aligned}
u_{ext}(x, y) = 2e^{-1.5(x^2+y^2)} &+ e^{-3((x+1)^2+(y+1)^2)} + e^{-3((x+1)^2+(y-1)^2)} \\
&+ e^{-3((x-1)^2+(y+1)^2)} + e^{-3((x-1)^2+(y-1)^2)}
\end{aligned} \tag{B.2}$$

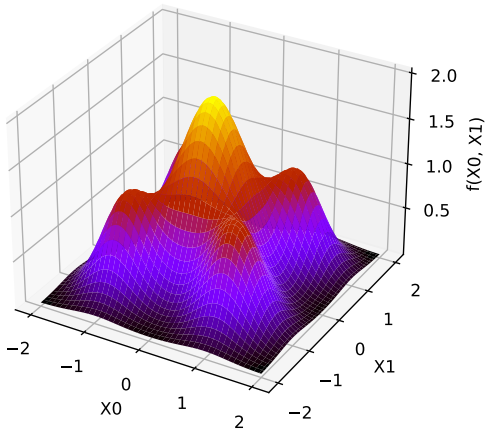

Figure B.1: PDE 0A Gauss Kernel solution plot

PDE 0B: Gauss Sine Kernel

Problem PDE:

$$\begin{aligned}
\frac{\partial^2 u}{\partial x^2} + \frac{\partial^2 u}{\partial y^2} = \\
2e^{-2(x^2+y^2)}(2sin(-2(x^2+y^2)) + 2(1-8x^2)cos(-2(x^2+y^2))) + \\
2e^{-2(x^2+y^2)}(2sin(-2(x^2+y^2)) + 2(1-8y^2)cos(-2(x^2+y^2))) + \\
2e^{-1(x^2+y^2)}(1sin(-1(x^2+y^2)) + 1(1-4x^2)cos(-1(x^2+y^2))) + \\
2e^{-1(x^2+y^2)}(1sin(-1(x^2+y^2)) + 1(1-4y^2)cos(-1(x^2+y^2))) + \\
2e^{-0.1(x^2+y^2)}(0.1sin(-0.1(x^2+y^2)) + 0.1(1-0.4x^2)cos(-0.1(x^2+y^2))) + \\
2e^{-0.1(x^2+y^2)}(0.1sin(-0.1(x^2+y^2)) + 0.1(1-0.4y^2)cos(-0.1(x^2+y^2))) \\
\text{on the domain } \Omega : x, y \in [-2, 2] \\
\text{subjected to:} \\
u(x,2) = e^{-2(x^2+4)}sin(2((x^2+4))) + e^{-1(x^2+4)}sin(1((x^2+4))) + e^{-0.1(x^2+4)}sin(0.1((x^2+4))) \\
u(x,-2) = e^{-2(x^2+4)}sin(2((x^2+4))) + e^{-1(x^2+4)}sin(1((x^2+4))) + e^{-0.1(x^2+4)}sin(0.1((x^2+4))) \\
u(2,y) = e^{-2(4+y^2)}sin(2((4+y^2))) + e^{-1(4+y^2)}sin(1((4+y^2))) + e^{-0.1(4+y^2)}sin(0.1((4+y^2))) \\
u(-2,y) = e^{-2(4+y^2)}sin(2((4+y^2))) + e^{-1(4+y^2)}sin(1((4+y^2))) + e^{-0.1(4+y^2)}sin(0.1((4+y^2)))
\end{aligned} \tag{B.3}$$

Solution:

$$\begin{aligned}
u_{ext}(x,y) =& e^{-2(x^2+y^2)}sin(2((x^2+y^2))) + e^{-1(x^2+y^2)}sin(1((x^2+y^2))) \\
&+ e^{-0.1(x^2+y^2)}sin(0.1((x^2+y^2)))
\end{aligned} \tag{B.4}$$

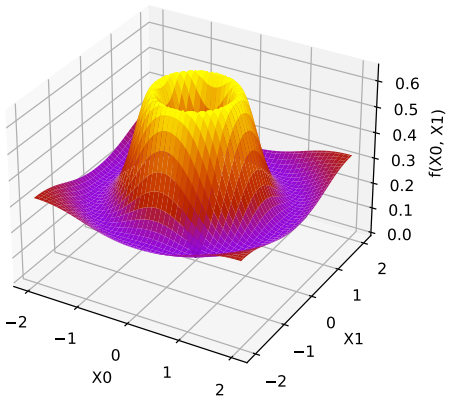

Figure B.2: PDE 0B Gauss Sine Kernel solution plot

PDE 1: Polynomial 2D

Problem PDE:

$$\begin{aligned} -\frac{\partial^2 u}{\partial x^2} - \frac{\partial^2 u}{\partial y^2} = \\ -2^{40} y^{10}(1-y)^{10}[90x^8(1-x)^{10} - 200x^9(1-x)^9 + 90x^{10}(1-x)^8] \\ -2^{40} x^{10}(1-x)^{10}[90y^8(1-y)^{10} - 200y^9(1-y)^9 + 90y^{10}(1-y)^8] \\ \text{on the domain } \Omega : x, y \in [0,1] \\ \text{subjected to:} \\ u(x,1) = 0 \\ u(x,0) = 0 \\ u(1,y) = 0 \\ u(0,y) = 0 \end{aligned} \tag{B.5}$$

Solution:

$$u_{ext}(x,y) = 2^{40} x^{10}(1-x)^{10} y^{10}(1-y)^{10} \tag{B.6}$$

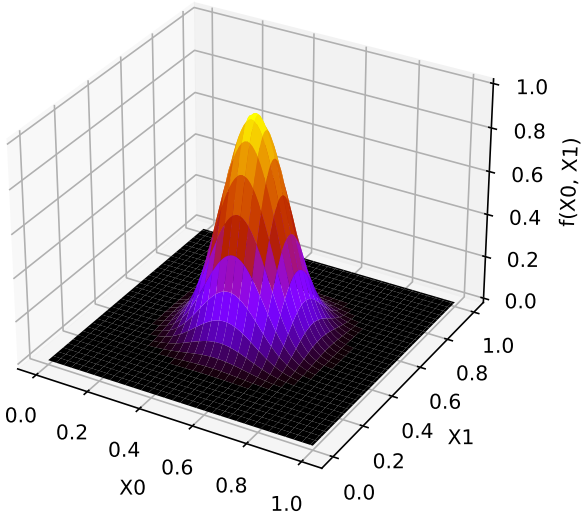

Figure B.3: PDE 1 Polynomial 2D solution plot

PDE 2: Chaquet PDE 1

Problem PDE:

$$\begin{aligned} \frac{\partial^2 u}{\partial x^2} + \frac{\partial^2 u}{\partial y^2} &= e^{-x}(x - 2 + y^3 + 6y) \\ \text{on the domain } \Omega : \mathbf{x} &\in [0, 1] \\ \text{subjected to:} & \\ u(x,0) = xe^{-x} u(x,1) = (x+1)e^{-x} u(0,y) &= y^3 \\ u(1,y) &= (1+y^3)e^{-1} \end{aligned} \tag{B.7}$$

Solution:

$$u_{ext}(x,y) = (x + y^3)e^{-x} \tag{B.8}$$

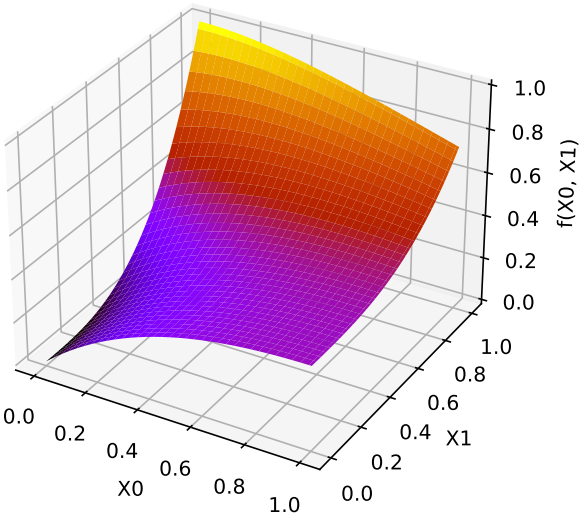

Figure B.4: PDE 2 Chaquet PDE 1 solution plot

PDE 3: Chaquet PDE 3

Problem PDE:

$$\begin{aligned} \frac{\partial^2 u}{\partial x^2} + \frac{\partial^2 u}{\partial y^2} &= 4 \\ \text{on the domain } \Omega : \mathbf{x} &\in [0,1] \\ \text{subjected to:} & \\ u(x,0) &= x^2 + x + 1 \\ u(x,1) &= x^2 + x + 3 \\ u(1,y) &= y^2 + y + 3 \\ u(0,y) &= y^2 + y + 1 \end{aligned} \tag{B.9}$$

Solution

$$u_{ext}(x,y) = x^2 + y^2 + x + y + 1 \tag{B.10}$$

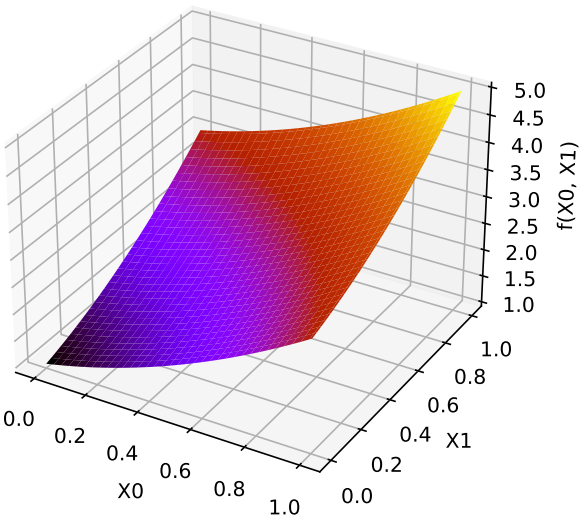

Figure B.5: PDE 3 Chaquet PDE 3 solution plot

PDE 4: Sine Bump 2D

Problem PDE:

$$\begin{aligned} -\frac{\partial^2 u}{\partial x^2} - \frac{\partial^2 u}{\partial y^2} &= 2\pi^2 sin(\pi x) sin(\pi y) \\ \text{on the domain } \Omega : \mathbf{x} &\in [0,1] \\ \text{subjected to:} & \\ u(x,0) &= 0 \\ u(x,1) &= 0 \\ u(0,y) &= 0 \\ u(1,y) &= 0 \end{aligned} \tag{B.11}$$

Solution:

$$u_{ext}(x,y) = sin(\pi x) sin(\pi y) \tag{B.12}$$

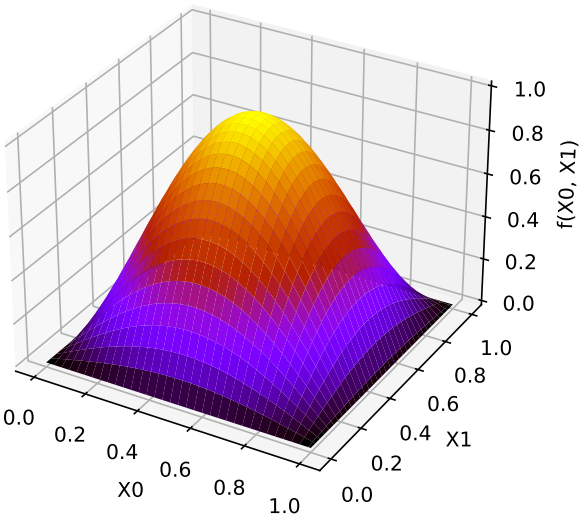

Figure B.6: PDE 4 Sine Bump 2D solution plot

PDE 5: Arctan Circular Wave Front

Problem PDE:

$$
\begin{aligned}
-\frac{\partial^2 u}{\partial x^2} - \frac{\partial^2 u}{\partial y^2} &= \frac{16000(\sqrt{(x-0.05)^2+(y-0.05)^2}-0.7)}{(1+400(-0.7+\sqrt{(x-0.05)^2+(y-0.05)^2})^2)^2} \\
&+ \frac{20(x-0.05)^2+20(y-0.05)^2}{(1+400(\sqrt{(x-0.05)^2+(y-0.05)^2}-0.7)^2)((x-0.05)^2+(y-0.05)^2)^{3/2}} \\
&- \frac{40}{(1+400(\sqrt{(y-0.05)^2+(x-0.05)^2}-0.7)^2)\sqrt{(y-0.05)^2+(x-0.05)^2}} \\
&\text{on the domain } \Omega : \mathbf{x} \in [0,1] \\
&\text{subjected to:} \\
u(x,0) &= tan^{-1}\left(20\left(\sqrt{(x-0.05)^2+0.0025}-0.7\right)\right) \\
u(x,1) &= tan^{-1}\left(20\left(\sqrt{(x-0.05)^2+0.9025}-0.7\right)\right) \\
u(0,y) &= tan^{-1}\left(20\left(\sqrt{0.0025+(y-0.05)^2}-0.7\right)\right) \\
u(1,y) &= tan^{-1}\left(20\left(\sqrt{0.9025+(y-0.05)^2}-0.7\right)\right)
\end{aligned}
\tag{B.13}
$$

Solution:

$$
u_{ext}(x,y) = tan^{-1}\left(20\left(\sqrt{(x-0.05)^2+(y-0.05)^2}-0.7\right)\right) \tag{B.14}
$$

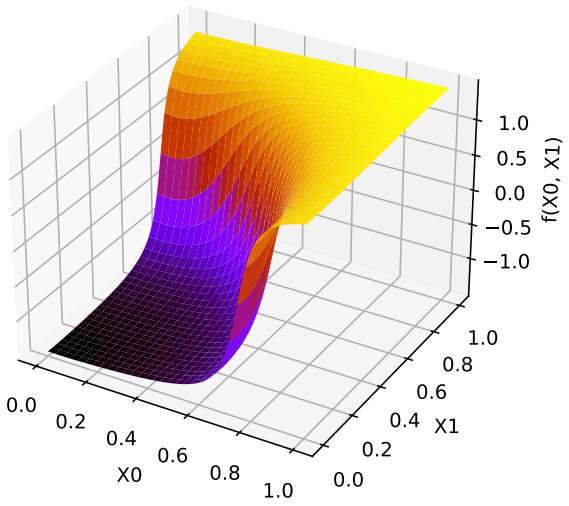

Figure B.7: PDE 5 Arctan Circular Wave Front solution plot

PDE 6: Peak 2D

Problem PDE:

$$\begin{aligned} -\frac{\partial^2 u}{\partial x^2} - \frac{\partial^2 u}{\partial y^2} = \\ -(4 \cdot 10^6 x^2 - 4 \cdot 10^6 x + 998 \cdot 10^3) e^{-1000((x-0.5)^2+(y-0.5)^2)} \\ -(4 \cdot 10^6 y^2 - 4 \cdot 10^6 y + 998 \cdot 10^3) e^{-1000((x-0.5)^2+(y-0.5)^2)} \\ \text{on the domain } \Omega : \mathbf{x} \in [0,1] \\ \text{subjected to:} \\ u(x,0) = e^{-1000((x-0.5)^2+0.25)} \\ u(x,1) = e^{-1000((x-0.5)^2+0.25)} \\ u(0,y) = e^{-1000(0.25+(y-0.5)^2)} \\ u(1,y) = e^{-1000(0.25+(y-0.5)^2)} \end{aligned} \tag{B.15}$$

Solution:

$$u_{ext}(x,y) = e^{-1000((x-0.5)^2+(y-0.5)^2)} \tag{B.16}$$

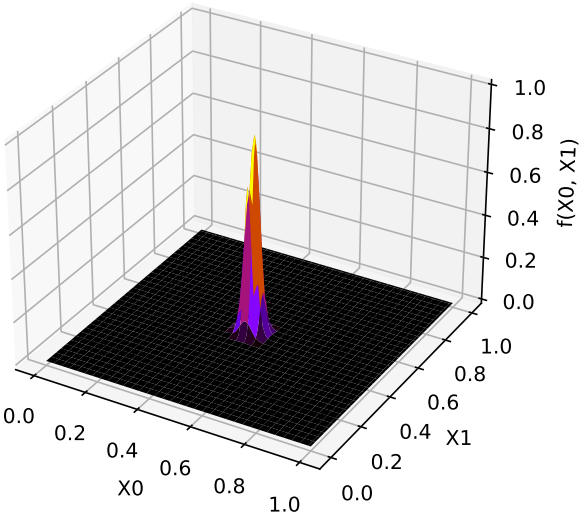

Figure B.8: PDE 6 Peak 2D solution plot

PDE 7: Boundary Line Singularity

Problem PDE:

$$\begin{aligned} -\frac{\partial^2 u}{\partial x^2} - \frac{\partial^2 u}{\partial y^2} &= 0.24x^{-1.4} \\ \text{on the domain } \Omega : \mathbf{x} &\in [0,1] \\ \text{subjected to:} & \\ u(x,0) &= x^{0.6} \\ u(x,1) &= x^{0.6} \\ u(0,y) &= 0 \\ u(1,y) &= 1^{0.6} \end{aligned} \tag{B.17}$$

Solution:

$$u_{ext}(x,y) = x^{0.6} \tag{B.18}$$

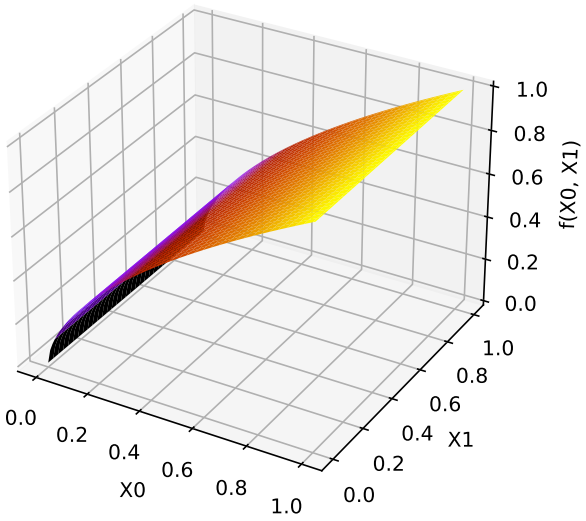

Figure B.9: PDE 7 Boundary Line Singularity solution plot

PDE 8: Interior Point Singularity

Problem PDE:

$$\begin{aligned} \frac{\partial^2 u}{\partial x^2} + \frac{\partial^2 u}{\partial y^2} &= \frac{1}{\sqrt{x^2 - x + y^2 - y + 0.5}} \\ \Omega : \mathbf{x} &\in [0,1] \\ \text{on the domain subjected to:} & \\ u(x,0) &= \sqrt{(x-0.5)^2 + 0.25} \\ u(x,1) &= \sqrt{(x-0.5)^2 + 0.25} \\ u(0,y) &= \sqrt{0.25 + (y-0.5)^2} \\ u(1,y) &= \sqrt{0.25 + (y-0.5)^2} \end{aligned} \tag{B.19}$$

Solution:

$$u_{ext}(x,y) = \sqrt{(x-0.5)^2 + (y-0.5)^2} \tag{B.20}$$

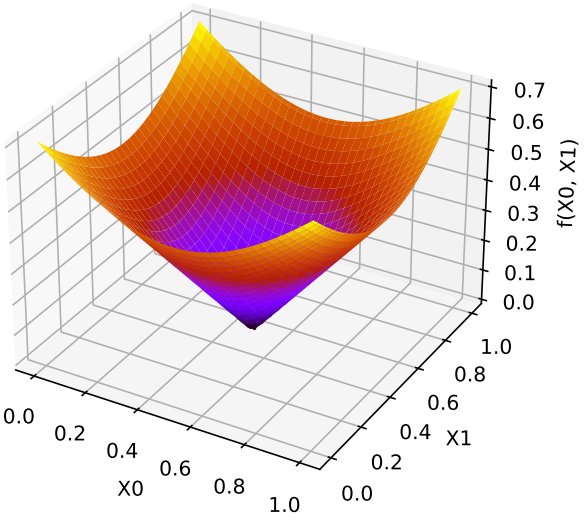

Figure B.10: PDE 8 Interior Point Singularity solution plot

PDE 9: Arctan Wave Front Homogeneous Boundary Conditions 2D

Problem PDE:

$$
\begin{aligned}
-\frac{\partial^2 u}{\partial x^2} - \frac{\partial^2 u}{\partial y^2} = \\
\frac{20\sqrt{2}(x^2+y^2-2x^2y-2xy^2+4xy-x-y)}{400(\frac{x+y}{\sqrt{2}}-0.8)^2+1} \\
+\frac{16000(1-x)x(1-y)y(\frac{x+y}{\sqrt{2}}-0.8)}{(400(\frac{x+y}{\sqrt{2}}-0.8)^2+1)^2} \\
+tan^{-1}\left(20\left(\frac{x+y}{\sqrt{2}}-0.8\right)\right)(2(1-y)y+2(1-x)x) \qquad \text{(B.21)} \\
\text{on the domain } \Omega : \mathbf{x} \in [0,1] \\
\text{subjected to:} \\
u(x,0) = 0 \\
u(x,1) = 0 \\
u(0,y) = 0 \\
u(1,y) = 0
\end{aligned}
$$

Solution:

$$
u_{ext}(x,y) = tan^{-1}\left(20\left(\frac{(x+y)}{\sqrt{2}}-0.8\right)\right)x(1-x)y(1-y) \qquad \text{(B.22)}
$$

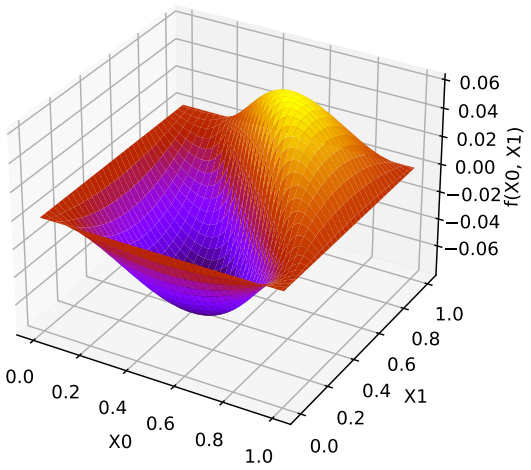

Figure B.11: PDE 9 Arctan Wave Front Homogeneous Boundary Conditions 2D solution plot

C Software Architecture

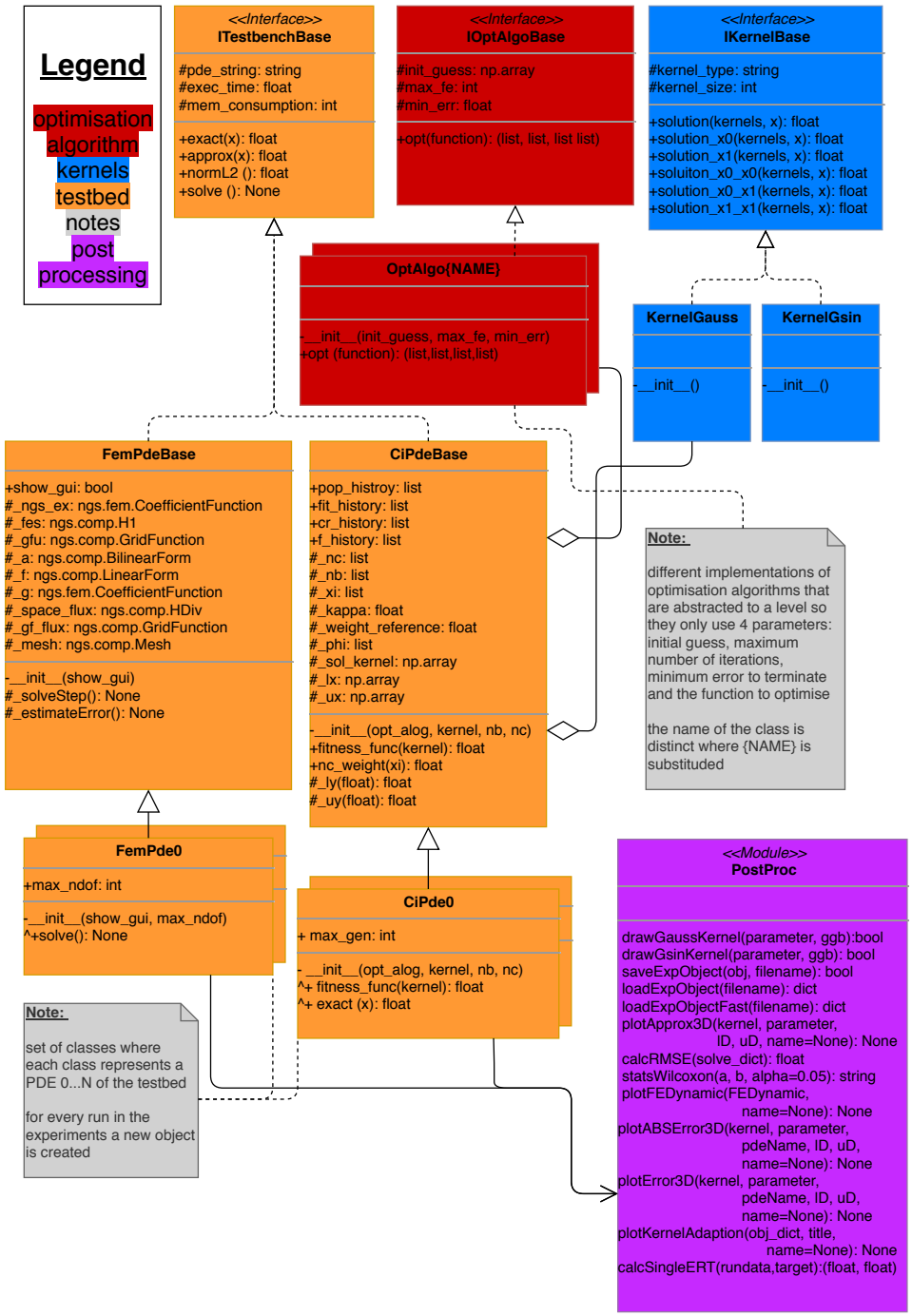

Figure C.1: This UML class diagram describes the software architecture defined to prepare, run and evaluate the experiments.

D Post-Processing Module Description

The post-processing module includes these functions. Their implementation is described in the following list. These functions are used to interpret the results in the experiments chapters.

- `bool saveExpObj(obj, filename)`
  Save an `CiPdeN` object as a JavaScript Object Notation (JSON) file. The filename parameter can include a path, but it must end with .json. The results execution time, memory usage, solution quality and all intergenerational data of the optimisation algorithm are stored in the file.
- `dict loadExpObject(filename)`
  Loads the JSON file located at the specified filename, which again can include a path. A dictionary with the saved `CiPdeN` parameters is returned.
- `dict loadExpObjectFast(filename)`
  When solving a PDE with more function evaluation, the result file can become very large (>400Mb @ 10^6 #FE). For evaluating such large files, this function can be used. It does not load the generation data (meaning population, function value, F and CR). Since the standard JSON interpreter in Python loads files in a serial manner, a new interpreter is needed. To that extent, *bigjson* from Heino 2020 is used. This package accesses only the parts of a JSON file that are actually needed.
- `bool drawGaussKernel(parameter, ggb)`
  Draws a solution approximated by Gauss kernels and with the specified parameters to a GeoGebra file. If the filename provided in the *ggb* argument does not exist, the function searches for a template and prints to a copy of that file.
- `bool drawGSinKernel(parameter, ggb)`
  This is similar to the `drawGaussKernel` method - but it takes parameters for a Gauss Sine kernel.
- `float calcRSME(solve_dict)`
  To compare the obtained results with previous works, the RMSE quality metric (as described in the chapter 4.3.3) must be computed. This is done

from a single dictionary, as obtained by the functions `loadExpObject` or `loadExpObjectFast`.

- `None plotApprox3D(kernel, parameter, lD, uD, name=None)`
  The approximate solution of a PDE can be plotted over the domain with this function. Only square sized domains are accepted, as specified by the lower and the upper domain parameters `lD` and `uD`. If *name* is of type string, the plot is saved as this file.

- `string statsWilcoxon(a, b, alpha=0.05)`
  This function is a wrapper for the `scipy.stats.wilcoxon` (SciPy 2020b). The default significance level is set to 0.05. A string is returned that describes if the mean and median of `a` is significantly smaller than the mean and median of `b`. The result is one of these strings:
  - sig. worse: the distributions are different; the mean and the median of `a` are larger than the mean and the median of `b`
  - sig. better: the distributions are different; the mean and the median of `a` are smaller than the mean and the median of `b`
  - unsig. worse: the distributions are similar; the mean and the median of `a` are larger than the mean and the median of `b`
  - unsig. better: the distributions are similar; the mean and the median of `a` are smaller than the mean and the median of `b`
  - unsig. undecided: the distributions are similar; the mean is larger, the median is smaller or vice versa

  Example distributions with the corresponding results are shown in figure D.1 below.

- `None plotFEDynamic(FEDynamic, name=None)`
  This method plots the function value dynamic of the population on a y-axis logarithmic plot. It can also cope with a varying population size. The plot can be saved with an optional argument.

- `None plotError3D(kernel, parameter, pdeName, lD, uD, name=None)`
  Similar to the `plotApprox3D` method, a 3D graph of the solution is plotted. Instead of the function value, the error is shown. The error is calculated by $E = u_{apx}(x, y) - u_{ext}(x, y) \forall x, y \in \Omega$.

- `None plotABSError3D(kernel, parameter, pdeName, lD, uD, name=None)`
  Similar to the `plotError3D` method, a 3D graph of the solution is plotted. The absolute error is shown. The error is calculated by $E_{abs} = |u_{apx}(x, y) - u_{ext}(x, y)| \, \forall x, y \in \Omega$.

- `None plotKernelAdaption(obj_dict, title, 'green', 'red', name=None)`
  This function plot the fitness difference over all generations. Additionally, it marks if the number of kernels (and thus the search dimension) is increased or reduced.
- `(float, float)calcSingleERT(rundata, target)`
  Calculates the expected running time and the success probability for a single target value. The expected running time is corrected by the success probability.

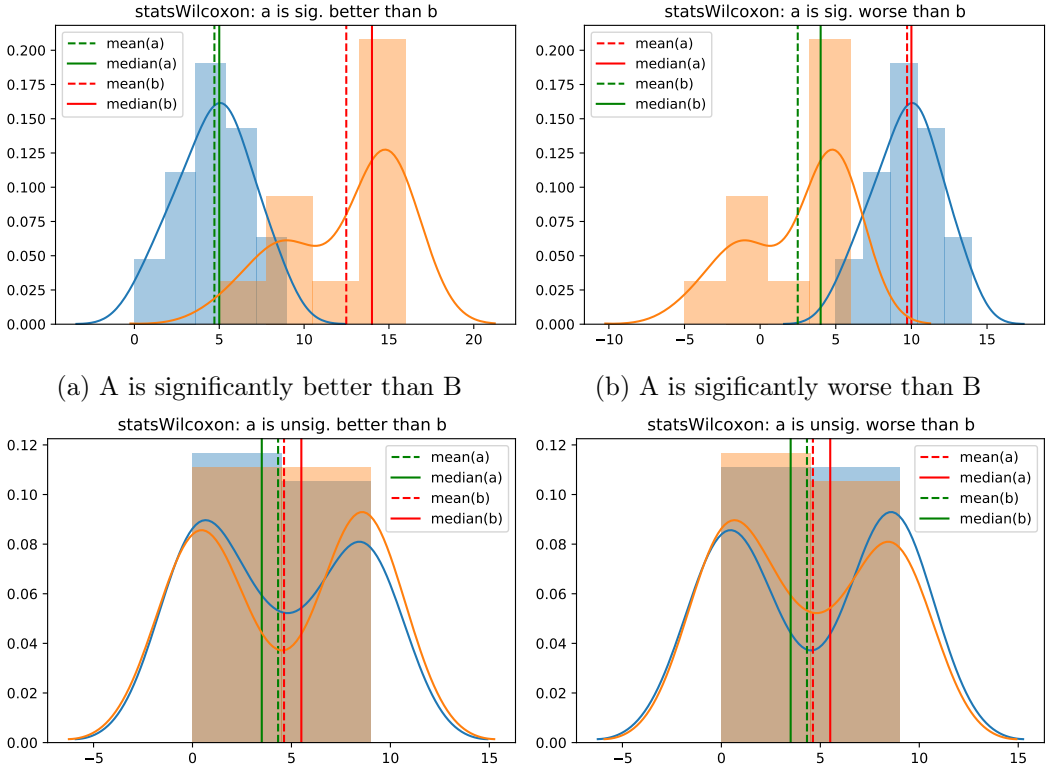

(a) A is significantly better than B

(b) A is sigificantly worse than B

(c) A is unsignificantly better than B

(d) A is unsignificatnly worse than B

Figure D.1: Example distributions for different results of the statsWilcoxon method.

E Solve Method

Algorithm E.1: Solve Method Pseudocode

```
1  Function solve():
2      gc.disable()
3      while gc.isenabled() do
4          time.sleep(0.1)
5      end
6      process = psutil.Process()
7      memstart = process.memory_info().vms
8      t_start = time.time()
9      // perform solver steps
10     // that are particular
11     // to FEM or CI solver
12     self._exec_time = time.time() − t_start
13     memstop = process.memory_info().vms − memstart
14     gc.enable()
15     gc.collect()
```

F pJADE

Algorithm F.1: Pseudocode of pJADE

Function pJADE($\mathbf{X}_{g=0}$, p, c, $function$, $minError$, $maxFE$):
  $fValue_{g=0} \leftarrow function(\mathbf{x}_{g=0})$
  $\mu_{CR} \leftarrow 0.5$
  $\mu_F \leftarrow 0.5$
  $A \leftarrow \emptyset$
  while $fe \leq maxFE$ **do**
    $g \leftarrow g + 1$
    $S_F \leftarrow \emptyset$
    $S_{CR} \leftarrow \emptyset$
    $pResults \leftarrow \emptyset$
    for $i = 1$ *to* NP **do parallel**
      $F_i \leftarrow randc_i(\mu_F, 0.1)$
      $v_i \leftarrow mutationCurrentToPBest1(\mathbf{x}_{i,g}, A, fValue_g, F_i, p)$
      $CR_i \leftarrow randn_i(\mu_{CR}, 0.1)$
      $u_i \leftarrow crossoverBIN(\mathbf{x}_{i,g}, v_i, CR_i)$
      $(u_i, function(u_i)) \rightarrow pResults$
    end
    for $i = 1$ *to* NP **do**
      if $function(\mathbf{x}_{i,g}) \geq pResults_{i,f,g}$ **then**
        $\mathbf{x}_{i,g+1} \leftarrow \mathbf{x}_{i,g}$
      end
      else
        $\mathbf{x}_{i,g+1} \leftarrow pResults_{i,u,g}$
        $fValue_{i,g+1} \leftarrow pResults_{i,f,g}$
        $\mathbf{x}_{i,g} \rightarrow \mathbf{A}$
        $CR_i \rightarrow S_{CR}$
        $F_i \rightarrow S_F$
      end
    end
    // resize A to size of $\mathbf{x}_g$
    if $|A| > NP$ **then**
      $A \leftarrow A \setminus A_{rand_i}$
    end
    $fe \leftarrow fe + size(\mathbf{X})$
    $\mu_{CR} \leftarrow (1 - c) \cdot \mu_{CR} + c \cdot arithmeticMean(S_{CR})$
    $\mu_F \leftarrow (1 - c) \cdot \mu_F + c \cdot lehmerMean(S_F)$
  end

G paJADE

Algorithm G.1: Pseudocode of paJADE

Function `paJADE(`$\mathbf{X}_{g=0}$, p, c, dT, $function$, $minError$, $maxFE$`):`
  $fValue_{g=0} \leftarrow function(\mathbf{x}_{g=0})$
  $\mu_{CR} \leftarrow 0.5$
  $\mu_F \leftarrow 0.5$
  $A \leftarrow \emptyset$
  while $fe \leq maxFE$ **do**
    $g \leftarrow g + 1$
    $S_F \leftarrow \emptyset$
    $S_{CR} \leftarrow \emptyset$
    $pResults \leftarrow \emptyset$
    for $i = 1$ *to* NP **do parallel**
      $F_i \leftarrow randc_i(\mu_F, 0.1)$
      $v_i \leftarrow mutationCurrentToPBest1(\mathbf{x}_{i,g}, A, fValue_g, F_i, p)$
      $CR_i \leftarrow randn_i(\mu_{CR}, 0.1)$
      $u_i \leftarrow crossoverBIN(\mathbf{x}_{i,g}, v_i, CR_i)$
      $(u_i, function(u_i)) \rightarrow pResults$
    end
    for $i = 1$ *to* NP **do**
      if $function(\mathbf{x}_{i,g}) \geq pResults_{i,f,g}$ **then**
        $\mathbf{x}_{i,g+1} \leftarrow \mathbf{x}_{i,g}$
      end
      else
        $\mathbf{x}_{i,g+1} \leftarrow pResults_{i,u,g}$
        $fValue_{i,g+1} \leftarrow pResults_{i,f,g}$
        $\mathbf{x}_{i,g} \rightarrow \mathbf{A}$
        $CR_i \rightarrow S_{CR}$
        $F_i \rightarrow S_F$
      end
    end
    `//` `resize` A `to size of` $\mathbf{x}_g$
    if $|A| > NP$ **then**
      $A \leftarrow A \setminus A_{rand_i}$
    end
    $fe \leftarrow fe + size(\mathbf{X})$
    $\mu_{CR} \leftarrow (1 - c) \cdot \mu_{CR} + c \cdot arithmeticMean(S_{CR})$
    $\mu_F \leftarrow (1 - c) \cdot \mu_F + c \cdot lehmerMean(S_F)$
    `//` `state detector`
    if $min(function(\mathbf{X}_{g-dT}) - function(\mathbf{X}_g)) < minError$ **then**
      break
    end
  end

H Adaptive Kernel Scheme

Algorithm H.1: Pseudocode of memetic parallel JADE with adaptive kernels

```
1  Function memeticpJADEadaptive(X, func, kSize, minErr, maxFE):
2      dim, popsize ← size(X)
3      // number of kernels
4      κ ← dim/kSize
5      p ← 0.3
6      c ← 0.5
7      dT ← 100
8      fecounter ← 0
9      bestFE ← ∞
10     bestPop ← ∅
11     popFactor ← popsize/dim
12     while fecounter < maxFE do
13         pop, FE, F, CR ← paJADE(X, p, c, dT, func, minErr,
            maxFE − 2 · dim )
14         fecounter ← fecounter + len(F) · popsize
15         bestIndex ← argmin(FE)
16         bestSol ← pop[bestIndex]
17         pop, FE ← ds(func, bestSol, minErr, 2 · dim)
18         fecounter ← fecounter + 2 · dim
19         if min(FE) < bestFE then
20             // increase dimension
21             X ← appendRndKernel(pop, popsize, kSize)
22             κ ← κ + 1
23             // adapt population size to dimension
24             X ← appendRndPop(X, popFactor, kSize)
25             bestFE ← min(FE)
26             bestPop ← pop
27             dim, popsize ← size(X)
28         end
29         else
30             // reduce dimension
31             // restart around previous best
32             X ← bestPop + N(size(bestPop))
33             κ ← κ − 1
34             dim, popsize ← size(X)
35         end
36     end
37     return pop, FE, F, CR
```

I PDE 2 3 4 and 7 Kernel Adaption

The following plots show the fitness difference in relation to the kernel adaption. Darker grey and black areas represent a strong decline of the fitness value over multiple generations, while lighter areas mean that the fitness value is stagnating. Following lighter areas, often comes a green bar, which means that a new kernel is introduced. Similarly, red lines represent the reduction by one kernel. The plots compare the best and the worst replications with $minError = 0$ produced in the experiment chapter 7.

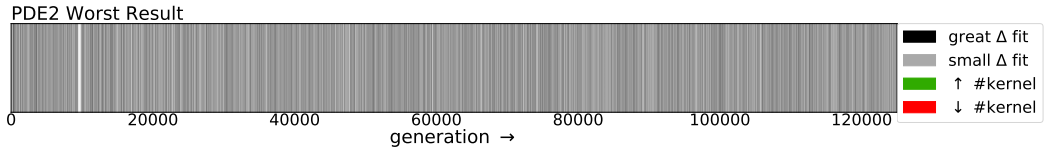

Figure I.1: Kernel Bars Plot on the worst result of PDE2 in experiment 2.

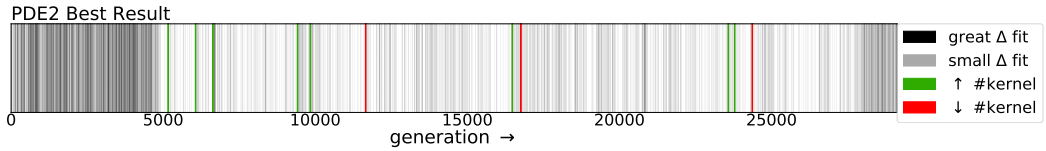

Figure I.2: Kernel Bars Plot on the best result of PDE2 in experiment 2.

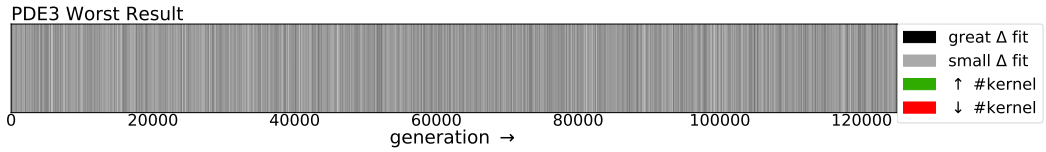

Figure I.3: Kernel Bars Plot on the worst result of PDE3 in experiment 2.

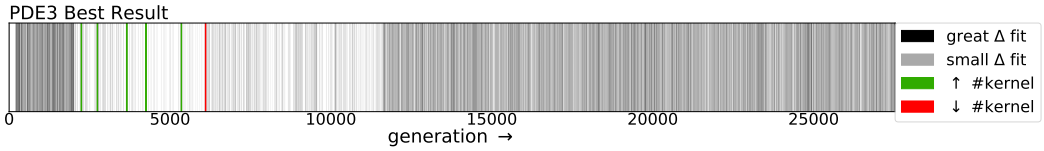

Figure I.4: Kernel Bars Plot on the best result of PDE3 in experiment 2.

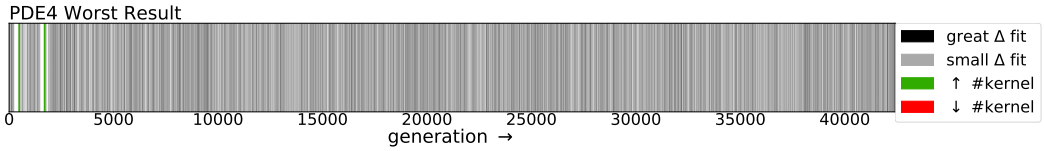

Figure I.5: Kernel Bars Plot on the worst result of PDE4 in experiment 2.

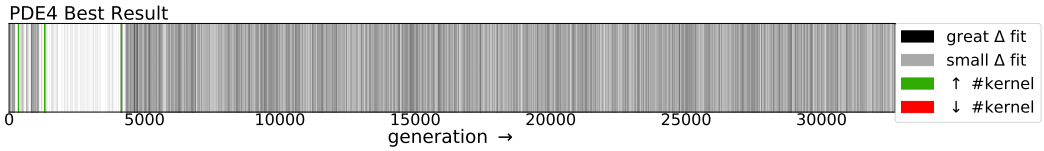

Figure I.6: Kernel Bars Plot on the best result of PDE4 in experiment 2.

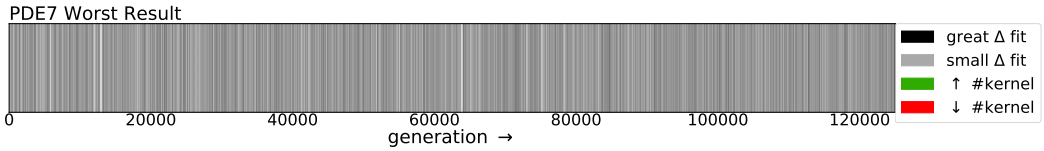

Figure I.7: Kernel Bars Plot on the worst result of PDE7 in experiment 2.

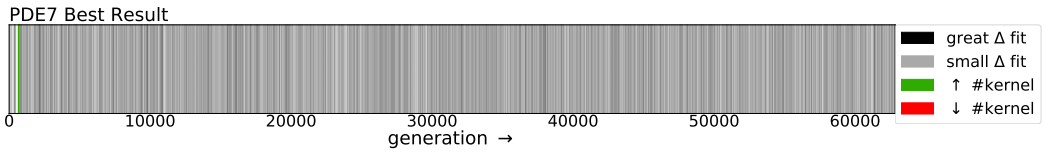

Figure I.8: Kernel Bars Plot on the best result of PDE7 in experiment 2.

Statement of Affirmation

I hereby declare that this thesis was in all parts exclusively prepared on my own, without using other resources than those stated. The thoughts taken directly or indirectly from external sources are properly marked as such. This thesis or parts of it were not previously submitted to another academic institution and have also not yet been published.

Dornbirn, 31.08.2020 Schwartze Nicolai, BSc